Biomechanics of artificial joints : the hip

Basic Orthopaedic Biomechanics, 2nd ed.,
edited by Van C. Mow and Wilson C. Hayes.
Lippincott–Raven Publishers, Philadelphia © 1997.

11

Biomechanics of Artificial Joints: The Hip

Rik Huiskes and Nico Verdonschot

Department of Musculoskeletal Biomechanics, Institute of Orthopaedics, University of Nijmegen, 6500 HB Nijmegen, The Netherlands.

TOTAL HIP REPLACEMENT

Development of Hip Replacement

Total hip replacement (THR) has become one of the major surgical advances of this century. At an estimated occurrence between 500,000 and 1 million operations per year (155), it is second only to dental reconstruction as an invasive treatment of body ailments. Its success rate as a satisfactory surgical therapy for serious disabilities or illnesses is probably surpassed only by removal of the appendix (W. H. Harris, *personal communication,* 1987).

Total hip replacement is an effective treatment for serious forms of osteoarthritis[1] and for disabling effects of rheumatoid arthritis, congenital deformities, and particular kinds of posttraumatic conditions. Osteoarthritis (OA) is the most frequent indication for THR, comprising about 65% of the total volume. According to an American study in 1981 (3), it is responsible for the majority of cases involving musculoskeletal discomfort and, second to cardiovascular conditions, is an important cause for complete or partial disabilities. About 17% of Americans have some form of arthritis (59,71,260). Ten percent of all Americans suffer from OA, half of them chronically.

The development and application of THR have achieved a tremendous reduction in disabilities, particularly in the older segment of the population. The economic effects of this surgical treatment on society as a whole in terms of savings in medical care, drugs, and disability aids and the reduction in sickness-related absence from jobs are significant (59,71,260). The personal effects on the happiness and life fulfillment of patients are overwhelming. The majority of patients receiving THR can hardly walk at all and suffer

[1]When the cause of degenerative joint disease is mechanically initiated, as is often the case, this disease is better referred to as osteoarthrosis.

serious continuous pain, day and night. A few weeks after the operation, they will, with few exceptions, be pain-free, able to function normally, and resume jobs and sometimes even active sports. Complications will usually not recur until after 10 to 20 years. When they do, as a result of eventual wear or loosening, a revision operation is possible. At least 90% of the patients live normal, pain-free lives for at least 10 years after the operation (29,76,155).

The successful application of THR on a large scale, which essentially evolved during the last three decades, is an accomplishment of scientific and technological developments in orthopaedic surgery and bioengineering, in particular from the scientific specialties of biomaterials and biomechanics sciences. The proliferation of applications started around 1960 with the introduction of two inventions by Sir John Charnley (25,26). One was the adoption of the "low-friction" principle, whereby a relatively small metal femoral head was made to rotate against a polyethylene acetabular cup. Another was the use of acrylic cement (polymethylmethacrylate or PMMA) as a filling material to accommodate uniform load transfer between the smooth-shaped prosthesis and the irregular texture of the bone. The PMMA, when introduced in a doughy phase, interdigitates with the bone and cures to form a solid but relatively flexible mantle between bone and prosthesis (Fig. 1). Polymethylmethacrylate is a relatively weak material, however, and long-term loosening of prostheses has been attributed to its mechanical disintegration.

Efforts to improve the endurance of implant fixation have resulted in better cementing techniques. Alternative prosthetic designs have been aimed at replacing acrylic cement with other means of fixation. Early noncemented prostheses were the press-fitted or screwed-in types. Noncemented porous-coated prostheses were introduced to provoke bony ingrowth for improved fixation. Hydroxyapatite-coated hip prostheses (64–66, 121,175) are meant to form a firm biological adhesive bond with bone (osseous integration). Some of these noncemented devices

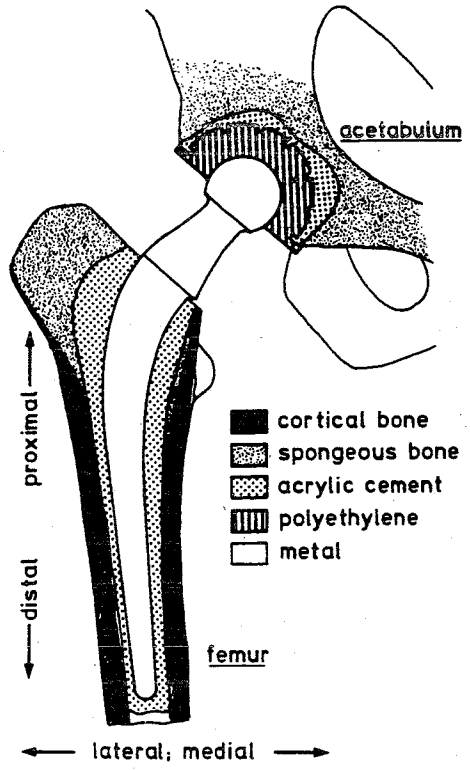

FIG. 1. Schematic section of a cemented Charnley prosthesis. (From Huiskes, ref. 93, with permission.)

have failed, but others are doing well in the mid- to long term. Definite conclusions about their ultimate clinical performances and about the best fixation methods or designs require longer-term studies. The noncemented prostheses are used predominantly in younger patients (<60 years), where it is assumed that these prostheses eventually simplify a revision operation (120). Epidemiologic studies show that for these younger patients, revision surgery would probably be needed if they were to receive a cemented prothesis.

Clinical Performance

The "quality" of a joint replacement depends on such clinical factors as medical complications the patient may suffer, presence of residual pain, motion restrictions, and loosen-

ing of the components. Although the precise relationships are not always evident, the quality is basically determined by prosthetic design factors (materials, prosthetic shape, fixation concept, and surgical instruments), surgical factors (surgical skills and experience, including patient and device selection, and patient instruction), and patient factors (bone mechanical quality, general health condition, age, weight, and level of physical activity). The most frequent complication is long-term loosening unrelated to infection, which is usually called aseptic or mechanical loosening. Aseptic loosening is a gradual process (52,68,128,191,207) whereby the mechanical integrity of the implant–bone interface is lost, and a fibrous tissue is formed between the two surfaces. A gradual increase in thickness occurs with time. As a result, the patient develops pain and functional restrictions. Aseptic loosening is the limiting factor for the functional life span of THR reconstructions. Most of the clinical and bioengineering research and development performed aims at understanding its causes and postponing its occurrence.

The precise mechanism of aseptic loosening of cemented THR is not entirely certain, but several factors are known to contribute. Some of these affect the biological processes at the cement–bone junction directly. Wear particles from the cup–head articulation and other origins may migrate in the cement–bone interface. They provoke reactions from macrophage cells, which cause bone to resorb (88, 128,178,207). As an effect, a fibrous tissue layer is formed between cement and bone, reducing the integrity of the fixation. Repeated application of load on the hip will create relative motions between bone and cement, which are known to provoke further bone resorption and loosening (69). A similar result can occur in an early stage through resorption of interface bone after bone death. Interface bone death, or necrosis, can be caused by the mechanical rasping procedure during the operation (58), by thermal damage from the heat of polymerizing of acrylic cement (58,93,165), or by cell-toxic effects of residual monomer in the cement (58,257).

Another class of causative factors for aseptic loosening has mechanical origins (1,72,89, 130,142,170,220). The loads on the hip joint are relatively high and frequent, up to 1 million cycles per year. Eventually this may cause fatigue failure of the components and junctions in the THR reconstruction. In particular, acrylic cement (36) and its interfaces with bone and THR components are vulnerable to fatigue processes. Indirectly, mechanical forces also affect the biological processes in bone. Bone reacts to chronic overloading by bone formation, and to underloading by resorption, which is called strain-adaptive bone remodeling (13,116,126,229). In this way, the bone morphology and the integrity of the fixation may gradually change over time. This also affects the stresses in the materials and their strength.

Long-term follow-up studies in large patient groups have shown that the average life span of cemented THR lies somewhere between 10 and 20 years. Although individual variations are large, the average in a group of patients depends very much on prosthetic design and on the average age of the patient population at the time of the operation (2,79, 155). Younger patients have significantly shorter endurance expectations than older ones, probably as a result of higher physical activity levels, metabolic turnover rates, and biologic remodeling processes.

Problems associated with noncemented prostheses arise from three sources. The first concerns the interface fixation stability. The fixation relies on a good mechanical fit because no cement is used to fill the gaps between the prosthesis and the host bone. Thus, the dimensions and shape of the prosthetic components in relation to the host bone are more important than for cemented prostheses. In addition, more precise bone preparation techniques are required. The problem of producing a good fit has not been solved for the available contemporary prosthetic designs (4,9,148,171,176,187,206). As a result, the initial postoperative fixation (or initial stability) of the implants is usually far from ideal. The patients may subsequently suffer (often

temporarily) from residual postoperative pain (midthigh pain) caused by relative motions of the implant during loading (50,255). These relative motions may also prevent bone ingrowth or osseous integration of the implant, thereby affecting the long-term stability of the device. The lack of adequate fit also leaves gaps at the implant–bone interface, which create routes for migrating wear debris, promoting long-term loosening.

Second, strain-adaptive bone remodeling phenomena affect the long-term postoperative behavior of noncemented joint replacements in particular. This is because these designs are usually relatively stiff, thereby affecting the strain patterns in bone more drastically than in the case of cemented replacements. This effect may be further amplified by the rigid interface formed by bone ingrowth or osseous integration. When this occurs, certain regions of the surrounding bone become understressed ("stress shielded" or "stress protected"), thus causing bone resorption to take place. The extent to which this mechanism affects the long-term clinical result is not known. However, certainly too much bone loss will eventually cause mechanical failure of the implant–bone structure. In addition, a weakened bone may create an unfavorable situation for revision surgery (53).

Third, prostheses that have been firmly fixed by bony ingrowth or by osseous integration are very difficult to remove, should it become necessary. Hence, it is not entirely certain that failed noncemented prostheses are more easily revised than failed cemented prostheses; this is often suggested as an advantage of the noncemented type.

To evaluate the quality of a hip prosthesis, relative to its potential for long-term endurance, survival rates are determined in patient series. Figure 2 shows an example of so-called survival-rate curves for two prosthetic types from the Swedish multicenter trials (155). The orthopaedic community in Sweden has developed a unique information system, the Swedish Register, for monitoring the long-term outcome of joint replacement. In this system, data on each THR procedure are

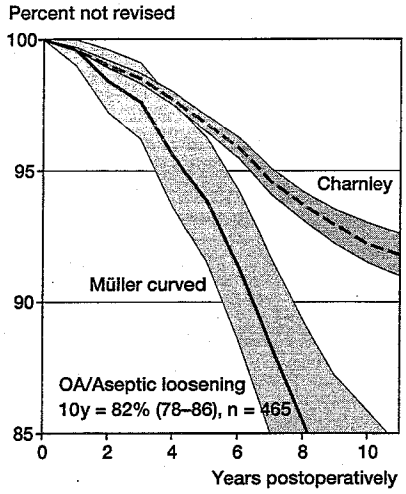

FIG. 2. Probability of survival (percentage not revised) of two cemented total hip replacements. The data are taken from the Swedish Register containing a total of 92,675 patients who received a THR between 1978 and 1990. The *shaded bands* give the 95% confidence intervals. (Adapted from Malchau et al., ref. 155.)

stored, including patient, surgical, and device-related information. Because virtually all surgeons contribute to providing the data, and each patient has a unique national identification number, all revisions are traceable and can be related to the specifications of the primary THR procedure. In this way, objective data can be obtained, whereby implant, patient, and surgical factors are correlated to prosthetic endurance with a high degree of statistical significance. This system has frequently enabled early detection of unsafe designs or provided information about the effectiveness of particular surgical procedures (76,77,79,155,225). It also gives feedback to individual orthopaedic centers about their relative performance. Similar follow-up studies in single or a restricted number of clinics have been less effective in discriminating causative factors for failures.

When revision is not taken as the indicator of failure, postoperative studies in patient series are less conclusive. Rating systems to score function and pain have been developed, but these mostly rely on patient interviews and

are not objective (256). Longitudinal postoperative radiograms are another source of information on the quality of hip reconstructions. However, radiographic exposure procedures are not standardized; hence, morphologic and bone-density parameters tend to be variable. In addition, conventional radiograms are two-dimensional reductions of a three-dimensional reality. As a result, measurements based on their use tend to be imprecise (123,157).

In recent years, methods have been developed that allow for more precise determinations of prosthetic behavior and hence for earlier detection of problems. It has been shown that aseptic loosening of prosthetic components is virtually always preceded by migration (63,135,247). Roentgen stereophotogrammetric analysis (RSA) permits these migrations to be detected with an accuracy of some 100 μm (134,135,166,214). The use of this method, discussed in more detail in another section of this chapter, allows significant predictions of pending loosenings of THR even after 6 months postoperatively (135). Dual-energy X-ray absorptiometry (DEXA) is a new method to measure bone mass *in vivo*, with an accuracy of about 5%. This method can be used to detect loss of bone around a prosthesis and predict pending problems or assess the effectiveness of particular prostheses in their bone-preserving potential (13,28,56). Gait analysis, finally, is another method for objectively measuring the quality of THR and detecting problems in an early stage (81,174,183).

Biomechanics and the Innovation Cycle

The development of new prostheses is motivated not only by requests from the orthopaedic community but also by commercial considerations. Marketing a reasonably successful device, even for a small number of users, can be quite profitable. As a result, new types appear frequently, not necessarily providing for better quality reconstructions. Traditionally, new designs have often been developed through "trial and error," using the operating room as the laboratory and the patient as the experimental model. This was justified at a time when no satisfactory alternative existed, and often the new hip replacement did at least offer the patients adequate and safe treatment for a limited number of years. Today, the traditional time-tested cemented hip replacements provide safe and effective solutions for a long period of time, relative to which new devices must be tested (57). Ideas for new designs tend to be based on clinical research, in which particular problems are identified, or on experimental research with new concepts or materials for THR.

Whatever the origin, the new design should be tested preclinically before marketing to prevent unsafe devices from being tried in patients. These tests can be performed in animal models, laboratory bench tests, or computer-simulation models, depending on the particular failure scenarios investigated (102). Deficiencies in a design are not always detected in a preclinical test because new designs may create hitherto unknown problems. Hence, to prevent unsafe designs from being widely marketed, they should be tested in restricted clinical trials. Because endurance of THR is the most critical issue, and the average life span is already on the order of 10 to 20 years, the efficacy of clinical trials is not a trivial matter. Obviously, innovators and companies will be reluctant to postpone marketing for a decade; on the other hand, a clinical trial period of 2 years (as, for example, required by the FDA) is much too short to establish long-term safety and efficacy of a new prosthetic design. When objective and precise measuring techniques are applied, such as RSA, DEXA, or gait analysis, as mentioned above, these short-term trials may be more effective in detecting design deficiencies. Nevertheless, postmarketing surveillance, such as applied in the Swedish Register, is necessary to prevent unsafe marketed devices from creating a disaster in a large patient population.

Biomechanics research is intimately involved with virtually all activities in the innovation cycle. To understand clinical failure mechanisms of THR requires knowledge about the forces acting on the hip, the stresses they generate in bone and implant materials, and

their effects on wear, damage accumulation, and bone remodeling. Biomechanics is important in the establishment of failure scenarios, which are required for effective preclinical testing (102). The development and validation of preclinical testing methods comprise another prominent area of biomechanics investigation, and, of course, biomechanicians are involved in designing new hip prostheses and surgical instruments. All these activities require basic information assessed in biomechanical studies, i.e., the evaluation of forces occurring in the joints and their related muscles in various functions, the study of motion characteristics of the joints, the assessment of geometric properties of the bones to which artificial components are to be connected, or the mechanical properties such as strength and elastic characteristics of bone and biomaterials involved.

This chapter on the biomechanics of THR emphasizes the analysis of load transfer from prosthesis to bone, its interaction with biological remodeling processes, and its effects on the mechanical behavior and endurance of hip reconstructions, both the cemented and the noncemented types. The principles of experimental design and analysis are emphasized, rather than the specifics of particular prostheses. Hence, the main purpose of this chapter is to acquaint the reader with the tools of research and development in this area. For illustrative purposes, some examples are also presented.

SOLID MECHANICS AND STRESS ANALYSIS

Some Principles of Solid Mechanics

In this section some definitions and principles of solid biomechanics are reviewed. For a more detailed discussion, the reader is referred to standard engineering textbooks (38,87,200,226).

Stress, Strain, and Hooke's Law

If a body is loaded, it deforms. Unless the body is regularly shaped (e.g., cube, bar, or beam), and the external load is evenly distributed and aligned with the geometry, these deformations produced in the body will not be uniform. The amount of deformation will vary throughout the body. To analyze the deformation, we select an infinitesimal cube of material inside the object and allow this cube to be stretched and compressed in the three edge directions. To quantify these deformations, we define a lineal strain along each edge, given as a change of length per original length (Fig. 3a). These three lineal strains also define the dilatation (change of volume per original volume; this is equal to the algebraic sum of the three lineal strains) of the cube. The lineal strains and dilatation depend on the applied loading and on the material that constitutes the object. We also allow the shape of the cube to distort in its three planes (Fig. 3b). These three angles are known as shear strains, and they also depend on the material and the external loading. These six variables completely describe the deformation of the tiny cube at any arbitrary point inside the body.

For a continuous body, load is transferred at every point inside the body. This implies that when we pass an imaginary plane through the body, the material on one side of the plane will exert a force on the material on the other side. These are internal forces, and they are transferred by chemical or physical bonds at the molecular level. Like the deformations, the magnitudes and orientations of these internal forces are not uniform but depend on the external loading, the shape of the object, and the intrinsic mechanical properties of the material

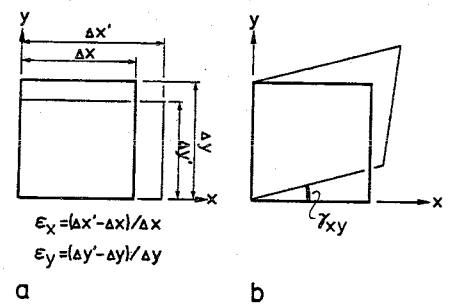

FIG. 3. Definitions of strain in the case of two-dimensional stress state. **(a)** direct strain; **(b)** shear strain. (From Huiskes, ref. 95, with permission.)

making up the object. To describe these internal forces, we must first define the concept of stress. Simply stated, stress is defined as force per unit area. For convenience, the areas we choose are the faces of the tiny cube described above (Fig. 4). On each face of the cube, the force vector may be arbitrarily oriented. This means that on each face of the cube the stress vector will also be arbitrarily oriented. This stress vector may be decomposed into a component perpendicular to the face of the cube (normal stress) and a component parallel to the face of the cube (shear stress). In general, the shear stress component will have two components, each parallel to an axis of the chosen coordinate system. Thus, a total of nine stress components (three normal stresses and six shear stresses) must be known to define the state of stress acting on the cube (Fig. 4). However, by conservation of angular momentum, the shear stresses are symmetric, i.e., $\tau_{xy} = \tau_{yx}$, $\tau_{yz} = \tau_{zy}$, $\tau_{zx} = \tau_{xz}$. Thus, only six independent stress components exist, three normal stress components (σ_x, σ_y, σ_z) and three shear stress components (τ_{xy}, τ_{yz}, τ_{zx}) (Fig. 4). We note that the normal stresses can be either tensile (positive) or compressive (negative). We also note that these stress values will vary with the orientation of the chosen cube (i.e., coordinate system) because the components of a vector will vary with the orientation of the chosen coordinate system.

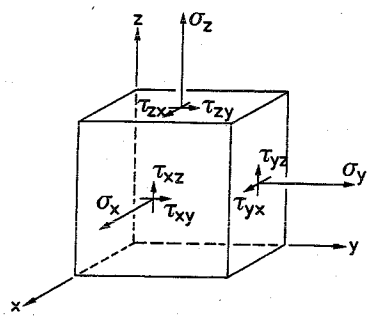

FIG. 4. Definition of the nine stress components relative to an infinitesimal cube in the material. Since $\tau_{zy} = \tau_{yz}$, $\tau_{xz} = \tau_{zx}$, and $\tau_{xy} = \tau_{yx}$, only six independent components remain to describe the three-dimensional stress state. (From Huiskes, ref. 95, with permission.)

Central to solid mechanics theory is the relationship between stresses and strains for the body. This relationship is given by a constitutive equation. The stiffness of the material depends on the intrinsic mechanical properties of the material, i.e., the coefficients of the constitutive equation or material constants. If this material is linearly elastic, the generalized Hooke's law may be applied (111). In this case, the six strain components are linearly related to the six stress components by a matrix of 36 elastic constants (of which 21 are independent) given by[2]

$$\begin{bmatrix} \varepsilon_x \\ \varepsilon_y \\ \varepsilon_z \\ \gamma_{xy} \\ \gamma_{yz} \\ \gamma_{zx} \end{bmatrix} = \begin{bmatrix} S_{11} S_{12} S_{13} S_{14} S_{15} S_{16} \\ S_{21} S_{22} S_{23} S_{24} S_{25} S_{26} \\ S_{31} S_{32} S_{33} S_{34} S_{35} S_{36} \\ S_{41} S_{42} S_{43} S_{44} S_{45} S_{46} \\ S_{51} S_{52} S_{53} S_{54} S_{55} S_{56} \\ S_{61} S_{62} S_{63} S_{64} S_{65} S_{66} \end{bmatrix} \cdot \begin{bmatrix} \sigma_x \\ \sigma_y \\ \sigma_z \\ \tau_{xy} \\ \tau_{yz} \\ \tau_{zx} \end{bmatrix} \quad (1)$$

This is a coupled set of six equations. It shows that a particular strain value may depend on all six stress values and vice versa. Irrespective of the kind of material considered, this matrix is always symmetric (i.e., $S_{ij} = S_{ji}$), which implies a maximum of 21 independent components. This set of six equations defines a completely anisotropic material if all these 21 elastic constants in the matrix are different. For most materials, some form of symmetry of the microstructure exists. If the material is orthotropic, all but the constants S_{ii}, S_{12}, S_{13}, and S_{23} reduce to zero, which leaves nine independent constants in the matrix. If the material is transversely isotropic, which means that the properties are equal for two of the three principal directions, the number of independent constants reduces to five. For the isotropic case, the number reduces to only two independent elastic constants. Most often, these are expressed in terms of the Young's modulus (or elastic modulus) E and Poisson's ratio ν. Other constants are commonly used as well, such as the Lame constants (λ,μ), modulus of rigidity or shear modulus (μ), and the

[2]This equation is defined by matrix multiplication. For example, $\varepsilon_x = S_{11}\sigma_x + S_{12}\sigma_y + S_{13}\sigma_z + S_{14}\tau_{xy} + S_{15}\tau_{yz} + S_{16}\tau_{zx}$, etc.

bulk modulus (κ). These constants may be expressed in terms of E and ν because only two constants are independent, and equation 1 may then be written as

$$\begin{bmatrix} \varepsilon_x \\ \varepsilon_y \\ \varepsilon_z \\ \gamma_{xy} \\ \gamma_{yz} \\ \gamma_{zx} \end{bmatrix} = \begin{bmatrix} 1/E & -\nu/E & -\nu/E & 0 & 0 & 0 \\ -\nu/E & 1/E & -\nu/E & 0 & 0 & 0 \\ -\nu/E & -\nu/E & 1/E & 0 & 0 & 0 \\ 0 & 0 & 0 & (2+2\nu)/E & 0 & 0 \\ 0 & 0 & 0 & 0 & (2+2\nu)/E & 0 \\ 0 & 0 & 0 & 0 & 0 & (2+2\nu)/E \end{bmatrix} \cdot \begin{bmatrix} \sigma_x \\ \sigma_y \\ \sigma_z \\ \tau_{xy} \\ \tau_{yz} \\ \tau_{zx} \end{bmatrix} \quad (2)$$

When the material is transversely isotropic, a total of five elastic constants are required (19, 193). For example, by approximation, cortical (haversian) bone is transversely isotropic. To describe cortical bone, a modulus is required for the longitudinal direction and another for the radial direction (the tangential direction has the same modulus as the radial one), along with two Poisson's ratios and a shear modulus.

We emphasize some important restrictions to linear elasticity theory and continuum mechanics. First, if a material is not linearly elastic, e.g., nonlinearly elastic, then Hooke's law does not apply. The material may also be plastic or viscoelastic in nature. For these types of material, the stress–strain laws are always much more complex. Biological materials can not, in general, be described by infinitesimal linear elasticity theory, although bone can, by reasonable approximation. Second, the definitions of stress and strain presume that the material is continuous. This implies that no matter how small a cube we have chosen, the properties in the cube are supposed to be identical to those of the material at a larger scale. This assumes that there are no imperfections or voids (discontinuities) in the material. For real materials, this is hardly ever true. Even metals have imperfections in their lattice structure and at grain boundaries. Plastics usually possess a certain degree of porosity, although the pore sizes are extremely small. Bone is essentially discontinuous, in particular trabecular bone. Hence, stress–strain relationships and the calculated stresses and strains are always approximations. The quality of these approximations ranges from very good (e.g., metal) to very rough (e.g., trabecular bone). The approach to a discontinuous material like bone is to designate a region in which dimensions are large relative to the characteristic size of the microstructure of imperfections and only consider the calculated stresses and strains in that region as average.

Three- and Two-Dimensional and Uniaxial Stress States

If the characteristic features of a structure can be represented in a plane, and the external loads are also in that plane, then the stress state in the structure is two-dimensional. A two-dimensional problem may be described as a plane stress or a plane strain problem. In the plane-stress problem, the material is free to expand in the out-of-plane direction, and the normal stress in that direction is zero. This implies for equations 1 and 2 that when z is the out-of-plane direction, $\gamma_{yz} = \gamma_{zx} = 0$, and $\sigma_z = \tau_{yz} = \tau_{zx} = 0$. For the plane-strain case, the material is constrained in the out-of-plane direction, and the lineal strain in that direction is zero. This implies for equations 1 and 2 that $\varepsilon_z = \gamma_{yz} = \gamma_{zx} = 0$ and $\tau_{yz} = \tau_{zx} = 0$. In both of these cases, the stress state within the plane can be characterized by three stress variables (e.g., σ_x, σ_y, and $\tau_{xy} = \tau_{yx} = \tau$).

In the uniaxial stress state, only one independent stress component exists. This implies for equations 1 and 2 that, if x is the uniaxial direction, $\gamma_{xy} = \gamma_{yz} = \gamma_{zx} = 0$ and $\sigma_y = \sigma_z = \tau_{xy} = \tau_{yz} = \tau_{zx} = 0$. This state of stress occurs predominantly in long, slender bodies of regular prismatic shape (bars or columns), which are loaded externally at the end by axial tension or compression, transverse forces, or bending moments. This state of stress is most often used for tensile or compressive tests to determine the Young's modulus and Poisson's ratio of isotropic materials.

Principal Stresses and Stress Tensors

If we rotate the cube of Fig. 4 relative to a fixed coordinate system external to the object, the values of the stress components will change even though the stress state within the material remains the same. Thus, different components may describe the same stress state inside the material. At one particular ori-

entation of the cube, all shear-stress components acting on the face of the cube will vanish. This orientation defines the principal directions for the state of stress at the cube inside the material. The associated normal stresses are known as the principal stresses. For any arbitrary state of stress, the principal stresses are the maximum and minimum stress at any point inside the object.

The state of stress is completely described by the six stress components. In its entirety, the state of stress is known as a stress tensor. Although the components may vary with the specific coordinate system chosen, the state of stress remains the same. In other words, the state of stress within an object does not depend on a specific chosen coordinate system (i.e., observer). It depends solely on the loading, geometry, and material properties of the object. The simplest representations of a state of stress are either in the principal coordinate system or by the three principal normal stress components.

Bone prosthesis structures often require stress information about "interfaces," where different materials are connected. These interfaces do not always align with the external coordinate system, nor do they generally align with the principal stress directions. For that purpose, local coordinate systems at the point of interest can be introduced relative to which the interface normal and shear stresses are expressed. The three methods of stress representation (coordinate, principal, and interface stresses) are illustrated in Fig. 5 for a two-dimensional example.

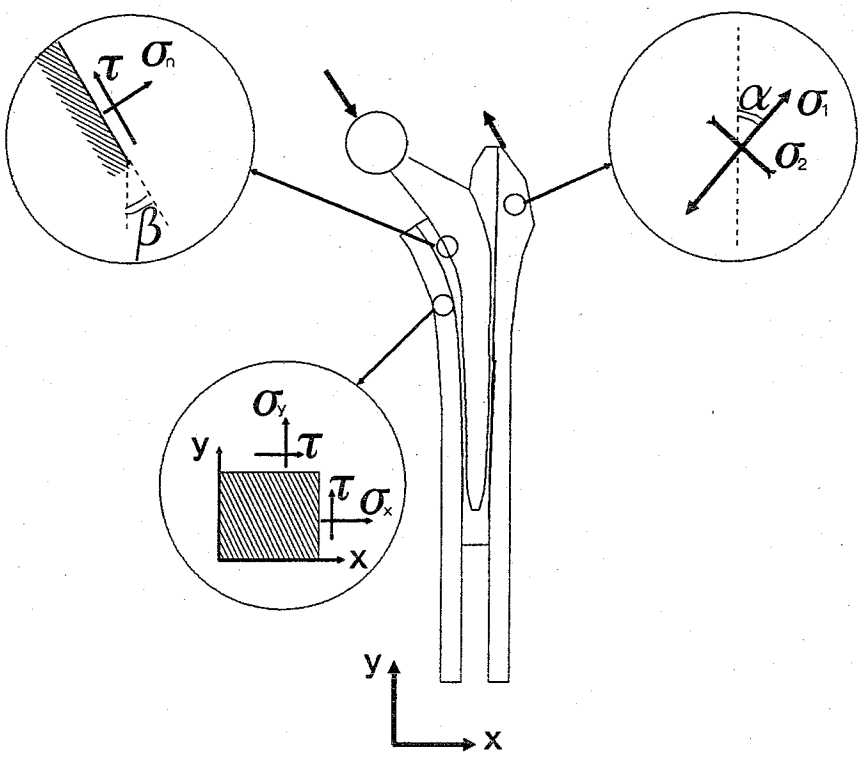

FIG. 5. The stress state in a point of a structure can be described in three ways: (i) principal stresses (σ_1, σ_2, and the principal-stress orientation α relative to the coordinate *xy* axes), (ii) coordinate stresses (σ_x, σ_y, and τ relative to a cube aligned with the coordinate axes), and (iii) interface stresses (compression/tension σ_n, normal to the interface, and shear τ, parallel to the interface, plus the orientation of the plane β). The principles of these representations are identical for three-dimensional stress states. One representation can directly and uniquely be converted to another by transformation of the coordinate system attitude.

Scalar Measures of Stress Intensity

The yield stress (or elastic limit) of a material is usually measured in uniaxial tensile and compressive or shear tests on material samples with simple geometric shapes. The question then is how to relate a two- or three-dimensional stress state, characterized by six stress components, to the yield stress data from uniaxial tests in order to estimate the probability of failure. For this purpose, an *equivalent* (or *effective*) *stress* is determined from a particular yield criterion. The von Mises yield criterion, for example, assumes that material will yield, i.e., deform plastically, when the distortion energy exceeds a certain value. The *von Mises stress* can be calculated from the equation

$$\sigma_{mi} = \{1/2[(\sigma_1 - \sigma_2)^2 + (\sigma_1 - \sigma_3)^2 + (\sigma_2 - \sigma_3)^2]\}^{1/2} \quad (3)$$

where σ_1, σ_2, and σ_3 are the principal stress values in the material point of interest. This von Mises equivalent stress value can simply be compared to stress values obtained from samples of the material tested in the laboratory in uniaxial tension or compression to estimate the probability of failure. It gives reasonable predictions for isotropic materials. It works less satisfactorily for anisotropic elastic materials (such as bone) or viscoelastic materials. Still, it is often used for these materials as well, to represent the six stress components in one generalized "stress intensity" factor, which greatly simplifies the interpretation and representation of results of stress analyses.

The *strain-energy density* (SED) also represents the stress state in a material but has not been directly related to a failure criterion. This quantity represents the elastic energy stored in the deformed material and can be calculated from the formula

$$U = 1/2(\varepsilon_1\sigma_1 + \varepsilon_2\sigma_2 + \varepsilon_3\sigma_3) \quad (4)$$

where ε_1, ε_2, and ε_3 and σ_1, σ_2, and σ_3 are the principal strains and stresses, respectively. This form of SED is valid only for isotropic materials, where the directions of principal strains and principal stress are parallel. The SED function is commonly used to formulate nonlinearly elastic constitutive equations (hyperelastic materials). It is also used in strain-adaptive bone-remodeling theory.

Stress Analysis

Stress analysis in solid mechanics involves a particular structure with a given geometry made out of a particular material(s) with known elastic properties (i.e., Young's modulus and Poisson's ratio). The structure is loaded externally by forces and/or moments and is connected to the environment in a certain way. The objective of stress analysis may be to determine the stress and strain fields in the structure to see if the structure gives rise to excessive deformations or stresses that could cause mechanical failure.

Stress analysis may be conducted either numerically on a computer or with closed-form mathematical solutions. In the former case, a computer model is used, i.e., the finite-element method. In the latter case, the solution is obtained in explicit mathematical formulas. These closed-form solutions are available only for particular, regularly shaped structures such as prismatic bars and beams. If applicable, closed-form solutions are always to be preferred over numerical ones because, in addition to the actual numerical results, they also render insight into the relationships among structural parameters, material properties, geometric factors, loads, and stress–strain patterns (95). As a rule, all calculated stresses and strains should be experimentally verified. Strains acting at the surface of a structure may be determined experimentally, either directly with measurements or indirectly, using a laboratory model.

It is noted that the results of a stress analysis, whether experimental or analytic, depend very much on the model constructed to represent the structure. The accuracy of the stress and strain calculations depends very much on the realism of the model (i.e., geometry, constitutive equation for the material, material coefficients, loading conditions, and boundary conditions). Models are abstractions of re-

ality, and they are used to simplify the actual problem. The essence of modeling is that each model must capture the salient characteristics of the problem appropriate to the needs of the situation. However, overly complex models are not necessarily better than simpler ones. There are no fixed rules for this modeling process. The question is never whether a model assumption is true in the real sense of the word (they almost never are) but whether a simplification is justified relative to the definition of the problem (107).

Finite-Element Analysis

The finite-element method (FEM) has become a widely used tool in orthopaedic biomechanics. It is a computer method suitable for determining stresses and strains at any given point inside a structure of arbitrary geometric and material complexity. A finite-element model relies on accurate constitutive representation of material characteristics (such as the elastic coefficients of generalized Hooke's law), geometric data, loading characteristics, and boundary and interfacial conditions. The principles of FE analysis are described in many textbooks (e.g., 91,264). Attempts at more general introductions to FEM, particularly for orthopaedic biomechanics, have been published elsewhere (95,107,117,154). Only the basic principles and a few pitfalls are reviewed here. To develop a FEM model, the shape of the structure to be analyzed is divided into small elements. For three-dimensional analysis, elemental volumes of a particular shape (e.g., bricks) are used, and for a two-dimensional analysis, elemental areas of a particular shape (e.g., triangles or quadrilaterals) are used. Each element has nodal points, usually at the corners of the element. At each nodal point three (or two in the case of two-dimensional analysis) displacement components and three force components (two in a two-dimensional analysis) are identified.

As an illustrative example, consider a two-dimensional model with triangular elements, each with three nodal points (Fig. 6). The displacement vector **u** and force vector **f** at each

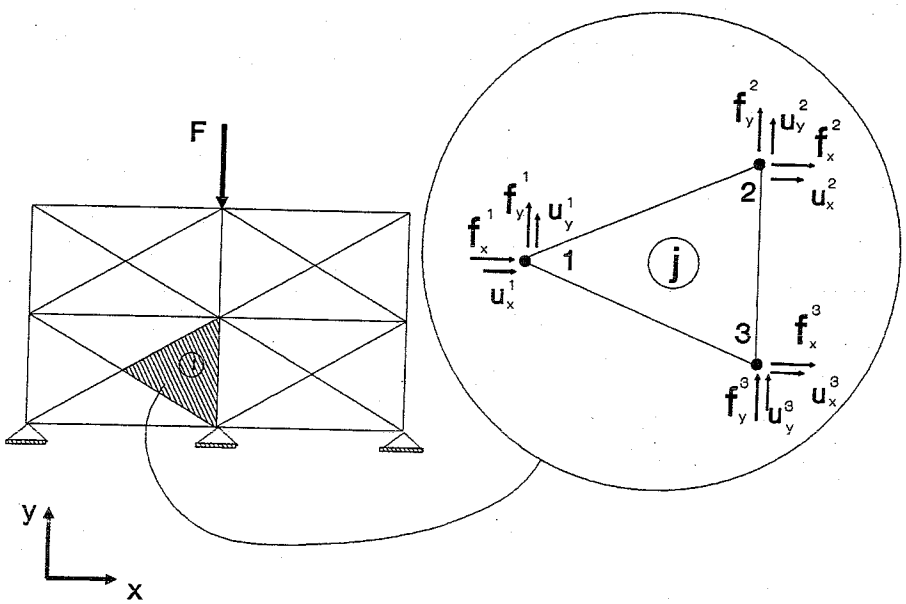

FIG. 6. A two-dimensional finite-element mesh and definition of nodal-point forces and nodal-point displacements.

nodal point i can be written in terms of their components:

$$\boldsymbol{u}^i = \begin{bmatrix} u_x^i \\ u_y^i \end{bmatrix} \quad \boldsymbol{f}^i = \begin{bmatrix} f_x^i \\ f_y^i \end{bmatrix} \quad (i = 1,2,3) \tag{5}$$

For the entire structure with n elements, these vectors at the j^{th} element may be written as

$$\boldsymbol{u}^j = \begin{bmatrix} u^1 \\ u^2 \\ u^3 \end{bmatrix} = \begin{bmatrix} u_x^1 \\ u_y^1 \\ u_x^2 \\ u_y^2 \\ u_x^3 \\ u_y^3 \end{bmatrix} \quad \boldsymbol{f}^j = \begin{bmatrix} f_x^1 \\ f_y^1 \\ f_x^2 \\ f_y^2 \\ f_x^3 \\ f_y^3 \end{bmatrix} \quad (j = 1,\ldots,n) \tag{6}$$

where n is the total number of elements in the mesh. When the material of the element is linearly elastic, and the deformations are small relative to the dimensions of the element, there is a linear relationship between the nodal point force and the nodal point displacement components, which may be written in vector notation as

$$\mathbf{f}^j = \mathbf{Q}^j \mathbf{u}^j \tag{7}$$

Here $\mathbf{Q}^j$ is called the "stiffness matrix" of the jth element and consists of 6×6 components. Let us assume for a moment that the values of all these 36 components are known for every one of the elements. The structure is then numerically "assembled," in the sense that all displacements and forces of the different elements belonging to the same nodal point are collected. Then one vector, $\mathbf{u}$, is formed in which all displacement components in all the nodal points are collected, and one vector, $\mathbf{f}$, is formed that contains all force components in all nodal points. Hence, we obtain an equation of the form

$$\mathbf{f} = \mathbf{Q}\,\mathbf{u} \tag{8}$$

where $\mathbf{Q}$ is the $m \times m$ "stiffness" matrix for the whole construction containing m^2 components, and m is the number of degrees of freedom in the model (usually $2n$ for a two-dimensional model or $3n$ if the model is three-dimensional). The value of each component is known from the assembling procedure. By Newton's third law of action and reaction, many of the force components at nodal points are zero. Hence, the components of the nodal-point force vector $\mathbf{f}$ are either zero where no external force is applied, have a known value where external forces are applied, or are unknown where boundary constraints are applied. The components of the nodal point displacement vector $\mathbf{u}$ where the boundary conditions are applied are either unknown where the forces are prescribed or known where the displacements are prescribed. Hence, for each component (degree of freedom) at each nodal point, either the displacement is known or the force is known. In other words, equation 8 is a system of m linear, algebraic equations with m unknowns and hence can be solved to give the values of all displacements in all nodal points.

To determine the components of the stiffness matrices in equation 8, we must go back to the individual element and equation 7. We assume that the deformation in each element takes a specific form in such a way that the deformation within the element is determined by the relative displacements of the nodal points. For instance, the strain distribution in each element may be assumed to be uniform. This assumption makes possible the determination of the components of the element stiffness matrix from the volume of the element and its shape, elastic modulus, and Poisson's ratio. And it also makes it possible to determine the strain in each element from the nodal point displacements and subsequently the stress in the element from Hooke's law.

In developing the FE code as described above, we have made two important simplifications. First, we have limited the admissible deformation of each element to a uniform strain pattern (i.e., a linear displacement field) within the element. Second, we have assumed that all load transmission between elements is concentrated in the nodal points. Thus, all results obtained are approximate. In fact, the accuracy of the approximation depends on the kind of elements used and on the degree of mesh refinement. When the element density approaches infinity, the results converge to the exact solution.

Today, using the finite element method is much simpler than suggested above because most of the work is done by readily available computer codes. The art of FE analysis now is really concerned with the development of the FE model and the interpretation of its results rather than with the performance of the calculations. However, the development of an adequate FE model for a hip reconstruction is still not a trivial matter (107). Of course, building a three-dimensional anatomically realistic mesh is a lot more time-consuming and complicated than building a two-dimensional mesh. In the three-dimensional case there could be significant restrictions on the maximum number of elements and nodal points used, depending on the capacity of the computer available. This is more problematic in prosthetic analysis because joint reconstructions are composite structures. For example, some parts of the composites have very small dimensions (e.g., acrylic cement layers) and require small elements. As a consequence of mesh continuity requirements, the adjacent material also needs relatively small elements, which increases the total number of elements in the structure. Potential solutions to this problem are limited by requirements for the minimal element aspect ratio; a brick element, for instance, that is relatively thin is said to be distorted and to produce errors.

The sophistication of the element and the displacement field must also be considered. Different types of elements are available in the FE packages. These elements use different interpolation functions to represent the coordinates and displacements in the subsequent calculations of strains and stresses. These interpolation functions can be relatively simple, such as a bilinear function for a two-dimensional four-node element or a trilinear function for three-dimensional eight-node brick elements. The advantage of these simple elements is that the number of degrees of freedom is relatively low, which limits the computer costs. However, these elements may not be able to capture the strain and stress states that are generated in reality. For example, these relatively simple elements behave too stiffly when they are exposed to a bending load. The reason for this is that the linear shear strain variation that is present in bending can not be described by the simple interpolation functions. In some FE codes this can be corrected to some extent by correcting the interpolation function. This procedure is called the assumed strain formulation. More complex elements have more complicated interpolation functions (two-dimensional eight-node elements and three-dimensional 20-node elements); they have quadratic interpolation functions and are more powerful to describe the true stress and strain distribution. If we use one element over the thickness of a substructure and a linear displacement field (i.e., constant strain element), then we will obtain constant stress and strain over that thickness. In reality, for such a structure, a strain gradient may exist such as that occurring in bending. If we want more detailed information, we must either use more elements or use a more sophisticated element with a quadratic displacement field (linear strain) that results in more nodal points per element. In both cases, the size of the computation problem increases. The number of nodal points or elements required for appropriate accuracy can be determined with so-called convergence tests (139).

When the mesh has been constructed, the computer code needs external loading characteristics, elastic constants for each element, and specifications for the boundary and composite interface conditions. This again is not a trivial step in the process of modeling THR reconstructions because, as discussed above, these characteristics tend to vary greatly in a patient population and over time, and in general they are not known precisely. Hence, in order to analyze some of the problems, again, simplifying approximations must be used.

Geometry and FE Mesh

The geometry or shape of the arthroplasty components is accounted for by the FE mesh itself. Conceptually, every detail of the structures can be taken into account by using sufficiently small elements, but in practice this

is hardly feasible; hence, the problem must be schematized to some degree. The refinement to which the structure is described by the mesh depends on the kind of information required (107). Figure 7 shows a few FE meshes of THR structures of variable complexity. In Fig. 7A a so-called "anatomic" mesh of a femoral component is shown, a three-dimensional model aimed at a realistic geometric representation of the reconstruction. The model in Fig. 7B is also three-dimensional but is symmetric relative to the midfrontal plane of the prosthesis. Although the general features of the load-transfer mechanism are reproduced in both models, the "anatomic" one is able to show details that are lost in the symmetric one. Although it seems intuitively obvious that the "anatomic" model is the more desirable one, this is not always true. The question is always whether details are relevant relative to the purpose of the model (107). Sometimes we would rather dispose of the details in order to obtain a more generic picture.

A simplified alternative to a three-dimensional model is a two-dimensional one, representing the midfrontal plane only. Such a model is quite easily assembled. However, it ignores the 3-D elastic integrity of the bone. This can be restored by using a "side plate" (93). This is essentially a second 2-D FE model, superimposed over the first one, or "front plate." When these requirements are fulfilled, then this model reproduces the relevant stress patterns of a three-dimensional one in the midfrontal plane reasonably accurately (235). Evidently, the effects of out-of-plane loading (i.e., torsion) can not be studied with a two-dimensional model, and out-of-plane stresses (e.g., hoop stresses) can not be determined.

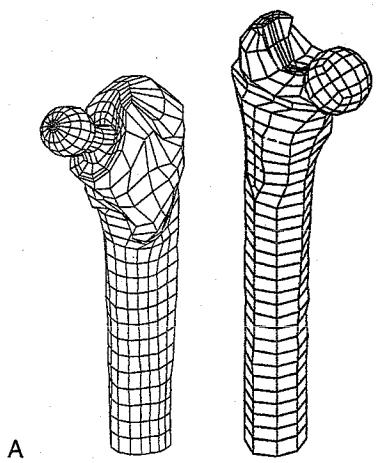

FIG. 7. Three-dimensional "anatomic" (**A**) and two-dimensional (**B**) finite-element models of femoral THA configurations.

In initiating an FE analysis, it is not advisable to immediately start developing the most expensive and complex model. As in all scientific endeavors, it is imperative to stop and think first what it is one wishes to accomplish and tune the model to those requirements. This, of course, requires an understanding of the relationships between model features and potential results.

Voxel Element Meshes

Increasingly, FE meshes of bones and THR structures are produced on the basis of geometric assessments from serial computed-tomography (CT) scanning (Fig. 8A). The CT delivers a three-dimensional voxel mesh of density values from which the shape of the bone can be graphically reconstructed using contour detection algorithms. The graphic reconstruction then serves as a basis for the element mesh (116,131,138). Advantages of this procedure are that mesh generation can be automated to some extent and that the apparent density of the bone material, by approximation related to its elastic modulus, is evaluated as well. Apart from this latter advantage and the convenience of the nondestructive geometric assessment, the problem of adequate mesh generation in a three-dimensional volume remains. This problem can be solved with voxel-conversion methods (86,208,254).

In principle, each voxel from a CT scan can be converted directly into a cubic element. The cube corners provide the coordi-

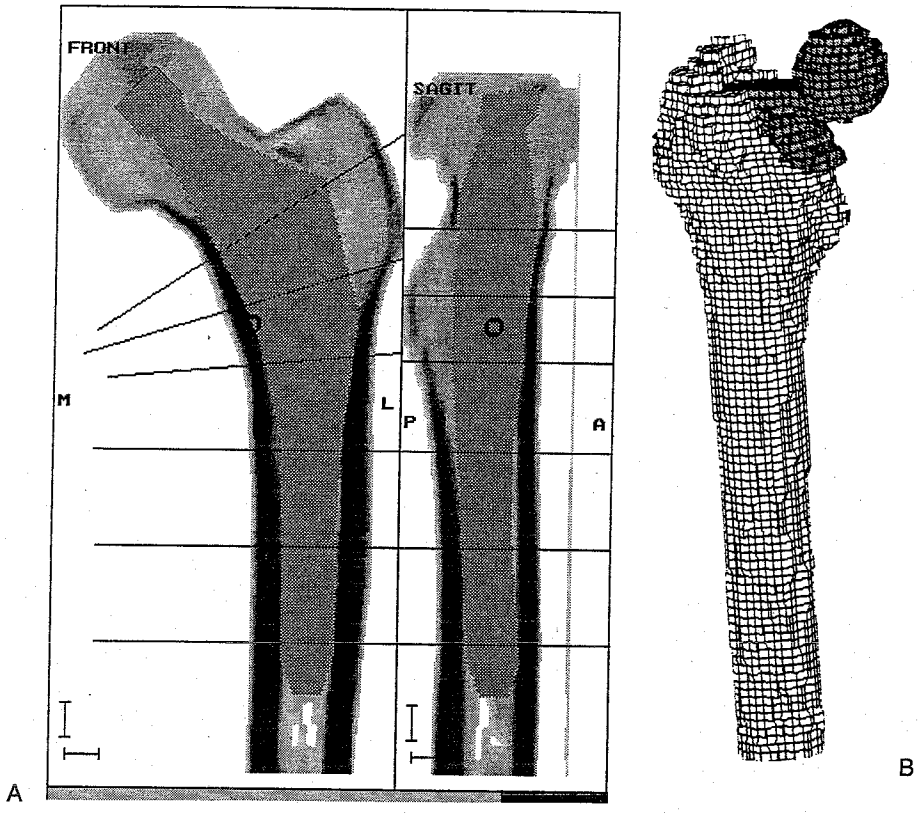

FIG. 8. (A) Example of a three-dimensional graphics computer program in which a CT-scanned bone can be imported, as well as the implant geometry. The implant can be moved relative to the bone in order to find the desired position. This is in fact an implantation-simulation procedure that can be done together with a surgeon. The finite-element mesh can be made directly from the geometric description. **(B)** Voxel model of an implanted femur. (Reproduced from 213a.)

nates of the nodal points, and the voxel density its elastic modulus. In fact, the whole mesh is available by the time the CT scan is made, ready for FEA. An example of such a mesh of a THR structure is shown in Fig. 8B. There are, however, disadvantages to this efficient procedure: the number of elements may be excessive, and the boundaries of the model are ragged instead of smooth. As was shown in comparative tests, the ragged boundaries hardly affect the mechanical behavior of a model at large. This implies that although the stress values calculated at the boundary are not dependable, those within the material are precise (85,125). The problem of excessive numbers of elements can be solved with alternative FE solution procedures that apply iterative optimization schemes. Examples are the element-by-element (EBE) procedure (84,92) and the row-by-row (RBR) procedure (231). The RBR procedure uses the fact that each element in the mesh has the same shape, dimension, and orientation, such that only a limited number of possible environments can exist. This makes the procedure much more efficient than EBE; hence, more elements can be used in the mesh. The RBR peocedure does require each element to have the same elastic constants, which is not the case for EBE.

Global Versus Local Mechanical Quantities

In many FE analyses of THR structures, local information about mechanical quantities is required. For example, one may need to evaluate the strength requirements of thin prosthetic coatings or study the stress environment of bone growing into pores. In such cases, the ratio between the typical volume to be studied and the dimensions of the whole THR structure may be on the order of 10^3. An adequate FE mesh for such a problem would imply too many elements for any computer. A traditional solution for this problem is to use FE models for different levels, applying the local nodal-point forces of a global model as boundary conditions for a local one. The precision of this method is questionable, however, because the stiffness characteristics of the local model are usually not equal to those of the corresponding volume in the global model (108). As a result, equal nodal-point forces produce different deformation patterns (nodal-point displacements). This problem can be solved by the application of homogenization theory (7,31,83,86,204).

In homogenization theory, a representative volume element (RVE) is produced from the stiffness characteristics of a local volume of interest, evaluated with an FE micromodel. The homogenized stiffness matrix of the RVE is substituted in the global mesh to determine its deformation characteristics, which then later serve as boundary conditions for an FE analysis of the local model, producing the local stresses and strains.

Loads

An FE analysis requires a numerical description of all external loads applied on the structure (point of application, magnitude, direction). These loads are usually variable and not always precisely known (12,14,15,34,46), so the question in FE analysis is often which approach to take in order to obtain useful information. A consideration that is always helpful is that FE analysis allows for easy parametric variation. Hence, the loads can be varied and the results studied in order to determine their relationships, and a "worst-case" situation can be defined. Often the worst-case (or typical-case) configuration is selected *a priori* from different possibilities. In such cases, it is advisable to investigate the sensitivity of the stress patterns to small deviations in the external loads. If different prosthetic designs are compared, different FE meshes are needed. Consequently, it is not trivial that the three-dimensional coordinates of the points where the external loads are applied are equal in all cases. Hence, the effects of different geometries on the stress and strain patterns are obscured by variations in load application location. This can be repaired by defining invariable points that are used to apply the external forces.

A set of three femoral loading cases can be considered that together represent average daily activities (Fig. 9; Table 1).Their magnitudes and directions have been chosen from telemetric measurements by Bergmann et al. (12) and Kotzar et al. (141) and are scaled for a person of 65 kg weight. The first two loading cases represent the peak joint forces that develop during the stance phase of normal walking (12,141), and the third loading case

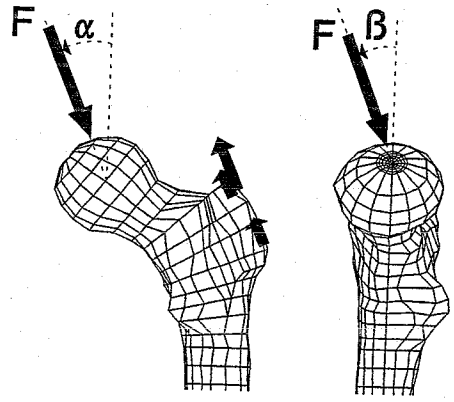

FIG. 9. The proximal part of a finite element model of a femoral bone. A set of three joint forces and three muscle forces can be selected, which represent typical daily loading configurations. Orientation is shown; values are listed in Table 1 (119,147).

TABLE 1. *Magnitudes and orientations of hip and muscle forces for three load cases (see Fig. 9)*

	Joint force	M. glut. max.	M. glut. med.	M. glut. min.
F_1 (N)	2132	637	637	214.5
α_1 (°)	23.4	39.9	24.6	28.4
β_1 (°)	5.7	43.0	24.8	28.4
F_2 (N)	1586	45.5	739	143
α_2 (°)	21.9	28.2	20.8	25.1
β_2 (°)	–4.6	24.3	10.5	1.9
F_3 (N)	1690	637	637	214.5
α_3 (°)	25	63.8	42.5	42.0
β_3 (°)	–15	62.0	57.7	55.1

represents the maximal joint load during stair climbing (141). The first loading case has the largest joint force (2132 N), whereas the third loading case has the largest out-of-plane component of this force. The insertions, orientations, and magnitudes of the corresponding forces in the three major muscles, the m. gluteus mimimus, the m. gluteus medius, and the m. gluteus maximus, have been taken from the work of Crowninshield and Brand (32) and Dostal and Andrews (49).

Hip-joint and muscle loads working at the acetabulum reconstruction during gait have been specified for FE analysis by Dalstra et al. (42), based on data from the same authors as mentioned above for the femur.

Figure 10 shows an example of the effects of variable loading in the hip joint during gait (12) on the bending stress patterns in a femoral THR structure (244). A worst-case load for the proximal stem would occur after 0.5 sec from the start of the stance phase. However, the distal stem stresses would reach a maximal value at 0.3 sec. This illustrates that a worst-case load for one part of the structure is not necessarily a worst case for another part.

Another approach to load selection is to use representative loading cases. This approach is especially useful when the effects of particular design features of a prosthesis are to be studied in a comparative analysis or when load-transfer mechanisms are to be studied. For instance, relative to femoral THR, the effects of the hip-joint force may be separated into those resulting from the axial force, bending, and torsional components. The problem can then be analyzed for those three cases separately or for just the most important one. Finally, it is important to realize that most FE models of implant structures use infinitesimal linear elastic theory and that the surfaces are perfectly bonded at the interfaces. In these models, the principle of superposition may be used. Hence, the stress patterns that result from the application of the hip-joint force and the muscle forces together can be found from adding the results obtained from treating those forces separately.

Material Properties

In the FE model, each element must be assigned the appropriate elastic constants of the material. For an isotropic linearly elastic material, two material constants are required, e.g., Young's modulus and Poisson's ratio. This is the case for metallic implant materials. Acrylic cement and plastic components may be included in this category only by rough approximation (177). Cortical bone, by reasonable approximation, can be considered as linearly elastic and transversely isotropic, requiring five elastic constants for a complete description of its stress–strain relationship (19,193). The elastic relationship for cortical bone can also be simplified from transverse isotropy if the stresses and strains in the transverse and tangential directions are of lesser importance for the problem investigated (94).

Modeling cancellous bone is more complicated. To the first-order approximation, its elastic modulus can be expressed as a function of its porosity, measured by its apparent density (20). If a volume V (cm^3) weighs w (g) without the fatty marrow, then the apparent density is defined by $\rho = w/V$ (g/cm^3). The relationship between apparent density and the elastic modulus can be empirically defined by (20)

$$E = C\rho^{\alpha} \qquad (9)$$

with C and α being constants; α is somewhere between 2 and 3, probably closer to 2 (195). The elastic properties of cancellous

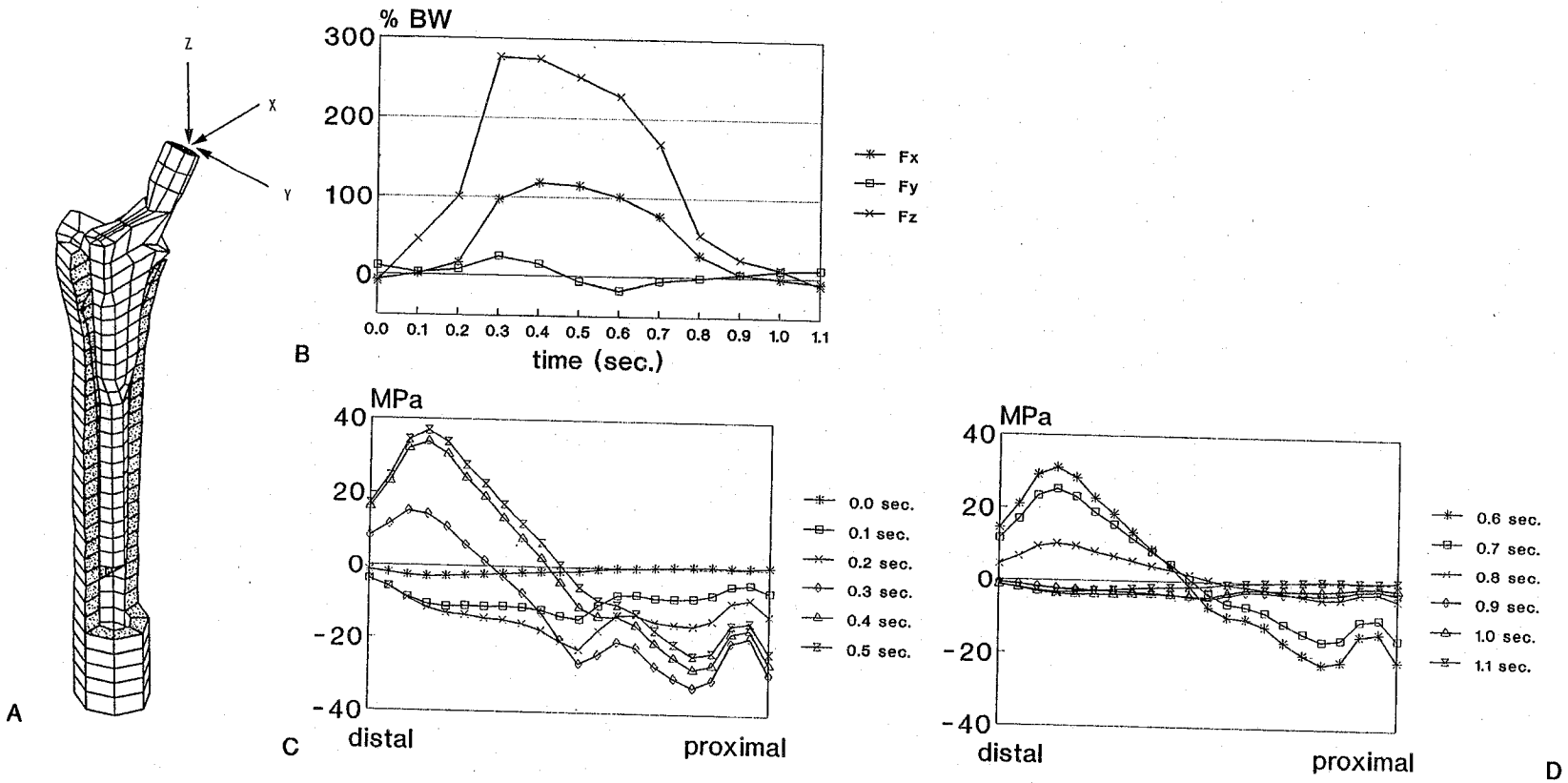

FIG. 10. (A) A finite-element model of a femoral stem–bone composite structure. **(B)** Hip joint forces determined from an *in vivo* instrumented prosthesis (12). **(C)** and **(D)** Distribution of the bending stresses at the medial side of the frontal plane of the prosthesis from 0 to 0.5 sec and from 0.6 to 1.1 sec (244).

TABLE 2. *Indicative values of Young's moduli and static strengths for most materials and interfaces used in THR reconstruction*

	Young's modulus	Static strength
CoCr alloy	200–220 GPa	800–1000 GPa under tension
Titanium	100–130 GPa	800–1500 GPa under tension
Acrylic cement (PMMA)	2–3 GPa	100 MPa under compression 25–40 MPa under tension
UHMWPE	1 GPa	20–30 MPa under tension
Cortical bone	15–20 GPa	20–50 MPa under tension 150–200 MPa under compression
Cancellous bone	500–1500 MPa	3–10 MPa under compression
Fibrous tissue	1 MPa	
Metal–acrylic cement interface		5–8 MPa under shear 5–10 MPa under tension
Hydroxylapatite–bone interface		30–50 MPa under shear
Acrylic cement–bone interface		2–4 MPa under shear 7–10 MPa under tension

bone also depend on the directionality of its structure, which can be the cause of its anisotropic behavior (78,227). The elastic constants of trabecular bone can be determined fully from measurements of its volume fraction, fabric, and degree of tissue mineralization (70,195,227,230,232). Of course, the elastic bone properties can be highly variable, depending on location and individual factors such as the degree of mineralization and osteoporosis (37).

To carry out an FE analysis, information about strength of materials is not needed. However, this information is required for the interpretation of results. In Table 2, indicative values for Young's moduli and the static strengths of the most important materials and interfaces used in THR are listed.

Nonlinear and Time-Dependent Materials

A bone–prosthesis structure can behave in a nonlinear elastic manner when one or more of its materials have nonlinear elastic properties, when deformations are large relative to the characteristic dimensions of the structure, or when its interfaces are not rigidly bonded (73,97,136,240). Examples of essentially nonlinear materials are collagenous tissues such as fibrous tissue membranes, articular cartilage, and ligaments. A finite deformation nonlinearity is illustrated in Fig. 11. Here a post consisting of two materials, a relatively stiff one with elastic modulus E' and length l_0 and a relatively soft and thin one with modulus E and thickness d_0, is considered. The cross-sectional area of the post is A, and the post is loaded by a uniformly distributed compressive force F over the thin layer. By simple linear elastic theory in uniaxial compression theory, it can easily be shown that in the deformed state, the length of the rigid post will reduce to $l = l_0 - l_0F/AE' = l_0(1 - F/AE')$, and the thickness of the layer will reduce to $d = d_0 - d_0 F/AE = d_0(1 - F/AE)$.

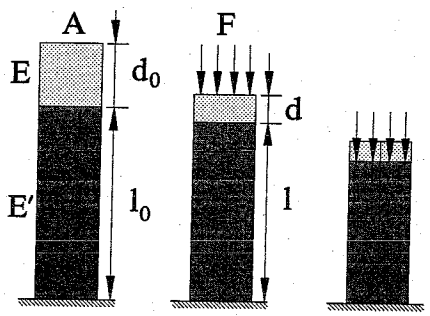

$$d = d_0 - \Delta d = d_0\left(1 - \frac{F}{AE}\right)$$

$$d < 0 \quad \text{if} \quad \frac{F}{AE} > 1$$

FIG. 11. A post consisting of a relatively rigid material (E') and a flexible layer (E) is compressed by a force F. If the ratio $F/AE > 1$, a linear analysis of the problem will predict a negative thickness of the soft layer.

Let us now assume that $A = 100$ mm^2, $F = 1000$ N, $E' = 100$ MPa, and $E = 5$ MPa. It follows that $l = 0.9l_0$, indicating a reduction in length of 10%. It also follows that $d = d_0 - 2d_0$ $0 = -d_0$, which implies a negative thickness of the soft thin layer! The reason for this unrealistic result is that the problem was treated as if it were linear and that infinitesimal strain assumptions remained valid. For finite deformation problems, the simple infinitesimal strain tensor must be replaced by finite deformation tensors, and an appropriate elastic constitutive law must be used. Constitutive laws for soft materials such as rubber and cartilage have been developed. A general feature of these laws is that they allow for the stiffness of the thin layer to gradually increase with increasing compressive load.

Similar problems occur with linear FE analyses of bone–prosthesis structures where thin layers of a low modulus exist next to more rigid materials (248). Thus, to analyze the fibrous tissue lining between bone and prostheses, a more complex FE code is required. If a structure behaves nonlinearly, the FE analysis must be performed in a stepwise fashion by increasing the external loads in small increments from zero until the desired end values are reached. The stiffness matrix in this algorithm is updated with every increment of load. Hence, instead of solving equation 8, one must solve

$$\Delta \mathbf{f} = \mathbf{Q}\,\Delta \mathbf{u} \qquad (10)$$

for each increment of load (80,91,264).

In a linear analysis, the external load is applied in one step because the deformations are always linearly related to the magnitude of the load. In a nonlinear analysis, one in fact simulates a process of structural deformation by gradually applied external loads, which introduces a time factor. If materials behave in a time-dependent way, the rate of the process becomes a factor of significance as well. Examples of such materials are viscoelastic ones (e.g., biphasic interface soft tissues) or plastics susceptible to creep or cold flow (e.g., PMMA and polyethylene). The strategy for the solutions of these problems is similar to the above, in the sense that the process of deformation is simulated iteratively, updating the stiffness matrix in every iteration, depending on the time-development of material constitutive parameters (168,188,219,237)

Boundary and Interface Conditions

The boundary conditions for the FE model are imposed on the exterior surfaces of the object. The boundaries can be divided into free, loaded, and fixed boundaries. At a free boundary, no stress (or load) is transferred, and it is not constrained by a connecting structure. At a loaded boundary, external loads are applied. At a fixed boundary, no motion is allowed, or the motion is constrained by some surrounding structure. The last ones are usually those where the FE model is cut off from the environment with which it normally interacts. The characteristics of this interaction must be accounted for by introducing prescribed displacements in the appropriate nodal points. This is not always easily realized, and as a result, artifacts can be introduced in the stress patterns near those boundaries. This is not a problem as long as the boundary region is remote from the region of interest.

Some problems that boundaries sometimes may present are illustrated in the example of Fig. 12, where an FE analysis is applied to an acetabular THR component. The right side of Fig. 12 represents the case in which the cup is assumed to be loaded internally by a distributed force, representing its interaction with an artificial metallic femoral head. The resulting surface deformation is shown (exaggerated to make it visible). Evidently, this is not a realistic representation because the inner cup boundary would in reality be forced to conform itself to the spherical contour of the stiff metallic femoral head. This problem can be solved by including the metal head in the FE model (left side of Fig. 12) and allowing only compressive stress to be transferred at the head–cup connection as in a contact problem. To do this, the hip-joint load is applied to the stem, and the femoral head then transfers the load to the cup in such a way that the

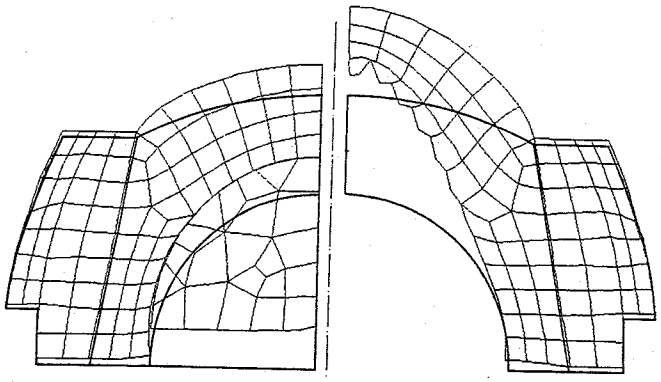

FIG. 12. Deformations determined by a finite-element model of an acetabular cup–bone composite structure (displacements are magnified to allow for visualization). When the femoral head is included in the model, the load transmission problem is a contact problem **(left).** In this case, the displacements at the surface of the cup are compatible. When the external force is applied directly on the inner surface of the cup with an assumed stress distribution, the resulting surface displacements may not be compatible with the form of the femoral head (109).

head is constrained to be in contact with the cup at all times.

At a connection (or interface) between two materials, which can be described as a surface, we can find stress transfer or relative motion, or a combination of both (Fig. 13). The stress transferred across the connecting surface can be represented by a normal stress (σ_n) perpendicular to the plane (tension or compression) and two shear-stress compo-

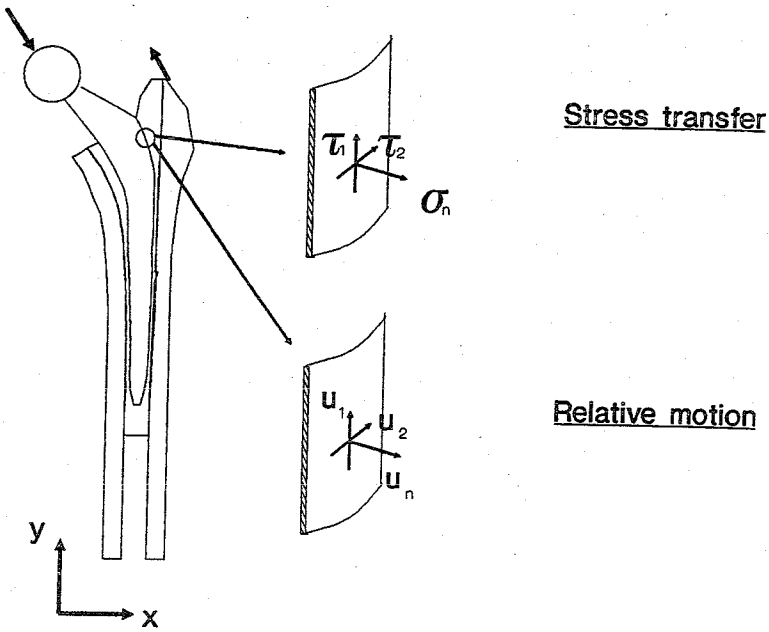

FIG. 13. Normal stress (σ_n) and shear stress (τ_1, τ_2) components transferred across a bonded interface. Normal (u_n) and tangential (u_1, u_2) displacement components are relative motions that may occur if the interface is unbonded.

nents (τ_1 and τ_2). The relative motions can also be characterized by three relative displacement components, u_n in the normal direction and u_1 and u_2 in the tangential directions. Various conditions at the boundary may now be written as follows:

- Bonded interfaces:

$$\sigma_n \neq 0, \tau_1 \neq 0, \tau_2 \neq 0,$$

$$u_n = u_1 = u_2 = 0 \qquad (11)$$

- Loose interfaces without friction:

$$\tau_1 = \tau_2 = 0, \sigma_n \leq 0 \text{ (i.e., } \sigma_n \text{ can only be compressive)}$$

$$u_n \geq 0 \text{ (i.e., } u_n \text{ can only be separation)}, \quad u_1 \neq 0, u_2 \neq 0 \qquad (12)$$

- Loose interfaces with Coulomb friction:

$$\sigma_n \leq 0, (\tau_1^2 + \tau_2^2)^{1/2} \leq \mu|\sigma_n|, \text{ where } \mu \text{ is the Coulomb coefficient of friction,}$$

$$u_n \geq 0, u_1 \neq 0, u_2 \neq 0 \qquad (13)$$

When interfaces are unbonded and hence loose without friction (equation 12) or loose with friction (equation 13), the problem becomes nonlinear and must be solved iteratively, using load increments. For this purpose, most FE packages use the so-called gap elements to account for separation and sliding of the surfaces. The load transfer from intramedullary implants (e.g., hip stems) is affected more dramatically by interface conditions than by any other structural parameter, in particular when comparing a fully bonded to a fully unbonded case (99).

STRESS TRANSFER IN COMPOSITE STRUCTURES

General Considerations

A bone–prosthesis structure is known as a composite structure. This implies that it consists of separate substructures with different elastic and geometric properties that are bonded to each other in some specified manner. The stress patterns in these composite structures are dependent on the bonding characteristics at the interfaces between the substructures and by the relative magnitudes of their elastic moduli.

The latter effect can be illustrated relative to the phenomenon of load sharing in a composite bar (Fig. 14A and B). Here, a tensile force F is transferred through a composite bar comprised of two bars bonded to each other. The two bars have different Young's moduli, E_1 and E_2, and cross-sectional areas A_1 and A_2. The quantity AE is known as the axial stiffness of a bar. When the loading is applied as shown, the individual bars of the composite will share in the load transfer from one to the other such that $F_1 + F_2 = F$. For this composite bar, the forces F_1 and F_2 are given by the ratio of axial stiffnesses:

$$F_1/F_2 = A_1E_1/A_2E_2 \qquad (14)$$

This formula shows that the bar with the higher axial stiffness will carry more load. We note that equation 14 is based on the assumption that the axial strains in the bars are equal, i.e., $\varepsilon_1 = \varepsilon_2 = \varepsilon$. Hence, from Hooke's law in uniaxial tension, $\sigma_1 = E_1\varepsilon$ and $\sigma_2 = E_2\varepsilon$, it follows that

$$\sigma_1/\sigma_2 = E_1/E_2 \qquad (15)$$

Equation 15 states that when a deformation (ε) is imposed on a composite bar, the material with higher elastic modulus will experience greater stresses. Similar formulas exist for the composite beam loaded transversely in bending or composite shafts loaded in torsion (95). For each case, the stiffer beam will carry a higher load.

The illustrative example of Fig. 14A and B is one of pure load sharing, because the external force F is applied on both bars simultaneously. If the force were only applied on bar 1, then load sharing would not occur in the segment of bar 1 to the right of bar 2 (Fig. 14C). Obviously, load sharing would take place only where bar 1 and bar 2 are bonded together. In this example, load transfer is via the shear stress developed at the interface between bar 1 and bar 2. In bar 1, in going from right to left, the load F_1 reduces from $F_1 = F$ to $F_1 =$

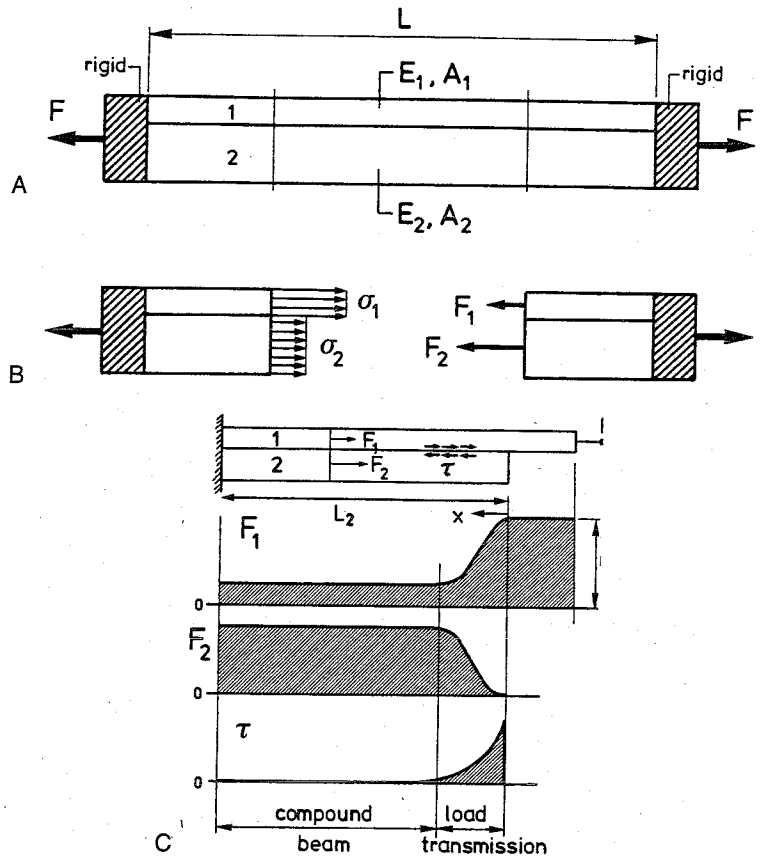

FIG. 14. (A) A composite structure consisting of two bonded bars with different elastic moduli and cross-sectional areas. The structure is uniformly stretched by an external axial force F. **(B)** The internal forces F_1 and F_2 differ by virtue of the different elastic moduli; the internal stresses $\sigma_1 = F_1/A_1$ and $\sigma_2 = F_2/A_2$ are also different. **(C)** Load transfer by means of shear stress τ at the interface between the two bars. The loads F_1 and F_2 inside the two bars and the shear-stress distribution τ at the interface are shown.(From Huiskes, ref. 95, with permission.)

$A_1E_1F/(A_1E_1 + A_2E_2)$, and in bar 2, the load F_2 increases from $F_2 = 0$ to $F_2 = A_2E_2F/(A_1E_1 + A_2E_2)$. This load transfer mechanism between the two bars is important, because the shear stresses it produces may cause the bond to fail at the interface.

Clearly, the total amount of load transferred from bar 1 to bar 2 must equal

$$F_2 = A_2E_2F/(A_1E_1 + A_2E_2) \qquad (16)$$

This force must act over the available area for the bar, L_2d_2, at the interface. Here, L_2 is the length of the bar, and d_2 its depth (in the perpendicular direction). Although the average shear stress over the length L_2 would be $\tau_{av} = F_2/L_2d_2$, the actual maximal stress is much higher because τ is far from uniform, with a peak value at L_2, where bar 2 begins to carry load. The actual shear-stress pattern $\tau(z)$ can be determined from a shear-lag distribution function given by

$$\tau(z) = \lambda F_2 e^{-\lambda z}/d_2 \qquad (17)$$

where λ is a structural parameter depending on the elastic moduli and the cross-sectional areas of the two bars (93). Again, similar formulas exist for beams in bending and shafts in torsion (93,95,96).

To review some basic aspects of compressive load transfer in composite structures, let

us consider a very simple model of a solid layer (prosthesis) fixed to a substrate (bone) (Fig. 15). We assume both materials, separately, to have uniform elastic properties and that the top layer is rigidly bonded to the substrate. Figure 15 presents von Mises stress patterns in materials for the case where the prosthesis is loaded by a single point force F. Figure 15A presents the case for which the prosthesis has the same elastic properties as bone ("isoelastic material"), whereas in Fig. 15B, the prosthesis is made out of a metal, say titanium, that is much stiffer than bone. From these results, we note the following characteristics:

1. The stresses are essentially nonuniform, concentrated predominantly in a central band in the structure, directly under the applied load.

2. When the moduli of the two materials are equal (Fig. 15A), the stresses are continuous over the interface; when the materials are different (Fig. 15B), the stresses are discontinuous over the interface.

3. The stress patterns are more uniformly distributed for the case of the stiff prosthesis (Fig. 15B) than in the case of the softer prosthesis (Fig. 15A). As a result, the stress magnitudes are higher for the case of the prosthesis made of softer material.

The normal (compressive) stress σ_y at the interfaces in Fig. 15 must balance the applied force F in the y direction. It would be immediately obvious from a free-body diagram of the prosthesis that the average compressive interface stress $\bar{\sigma}_y$ equals F/Ld, where L is the length and d the width of the elastic layer. The *actual* stress, σ_y, is nonuniform and must also

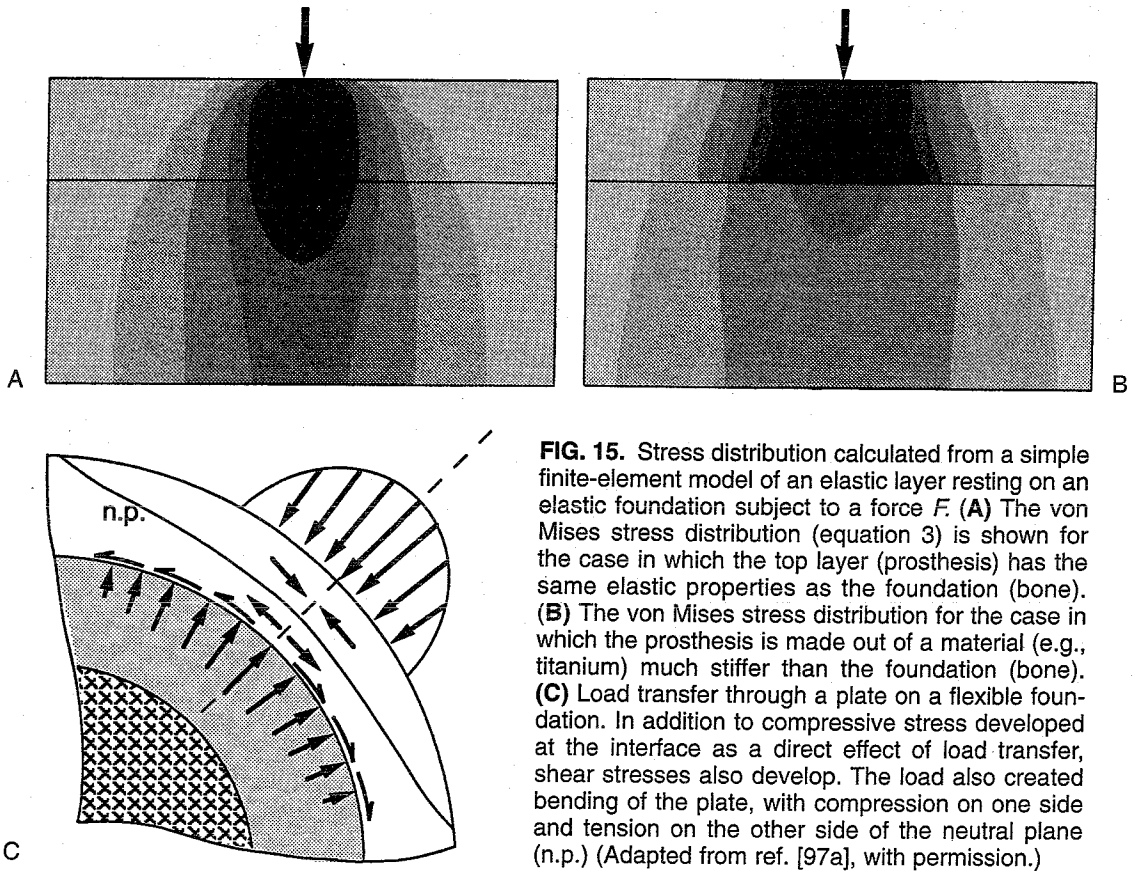

FIG. 15. Stress distribution calculated from a simple finite-element model of an elastic layer resting on an elastic foundation subject to a force F. **(A)** The von Mises stress distribution (equation 3) is shown for the case in which the top layer (prosthesis) has the same elastic properties as the foundation (bone). **(B)** The von Mises stress distribution for the case in which the prosthesis is made out of a material (e.g., titanium) much stiffer than the foundation (bone). **(C)** Load transfer through a plate on a flexible foundation. In addition to compressive stress developed at the interface as a direct effect of load transfer, shear stresses also develop. The load also created bending of the plate, with compression on one side and tension on the other side of the neutral plane (n.p.) (Adapted from ref. [97a], with permission.)

satisfy the equilibrium condition. Thus, a simple relationship exists relating the average stress, $\bar{\sigma}_y$, and the actual stress:

$$\bar{\sigma}_y L d = d\int_0^L \sigma_y dx = F \qquad (18)$$

We note that although the average stress may be used in certain situations, when suspected stress concentrations exist in the composite structure, the average stress should not be taken as representative of the maximal stress value. Equation 18 also shows that since the stress distribution σ_y must always balance the applied load F, a composite structure that leads to a narrower load distribution (Fig. 15A), when compared to that in Fig. 15B, has a higher maximal value. This demonstrates that our intuitive expectation that a material with similar elastic properties to bone would be ideal for implants in fact may not be true. In general, the stress patterns in a surface-fixation structure depend not only on the articular loading characteristics (magnitude, direction, contact location, and contact area size) but also the flexural rigidity (elastic moduli and dimensions) of the component, the elastic characteristics of the supporting bone, and the bonding characteristics.

This illustrates that the load-transfer and load-sharing mechanisms in composite structures can be complex, even in relatively simple regular structures. In general, stresses within a structure cannot simply be determined by dividing the load to be transferred by the area available for load transfer. As a rule, the stresses are not uniform over a particular area, and peak values are bound to occur, depending on the geometry and the material characteristics of the separate components in the composite. High values of stresses generally occur in structures with notches, sharp corners, and holes. These high values are known as stress concentrations.

Very often, stresses in composite structures are generated not as a direct effect of load sharing or load transfer but as an indirect effect of deformational variations caused by differences in elastic moduli (Fig. 15C). Because of the compressive force, compressive stresses will arise at the interface as direct effects of the load transfer mechanism. However, high shear stresses at the interface may also arise as an indirect effect. This is caused by the difference in lateral displacements of the plate and the foundation. If the elastic foundation has a lower elastic modulus than the plate, it will tend to expand more in the lateral direction. This expansion is resisted by the shear stresses developed at the interface. Another mechanism occurs as well. The external load causes the plate to deform in bending. Hence, we find a "neutral plane" (n.p.) where the bending stress in the plate is zero. Above it, compression occurs, and under it, tension. These three mechanisms are, of course, interrelated and dependent on the precise characteristics of the structure. For instance, if the plate is relatively stiff, it deforms less, which will also affect the interface stress distribution.

In the above example, we assumed that the stiffness characteristics of the elastic foundation (i.e., bone) are uniform. This, however, is hardly ever the case in prosthetic composite structures. The stiffness S of a layer of material through which load is to be transferred (e.g., cement or cancellous bone), in terms of the ratio between normal stress (σ_n) and deflection (δ), depends on its Young's modulus (E) and its thickness (t): $S = \sigma_n/\delta = E/t$ (i.e., this is Hooke's law for uniaxial compression). Hence, from the surface, a nonuniform layer bonded to a rigid substrate would appear stiff if either its elastic modulus is high and/or its thickness is relatively small. These stiff parts of the layer (high E or small t) would tend to develop higher stresses and thereby carry more loads than the softer regions. This concept is illustrated in Fig. 16A. This figure shows graphic representations of stresses calculated from finite-element models used to study the effects of prosthetic femoral stem placement in the medullary canal. Clearly, the thin bony regions develop more stress than the thick regions. When the stem is more centrally placed, the layer thickness is more uniform (Fig. 16B), and thus, no stress concentrations are developed.

Stress transfer in composite structures is very much affected by the bonding characteris-

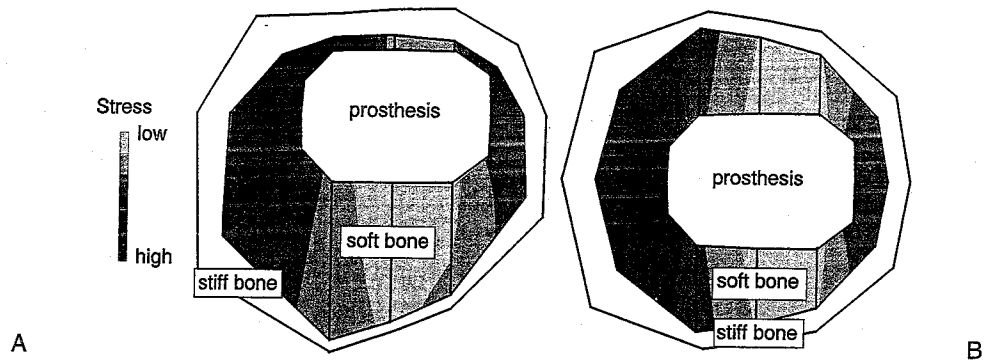

FIG. 16. The von Mises stress distributions in the trabecular bone at a cross section of a proximal femur with a noncemented bonded stem: **(A)** determined from a three-dimensional anatomic finite-element model and **(B)** determined in a three-dimensional symmetric finite-element model (235).

tics at the interface. The frictional and adhesive characteristics of the surfaces are important factors. The orientation of the interface relative to the dominant direction of loading is also important. So are surface microstructures and textures important. If the interface is smooth, unbonded, and lubricated, then no shear stress will be developed no matter how large the disparity in the lateral displacement. The difference between bonded (adhesive) and unbonded (lubricated) interfaces can be most simply seen for uniaxial loading (Fig. 17). For the unbonded or lubricated case (right), only compressive stress is developed in the material; the material is in a state of uniaxial compression. For the bonded or perfectly adhesive case (left), shear stresses are developed at the interface as well. The compressive stresses at the interface are sufficient to balance the external force. The shear stresses merely develop as a secondary effect, and they must balance themselves.

This is no longer true when the interface is not perpendicular to the applied force. Figure 18 depicts a cone-shaped object (implant) inserted into a tubular structure (bone) where the interface is bonded by cement or by some other mechanism. In this case, the applied force will create compressive and shear stresses along the interface. If the cone angle is relatively small, as is the case with most hip prostheses, the magnitude of the shear stress developed will be much greater than the compressive stress. This load transfer would occur predominantly by the shear stress, as shown in

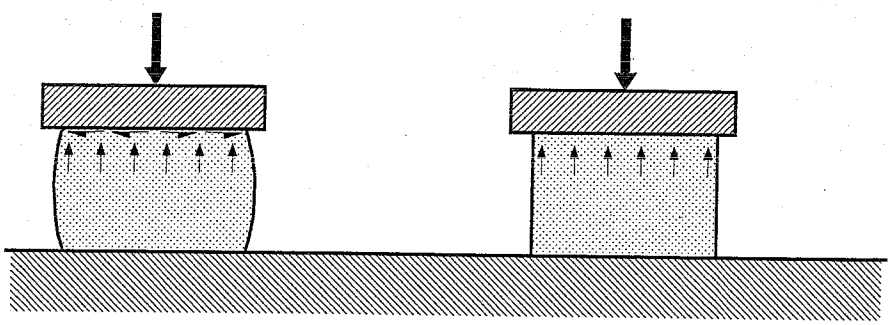

FIG. 17. Compression of a material by a force applied onto an adhesive interface will create both compression and shear at the interface **(left).** When the interface is unbonded and lubricated, it can slide without friction at the interface. In this case, only compressive stresses occur **(right).**

Fig. 18. When the interface is unbonded and lubricated (e.g., by body fluids at the bone surface), shear stress at the interface can no longer exist or is minimal. To develop a significant reaction force to equilibrate the applied load (Fig. 18), the cone-shaped prosthesis must subside into the tubular bone to create a significant compressive stress at the interface. Again because of the small cone angle, a very large compressive stress must be developed at the interface to generate a sufficient amount of force to equilibrate the applied load. In this process, a tensile hoop stress must be developed in the bone to prevent expansion.

The basic concepts discussed above are of importance for any composite implant structure. In the next two sections, the intramedullary stem fixation of the femoral component in THR and the acetabular cup fixation are considered in more detail.

Intramedullary Stem Fixation

The principles of load transfer in intramedullary fixation are based on load sharing, similar to the principles in Fig. 14. As a simplified model, we choose a metal rod (the stem) fixed in a tubular bone. The stem is loaded by an axial force (Fig. 19A) that must be transferred to the bone. Again, the load transfer between the stem and the bone is realized by shear stresses at the interfaces. In fact, a free-body diagram of the stem would indicate that these shear stresses must balance the external load; hence, the average shear stress times the surface area of the stem equals the axial force. But again, these shear stresses are not uniformly distributed; rather, stress concentrations occur on the distal and the proximal sides. This is illustrated in Fig. 19A, together with the load-sharing patterns in the stem and the bone.

When the stem is loaded in bending (Fig. 19B), a very similar load-transfer mechanism occurs. This time, however, the bending moment is to be transferred from the stem to the bone via interface stresses (tension, compression, and tangential shear) to effectuate this moment transfer. These stresses are again nonuniform and are concentrated mainly at the proximal and distal sides.

The graphs of Fig. 19 illustrate the most important basic principles of load transfer in intramedullary fixation of artificial joints (93,95,96):

1. The structure can be divided into three regions, a middle region where load sharing occurs and two load-transfer regions on the proximal and distal sides.

2. In the middle region, pure load sharing occurs, whereby the stem carries $\varepsilon_n \times 100\%$ of the axial force or $\varepsilon_t \times 100\%$ of the bending moment. Here, ε_n and ε_t are relative axial and flexural rigidities defined as:

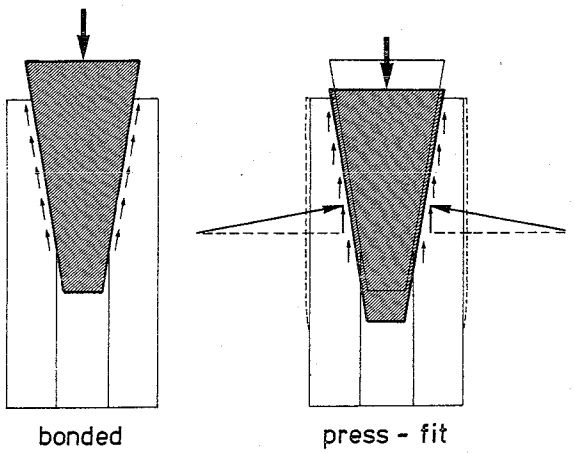

FIG. 18. Load transfer via a straight-tapered cone pushed into a cylindrical counterpart. **(Left)** The shear stress at the bonded interface can equilibrate the applied force. **(Right)** At a smooth, press-fitted interface, equilibrium relies on the vertical component of compressive interface stress. For slightly tapered cones, a significant amount of subsidence must occur in order for the compressive stress required for equilibrium to develop. (From Huiskes, ref. 99, with permission.)

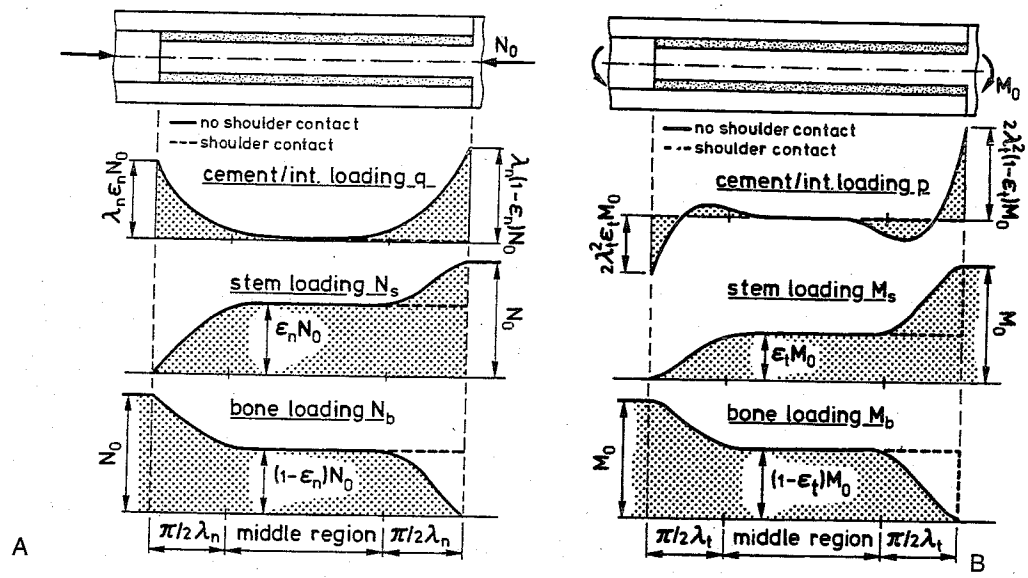

FIG. 19. The load-transfer characteristics in a simple model of a straight stem cemented in tubular bone with and without shoulder contact **(A)** Axial loading. **(B)** Bending. In both drawings, left is distal, right proximal. From top to bottom: **(A)** distributions of shear loading, and **(B)** the bending moment in the stem; and **(A)** the axial force, and **(B)** the bending moment in the bone. (From Huiskes, ref. 96, with permission.)

$$\varepsilon_n = A_s E_s/(A_s E_s + A_b E_b) \qquad (19)$$

$$\varepsilon_t = I_s E_s/(I_s E_s + I_b E_b) \qquad (20)$$

where E, A, and I are the elastic moduli, the cross-sectional areas, and the second moments of inertia of the stem (s) and the bone (b).

3. The load carried by the stem and the bone is normally carried by the bone alone; hence, the bone is stress-shielded by the stem. The higher ε_n and ε_t are, the higher is the percentage of load that is carried by the stem, and the more extensive the stress-shielding effect.

4. The higher the percentage of load carried by the stem in the middle region, the less is transferred proximally and the more distally, and vice versa. As can be seen in Fig. 19, the proximal load transfer is proportional to $(1 - \varepsilon_n)$ and $(1 - \varepsilon_t)$, and the distal load transfer to ε_n and ε_t, respectively. Hence, the stiffer the stem, the higher the distal interface stresses; the more flexible the stem, the higher the proximal interface stresses.

5. The length of the distal and proximal load-transfer regions and the peak interface loads on the distal and proximal sides depend on the parameters λ_n and λ_t, the fixation exponents for axial and transverse loading (93,95,96). These parameters depend not only on the axial and flexural rigidities of the stem and the bone but also, and most predominantly, on the elastic modulus and the thickness of an intermediate layer (e.g., acrylic cement or cancellous bone). A stiff intermediate layer (i.e., high modulus and/or thin layer) reduces the length of the load-transfer regions and thus increases the gradients in the interface loads.

6. The peak interface stresses do not necessarily reduce when the stem is made longer. Here again, the notion "stress is load per available area" is misleading. When the stem is made longer, the load-transfer regions merely shift further apart, and nothing else changes. It is only when the stem is made short (less than π/λ_n or π/λ_t) (Fig. 19), which makes the middle region disappear, that a fur-

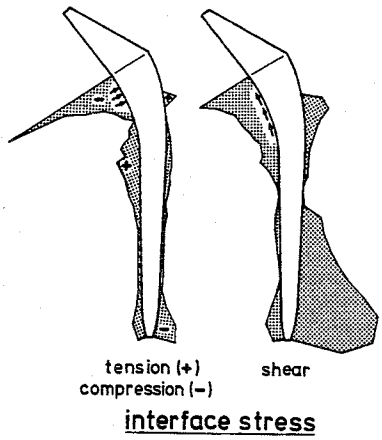

FIG. 20. Distribution of tensile, compressive, and shear stresses at a stem–cement interface for a loaded cemented THA stem from a two-dimensional finite-element model. **(Left)** Stress normal to the interface (tension–compression). **(Right)** Shear stress. (From Huiskes, ref. 99, with permission.)

ther reduction in length starts to affect the interface stresses.

7. If a collar on the proximal stem is bonded to the proximal bone (Fig. 19), the proximal load-transfer region is bypassed. Hence, conceptually, no load is transferred on the proximal side over the interfaces.

The above considerations are basic principles derived from a simplified, generalized model (93) and in fact are very helpful as baseline information for prosthetic design. In reality, of course, the load-transfer mechanism and the stress patterns are much more complex. Loads do not occur as isolated axial compression or bending, stems are usually not straight, interfaces are not always rigidly bonded, and bone has more complex properties and shapes than in this model. However, awareness of these basic phenomena facilitates the interpretation of more realistic, and complicated, analyses. If we formulate the conceptual analytic model of Fig. 19 in an FE model, we see the basic principles reflected in the results (93). We can recognize the proximal and distal load-transfer regions in the interface shear stresses and in the bone-bending stresses. The middle region of load sharing is obvious as well. Such an analysis also confirms that the ratios of proximal to distal interface stress transfer and of middle region load sharing both change when a more flexible stem material (metal versus isoelastic) is used.

In the case of a more realistically tapered stem in an "anatomic" bone model, these basic principles are less obvious, but still recognizable, as illustrated in Figs. 20 (99) and 21 (240). The interface stress patterns in the two-dimensional (Fig. 20) and three-dimensional FE models (Fig. 21) clearly demonstrate the proximal and distal stress-concentration regions. The ratio between proximal and distal stresses in these "anatomic" cases is regulated not just by the stiffness of the stem but also by the prominence of the taper shape. The stronger the distal taper of the stem, the more the distal stresses are reduced (93). Hence, although the principles of the load-transfer mechanism remain intact, the actual stress patterns are affected by stem design (112).

The rigidity of the stem is an important design parameter, as it affects both the bone stresses (which may provoke bone resorption) and the interface stresses (which may provoke interface loosening). Using the same stem design, we obtain less abnormal bone

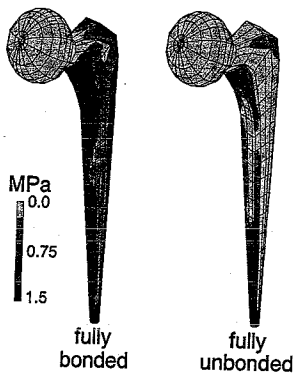

FIG. 21. Shear stresses at the stem–cement interface generated by stems that are either fully bonded **(left)** or unbonded **(right)** to the cement mantle, calculated with a CT-based three-dimensional finite-element model. (From Verdonschot and Huiskes, ref. 241, with permission.)

stresses but higher proximal interface stresses when a flexible (isoelastic) material is used instead of a metal. We see that confirmed in a three-dimensional FE study (116). In view of the potential problems of bone resorption and interface loosening, this principle presents incompatible design goals for which a compromise must be sought. Noncemented stems tend to be medullary-canal filling and much thicker, hence stiffer, than cemented ones. This means that stress shielding is more of a problem in noncemented THR, whereas proximal cement and interface stresses are more of a concern in the cemented ones.

Many designers do not realize, however, that the governing parameter for the load-sharing ratio between stem and bone is not the stem rigidity but the ratio between stem rigidity and bone rigidity (13,93,105). The basis for this relationship was shown in equations 19 and 20. It was found both clinically and analytically that long-term adaptive bone resorption around hip stems, as a result of stress shielding, is highly sensitive for initial bone rigidity (55,101,104,116). These results suggest that, in the above relationship, the bone stiffness plays a more important role in load transfer than the stem stiffness because the former is more highly variable than the latter in a patient population. Hence, bone stiffness, as dependent on density and thickness, is a significant "design" parameter.

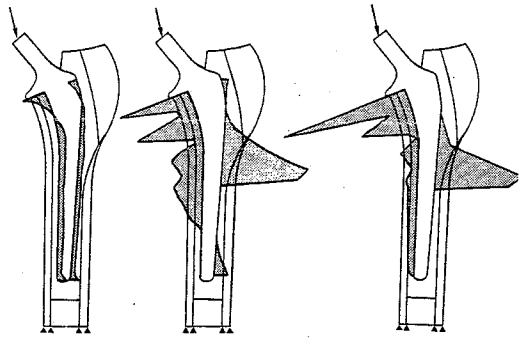

FIG. 23. Normal stresses in the cement at the stem–cement interface assuming bonded interface conditions **(left),** frictionless unbonded conditions **(middle),** and frictionless unbonded conditions with fibrous-tissue interposition **(right)** at the cement–bone interface. (Adapted from Weinans et al., ref. 248.)

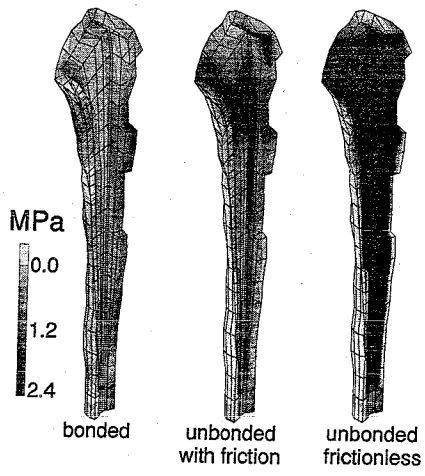

FIG. 22. Tensile stress distribution in the cement mantle assuming bonded or unbonded (frictionless and frictional) stem–cement interface conditions. Only the anterior half of the cement mantle is shown. (Adapted from Verdonschot and Huiskes, ref. 240.)

Another set of parameters that play an important role for the load-transfer mechanism are the mechanical characteristics of bonds between the different materials. Above (Fig. 18), we have seen that an unbonded, conically shaped stem has a different load-transfer mechanism than a bonded one. An unbonded, frictionless cone pushed in a tube must subside to create enough compressive interface stress for equilibrium, which also produces excessive tensile hoop stress in the tube. Cemented stems in THR tend to become debonded from the cement early postoperatively (127). Figure 22 illustrates the effects of debonding on cement stresses, as determined in a three-dimensional FE analysis. We see dramatic increases in cement stresses from a bonded (Fig. 22, left) to a debonded, frictionless configuration (Fig. 22, right). If we do assume friction to occur (Fig. 22, middle), the cement stresses are still higher than those in the bonded case, but not that much higher. Evidently, the bonding and friction conditions are

very important for the cement stresses and the probability of cement failure (73,160,240).

Another effect of similar consequences is that of cement–bone interface loosening, resorption, and fibrous-tissue interposition. Figure 23 shows an example of that, as determined in a two-dimensional FE model, applying nonlinear interface conditions to model the effects of loosening and a nonlinear constitutive description of a 1-mm-thick fibrous tissue membrane (248). As evident from Fig. 23, the load-transfer mechanism (as represented by stem–cement interface normal stresses) changes drastically from a bonded to a (frictionless) debonded cement–bone interface and then again somewhat from a debonded interface to one with the fibrous membrane interposed. The most drastic effect, however, is caused by debonding.

The stem–bone bonding conditions also play important roles in the load-transfer mechanism of noncemented THR, particularly concerning interface stresses and relative motions (17,67,136). These conditions depend largely on the precision of fit of the stem and on the extent and location of ingrowth coatings. Where debonding from the bone and friction are concerned, similar relationships occur in the load-transfer mechanism as for stem debonding from cement (160,240). An important difference is, of course, that cemented stems are bonded best in the beginning, whereas noncemented ones become bonded only later on. During the ingrowth period, stem design and interface-stress transfer play important roles for the ingrowth process (105). For noncoated, press-fitted stems, the interface coefficient of friction is very important for the eventual fixation characteristics, as these stems tend to sink in the bone and find fixation later. In this process, proximal load transfer may shift to distal, with stress shielding and bone resorption as a result (229).

Usually, a noncemented stem is not fully coated for bone ingrowth, but only proximally. The reason for that is twofold. First, this is thought to promote proximal stress transfer rather than distal stress transfer, so stress shielding and adaptive bone resorption would be reduced. This can be confirmed in FE analyses, but the effect is not as pronounced as sometimes expected when the distal stem is still in (compressive stress-transferring) contact with the bone (119,253). Second, it facilitates a possible revision operation. Full coatings are sometimes preferred because they are thought to enhance the extent of ingrowth, thereby reducing the probability of interface debonding. This thought is partly based on the idea that interface stresses reduce when the contact area is increased. As we have seen above, however, one must be very careful with the notion that stress is force per unit area. If we compare the interface stresses for the same prosthesis in the same bone, coated fully, proximally and with 5 proximal bands, we find that the differences in maximal values are very small (119; Fig. 24). The reason, again, is that all parts of the interfaces do not participate equally in stress transfer. So ingrowth at mechanically strategic locations is more important than the total area it occupies.

Acetabular Cup Fixation

The acetabulum is structurally more complex than the femur and does not easily lend itself to reduction to a simpler geometry, which would make it accessible for conceptual analytic studies, in the same way as composite beam theory provided the basis for the femoral reconstruction. In addition, in comparison to the femoral reconstruction, far fewer stress analyses have been conducted. Some strain gauge experiments to study the effects of cup fixation on acetabular surface stress transfer have been reported (40,60,124, 152,184,196). Finite-element analyses of the acetabular reconstruction were conducted, using two-dimensional (21,192,233), axisymmetric (98,179), or three-dimensional models (42,149,194). In addition, the stresses in the polyethylene (PE) liner were analyzed, particularly with regard to friction, wear, and PE failure prospects (10). Some generic information is discussed here, mostly as it resulted

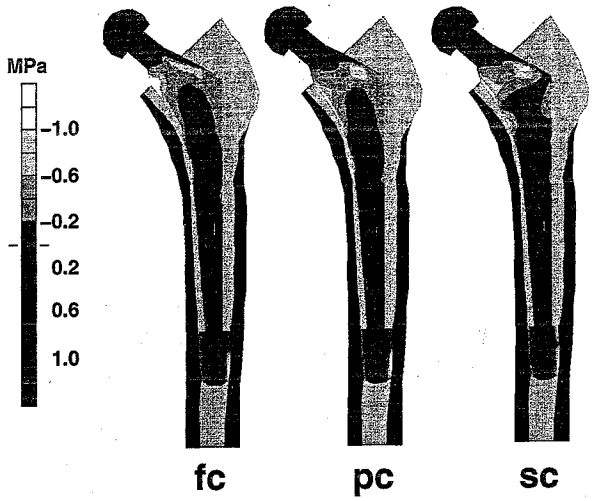

FIG. 24. Normal stress distributions at the implant–bone interface for different coating configurations, shown as shades on the stem surface. High tensile stresses (positive) are white, and high compressive stresses black; zero stress is a medium gray shade. (fc, fully coated; pc, proximally coated; sc, proximally stripe coated). (Adapted from Huiskes, and Van Rietbergen, ref. 119).

from our own three-dimensional FE model (39,41–43).

The hip-joint force is introduced by the contact between femoral head and PE liner and varies greatly in magnitude and orientation during gait. The stresses in the pelvis reach a maximum at the beginning of the single-leg stance phase (41). The distribution of the stresses over the articulating surface of the PE liner depends on its stiffness characteristics, which are determined by the PE thickness and whether or not a metal backing is present (10,43). A thicker PE liner distributes stress better and reduces the peak value. This mechanism is similar to what was discussed relative to Fig. 15. At the time of heel strike, when the force is maximal, the superior-anterior rim is the high-stress location. From the liner the stress is then distributed to the bone, through the cement (if a cemented cup is used) and the metal backing (if present). The stress-transfer mechanism here again depends mostly on the rigidity of the structure. Metal backing, providing a higher stiffness, tends to distribute stress better over the cement and the subchondral bone. This was originally thought to be its

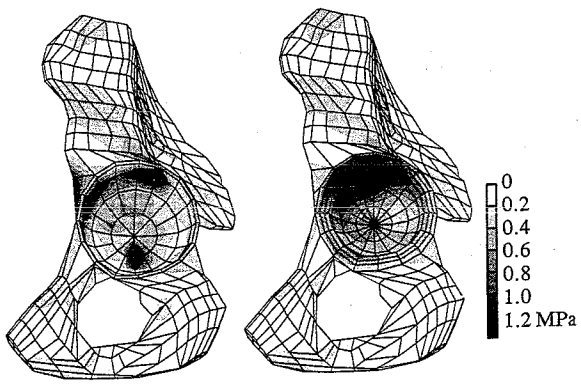

FIG. 25. Distributions of the Von Mises stresses in the trabecular bone of a normal bone **(left)** and a pelvic bone with a cemented non-backed cup **(right).** (Reproduced from Dalstra and Huiskes, ref. 43.)

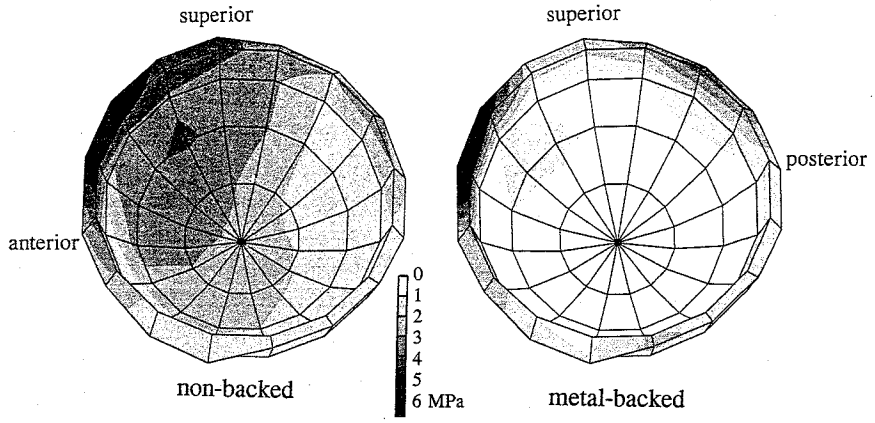

FIG. 26. Von Mises stresses in the cement mantle for a nonbacked polyethylene cup **(left)** and a metal-backed cup **(right).** (From Dalstra, ref. 39, with permission.)

greatest mechanical advantage (35). However, three-dimensional FE analysis has shown that it does provide cement and interface stress concentrations at the rim of the fixation (Fig. 26). As an effect, the maximal cement and bone interface stress peaks of the metal-backed cup surpass those of a nonbacked one, providing higher failure probabilities. This is a result of the fact that the bone rim and the metal backing are both stiff relative to their environments in the structure.

The stress transfer to the subchondral trabecular bone differs between an intact and the reconstructed case (Fig. 25). Whereas in the intact acetabulum the stresses are well distributed, in the reconstructed case they are concentrated in the anterior-superior region (39). It is also clear that stress shielding in the acetabular bone does occur, particularly in the dome region. This region is also the one where bone resorption is often seen (185), which is usually attributed to a loosening process. The stress patterns, however, do suggest that it might be a result of mechanical disuse, similar to what occurs in the femur. Further away from the cup in the cortical shells, there is very little difference between the stress patterns of the intact and reconstructed cases. The consequence of this is that little information about the local stresses in and around the implant can be obtained from experiments involving strain gauges on the external bone surfaces. The strains here are simply not very sensitive to the design and fixation characteristics of the cup.

DESIGN ASSESSMENT AND DEVELOPMENT

In the first section of this chapter, we discussed the performance and endurance of THR and summarized what is known about failure mechanisms. It was argued that biomechanics is important in all activities of the innovation cycle. This is particularly so for design and design assessment of new prostheses, in which the engineering task is substantial (102,103). In order to rationalize the design process, five questions must always be addressed: (a) What clinical problem creates a traditional design? (b) How does this problem relate to the design characteristics? (c) What innovative feature would improve the design? (d) Does this feature indeed solve the clinical problem? (e) Will this innovative design cause another clinical problem, worse than the original one? To answer these questions is not an easy task, first because patient factors (both biological and functional ones) and surgical factors (technical feasibilities and skills) can hold many surprises in waiting. Second, al-

though a clinical problem may be well documented, its cause in terms of precise failure mechanisms often remains obscure. Third, engineering design goals in THR tend to be incompatible; i.e., what prevents one failure mechanism often promotes another (102,103). In this section a few biomechanical methods are discussed that are useful to analyze these questions and problems.

Failure Scenarios and Design Assessment

It is essential that new designs for THR be preclinically tested before they are applied in patients and clinically tested before they reach the market. This seems trivial, but in the orthopaedic trial-and-error culture, this is not always evident (102,156). It is also not easily realized because of two principal problems. First, the endurance of a THR design can only be established in fact in long-term clinical trials with large patient series, using sophisticated actuarial methods (79,155). Conventional methods of THR performance assessment, such as radiography and patient interviews, are notoriously imprecise and subjective. However, new clinical methods have been developed in the recent past that enable more precise assessment of THR performance within a reasonable time period. The most powerful of these is roentgen stereophotogrammetric analysis (RSA) (212), which allows precise evaluations of three-dimensional relative displacements of the implant relative to the bone in the course of time.

It is known that the extent of these motions is correlated with endurance of the THR. With RSA, these migrations can be detected in an early stage. This method is discussed separately below. A less sensitive method with the same purpose, but more easily conducted, is digital radiography (63,123,157,247). Digitizing radiographs makes them accessible for computer-graphics evaluations, which improves the precision and the objectivity of radiographic measurements. Another radiographic method with high precision is dual-energy X-ray absorptiometry (DEXA), useful to determine the development of bone density in the course of time (13,28,56,189). Whether a particular prosthetic design provokes excessive bone resorption can be checked early postoperatively with this method. It is also useful in laboratory studies with postmortem bones (56). A fourth clinical evaluation method sensitive to THR performance in an early stage is gait analysis (81,174,183).

The second problem in design confirmation of innovative THR components is the difficulty of defining valid preclinical tests. In order to preclinically check a prosthetic design in a laboratory or computer-simulation test, one has to know what to test for. Because failure mechanisms are not always well understood, the design of valid testing methods is not trivial. In order to facilitate that, we propose the application of failure scenarios to which testing methods can be tailored (102). A failure scenario is a paradigm of a failure mechanism. It is a course of events that does or does not occur but is always latent. Preclinical tests can be designed to establish how sensitive a THR prosthesis is for a particular failure scenario.

In an example of a definite failure scenario for cemented THR stems, it is proposed that, as a result of the weakness of the metal–cement bond, debonding is likely to occur early postoperatively. This promotes, on the one hand, stem subsidence in cement, cement stress increase, and crack formation (compare discussion in relation to Fig. 22). On the other hand, the debonded stem will rub against the cement and produce wear particles. Both mechanisms in this scenario are likely to cause cement–bone interface resorption and clinical failure of the reconstruction. Questions to be answered relative to this scenario, for the assessment of a new prothesis, are: Will the stem easily debond? If debonded, to what extent does it increase cement stresses and the probability of failure? If debonded, what metal–cement relative motions does it produce, and will these promote excessive production of wear particles? As described later below, laboratory and computer-simulation methods are now available to analyze these questions for preclinically testing new designs.

The above specified failure scenario is a mixture of two generic scenarios for long-term aseptic (noninfected) loosening, out of a total of six proposed (102). The first of these is the *accumulated-damage* scenario. This is based on gradual accumulation of mechanical damage in materials and interfaces from repetitive dynamic loading. The damaging process eventually proliferates to disruption of the implant from the bone, interface micromotion, bone resorption and fibrous interposition, and finally, gross loosening. As a generic scenario, it is certainly relevant not only for cemented stems, as in the above example, but also for cemented acetabular cups and for noncemented components of both sides (e.g., it may lead to disruption of prosthetic coatings). The fact that cemented stems are more sensitive than other types of components for this scenario is not the issue here. The whole point of failure scenarios is how easily they could be provoked by a new design.

The second, also involved in the above example, is the *particulate-reaction* scenario. Wear particles from articulating surfaces, debonded interfaces, or modular-component connections can migrate into the cement–bone (cemented) or implant–bone (noncemented) interfaces. These small particles activate microphages at the interface into inflammatory responses of local bone resorption (lysis), thereby gradually debonding cement and bone (5,47,207). Eventually, this process produces relative interface motions and proliferates to gross loosening in much the same way as the final stage of the accumulated-damage scenario described above. This means that one can usually not discriminate between these two scenarios by studying radiograms or retrieved specimens, because the eventual results are the same. The elements of the particulate-reaction scenario include, besides wear-particle production, particle transport and biological bone reactions. Although the latter is a patient rather than an implant design factor, the characteristics of wear particles in terms of material, size, and shape are certainly relevant for this scenario (159,213). This could be tested preclinically. The same is true for the potential of a design, and its inherent fixation method, to produce excessive wear particles and provoke transportation to the implant–bone interface.

The next, valid for noncemented components only, is the *failed-bonding* scenario. This implies that ingrowth or osseus integration does not occur because of gaps and relative motions at the implant–bone interface (54,205,216). The biological bonding or ingrowth processes require a certain quiescence at the interface to succeed. If relative motions occur beyond some 150 μm (186), ingrowth will be prevented, and motions will be enhanced, provoking bone resorption, fibrous-tissue formation, and eventually, loosening. The elements of this scenario are initial fit, osseus induction (the capacity of a coating material to induce bony adhesion and fill gaps), initial relative interface motions, and interface motion-induced bone resorption. Methods to test for the latter biomechanical interface phenomena are discussed below. Where fit is concerned, preclinical tests can be performed in series of postmortem bones (171,172,206). This seems rather trivial, but tests like this are hardly ever reported.

The *stress-shielding* scenario particularly involves the bone around the femoral stem. Because the bone is stress-shielded by the stem, the bone stresses are subnormal (see Fig. 19). In accordance with Wolff's law (198,258), resorption develops. Although this does not automatically lead to prosthetic loosening, it may enhance bone or stem fracture and complicate a possible revision operation. The potential of a particular stem design to provoke excessive bone resorption can now be preclinically tested with computer-simulation methods with good accuracy, as discussed below.

A fifth model is the *stress-bypass* scenario. This is similar to the stress-shielding scenario but develops through another route, when proximal load transfer in the noncemented femoral THR is bypassed in favor of distal load transfer. As a result, the proximal bone is again understressed. Its cause can be inadequate proximal fit, either initially as an effect of inadequate fit or bone preparation, or gradually

postoperatively as an effect of stem subsidence (229).

The final one proposed until now is the *destructive-wear* scenario, which implies that articulating surfaces or modular–component connections (e.g., cone connections between metal head and stem of the femoral component, or connections between PE liner and metal backing in the acetabulum) simply wear out, to the extent that mechanical integrity can no longer be maintained (203). The sensitivity of a design for this scenario can be preclinically tested in hip simulators (162,203).

It must be noted that whether or not an innovative design will be successful can not be determined preclinically with certainty. This also depends on patient and surgical factors independent of design. In addition, new materials or shapes may introduce failure mechanisms hitherto unknown. In this respect, the scenarios discussed above may not be complete or sufficiently detailed. Further research will have to provide more certainty. In any case, preclinical testing can only provide a first sieve for unsafe devices.

Roentgen Stereophotogrammetric Analysis

Roentgen stereophotogrammetric analysis (RSA) was developed by the late Dr. Goran Selvik (212). The method is based on the principle that three-dimensional coordinates can be reconstructed from two radiographic images (Fig. 27A). To be able to determine the three-dimensional position of a point in space, the space has to be defined in the so-called laboratory coordinate system. When the positions of the two X-ray foci and the radiographic plates are known, the position of an object point can be reconstructed by calculating the intersection of the X-ray beams. The laboratory coordinate system is determined by a calibration cage. To this cage, markers made out of a high-density material (tantalum) have been attached, and their relative positions are accurately measured. Within the calibration cage, two planes with markers can be distinguished. The plane closer to the foci contains the "control markers" and is called the "control plane." The plane closer to the radiographic films contains the "fiducial markers" and is called the "fiducial plane." The fiducial markers are used to define the laboratory coordinate system, whereas the control points are used to calculate the positions of the two foci.

If we want to determine the three-dimensional coordinates of an object point somewhere in the calibration cage, we obtain two images. Both images have a two-dimensional local coordinate system (x',y'). The relationship between the global coordinates (x,y) of the fiducial markers and those on the images (x',y') can be determined using the Hallert transformation (212):

$$x = \frac{a_1 \cdot x' + b_1 \cdot y' + d_1}{a_4 \cdot x' + b_4 \cdot y' + 1} \quad \text{and}$$

$$y = \frac{a_2 \cdot x' + b_2 \cdot y' + d_2}{a_4 \cdot x' + b_4 \cdot y' + 1} \qquad (21)$$

These relations have four unknown variables (a_1, b_1, d_1, a_2, b_2, d_2, a_4, b_4), which depend on the position and orientation of the fiducial plane relative to the radiographic films and on the positions of the two foci. If four fiducial markers of the calibration cage are projected on both X-ray films, the eight measuring points can be used to solve the eight unknown variables in equation 21. After this procedure, the (imaginary) projection of an object point in the fiducial plane can be calculated. Subsequently, the positions of the foci can now be reconstructed by using the control coordinates of the calibration cage and the calculated projections of these points in the fiducial plane. After this procedure, the three-dimensional position of any point in space, provided that it is projected on both radiographic films, can be reconstructed by calculation of the intersection of the two lines between the foci and the projection of the object point on the (x,y) fiducial plane. Once the coordinates of the foci are determined and remain steady with respect to the fiducial plane, the control plane becomes redundant for the duration of a measurement session. For that reason, a "reference plate" with markers is

commonly added to the configuration, to represent the fiducial plane after calibration (212). This implies that the calibration cage can be removed, and the object no longer needs to be positioned within its constraints. Because of measuring errors, the two lines do not usually intersect mathematically, which leads to inaccuracies in the results. The accuracy can be improved by using a redundant system of fiducial and control markers (for example, nine of each). A computer program (X-RAY; 212) is used to determine the most probable intersection point by mathematical optimization. In addition, the program provides information about the accuracy of the measurements, based on the standard deviations of the redundant system. With this technique, the three-dimensional coordinates of an object point can be reconstructed with an accuracy of about 25 μm (212).

Usually, one is interested in the position of a rigid body (prosthesis) relative to another one (bone), and how this changes in time. The position of each of these rigid bodies can be determined from at least three marked points in the bodies. When two or more pairs of radiographs in a particular time sequence are available, the migration of one rigid body rel-

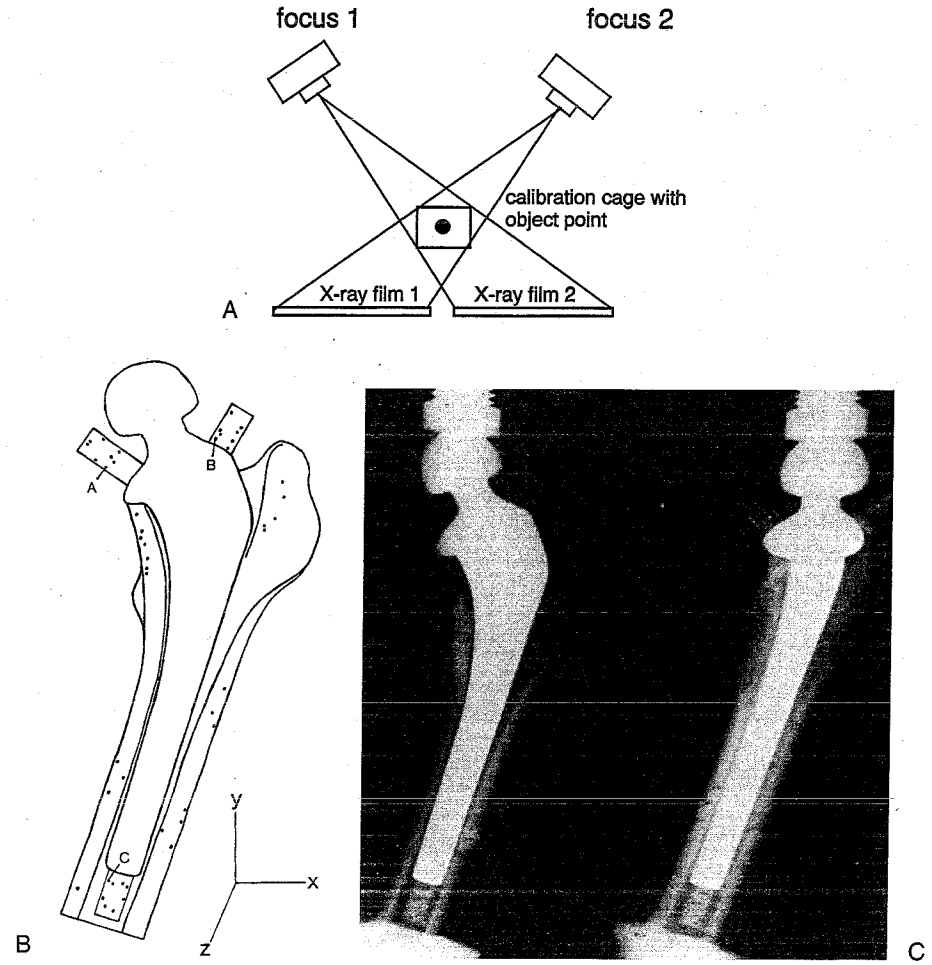

FIG. 27. For the RSA analysis, the bone and stem with attached acrylic posts are provided with tantalum pellets. **(A)** The projections of the calibration cage markers and object point on two radiographic films. **(B)** Schematic. **(C)** Double X-rays.

ative to the other over time can be determined in terms of three rotations and three translations (212). To minimize errors, more than three markers should be used, particularly when it is expected that the bodies do not behave as ideally rigid. A computer program (KINEMA; 212) is used to determine the relative kinematics of the two rigid bodies. In addition to the information about the measuring errors produced by X-RAY, the computer program KINEMA provides information about the rigidity of the bodies. For this purpose, the program calculates the distances between the marker points in the rigid body. If the body is ideally rigid, these distances are constant in time. If this is not the case, the body does not behave as a rigid one, meaning that the body is very flexible or that one marker may have come loose.

An experimental setup to measure relative motion (migration) of a femoral component of a THR requires, apart from a testing machine, two X-ray tubes, specially prepared X-ray cassettes with optimally flat films, tantalum pellets to mark the bone and the prosthesis, and a calibration cage. Figure 27B shows the arrangements of the tantalum pellets in bone, cement, and prosthesis. In order to minimize measurement errors, the scattering of the pellets should be optimal. The scattering can be quantified using a condition number as defined by Söderqvist and Wedin (217). It is possible to use clear markings on the prosthetic components for the RSA measurements, such as the metal ring in the PE cup, the prosthetic tip, the center of the prosthetic head, or the collar of the prosthesis. In an experimental setup one could come close to the optimal scattering of the pellets. However, under *in vivo* conditions the surgeon has a limited region where the pellets can be inserted (only the proximal femur); some pellets may migrate as a result of bone remodeling; and the images of the pellets may not always be visible on the radiograph as they are obscured by the image of the metal implant. The latter problem can be minimized by standardizing the way in which the pellets are inserted and the radiographs are made. Figure 27C shows the radiographic pair of the specimen. First, all markers must be identified and numbered, and then digitized. The digitizer must have a high resolution (about 5 μm). The identification and digitization procedures are time consuming but can be automated.

The RSA system was originally developed as a method to accurately determine three-dimensional motion patterns between bone segments, such as in human joints. In addition to this application, the method has been used in studies concerning bone growth, the stability of joints, bone fractures and spinal segments, volume measurements, and fixation of prostheses (133). With respect to joint reconstructions, the method was applied to study permanent displacements (migration) and induced relative motions between prosthetic components and bone *in vivo* (135,167,201,215). These studies have shown that early excessive migration of components is correlated with early revision and that the RSA technique has appropriate sensitivity to detect these early micromotions (Fig. 28). Kärrholm et al. (135) could identify a migration threshold by 6 months, beyond which there was an increased risk of subsequent revision.

The advantage of RSA is that it can provide significant information about the quality of THR designs early postoperatively (6 to 24 months). The RSA technique is very precise and dependable, and it provides real three-dimensional relative motions between two segments, which are impossible to obtain with other techniques. On the negative side, the evaluation tends to be rather tedious and time consuming. In addition, the technique is suitable for quasistatic loading only, because radiographs must be made after each load increment. In the near future, dynamic RSA studies will be possible as the techniques for synchronization of the roentgen cameras are developed and high-speed film exchangers become available. Using this dynamic technique in addition to the quasistatic one will make the RSA technique even more effective as an *in vivo* tool

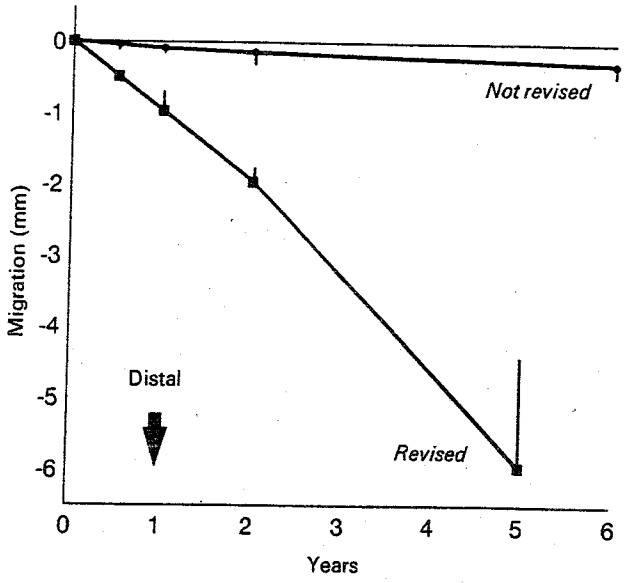

FIG. 28. *In vivo* proximal/distal migration (mm) of the center of the femoral head (mean and standard error) determined with RSA techniques in a series of 80 cemented THR reconstructions. The reconstructions that were revised within 6 years because of failure, and those that were not, could be discriminated significantly within 1 year postoperatively by using RSA. (From Kärrholm and Snorrason, ref. 135, with permission.)

to analyze failure processes in THR reconstructions.

Laboratory Bench Tests

Laboratory experiments to investigate or preclinicallly test the mechanical behavior of THR reconstructions can grossly be divided into two types. The first type aims at determining the relative motions of the components under (dynamic) loading (17,158,209–211,223, 224,246). As discussed earlier, the amount of micromotion between implant and bone is a critical factor in the fixation mechanism of cementless prostheses. These implants require minimal motions at the implant–bone interface to allow bony ingrowth into porous surfaces or bonding to hydroxylapatite coatings (186). High relative motions may also cause bone to resorb at the interface and create a fibrous-tissue membrane (114,181,251). Hence, it is important for noncemented stems to have adequate "initial stability," which can be tested in laboratory bench tests. Laboratory micromotion analyses can also be applied to cemented THR reconstruction (17,158,246). These analyses are meant to test whether micromotions between the stem and the cement mantle are produced when the structure is dynamically loaded. The detection of relative motions would indicate that the stems had debonded from the cement mantles, thereby giving rise to the accumulated-damage and particulate-reaction failure scenarios.

In a laboratory micromotion analysis, the structure is (dynamically) loaded, and the motions of the components are recorded. The (micro)motions can be measured experimentally, for instance, by providing the prosthesis with sensors that measure the displacements at one or more points of the prosthesis, relative to the bone (209,210,223,224,246). Sometimes only particular motion components are measured, for instance, subsidence in axial or rotation in torsional loading of femoral stems. A complete evaluation of prosthetic motions is not trivial. The rigid-body motion of a prosthetic component relative to the bone can be described by three translations of a chosen base point (e.g., superior–inferior subsidence, AP translation, and medial-lateral translation) and three rotations about mutually perpendicular axes (e.g., axial rotation, flexion, and varus–valgus rotation). In order to determine these six rigid-body motions, at least six relative displacements of three points must be determined (e.g., the x, y, and z displacement of one point, the x and y displacements of a sec-

ond point, and the z displacement of a third point). An additional complication is that some prosthetic components undergo nonnegligible deformations when loaded, for instance, the bending of a hip stem. Hence, the prosthesis does not always behave as a rigid body, which requires additional displacement sensors in particular regions far removed from the base point.

Figure 29A shows an example of an experimental setup (209) in which three rigid-body translations and one (axial) rigid-body rotation are measured in addition to four local relative interface motions at the proximal and distal ends of the hip stem. The load can be applied dynamically, and the sensors allow for continuous data sampling. When tests of this kind are conducted, the displacements must

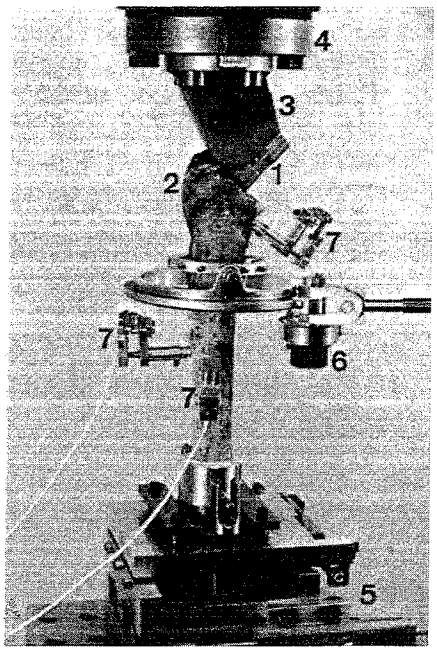

A

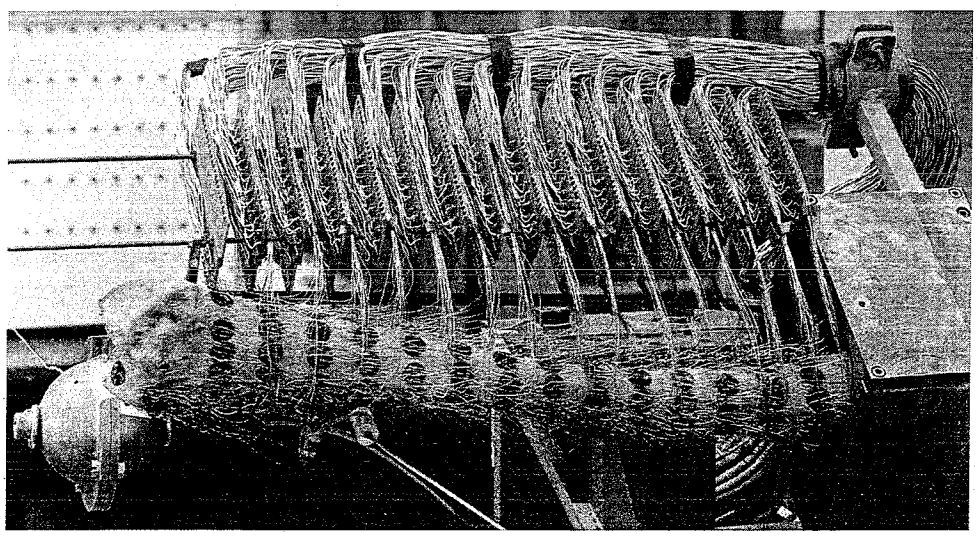

B

FIG. 29. (A) An experimental setup for direct measurements of motion of a prosthesis implanted in bone: (1) prosthesis, (2) bone specimen, (3) clamping flanges, (4) load cell, (5) an xy translation table that allows measurement of horizontal motion and transmits axial and torsional loads, (6) rotation transducer, and (7) interface transducers for measurement of local prosthetic motion. (From Schneider, ref. 209, with permission.) **(B)** Femur specimen with 100 strain-gauge rosettes for strain analysis on the periosteal bone. (Reprinted from ref. [106], with permission.)

be divided into permanent ones, representing a setting process or migration of the prosthesis, and recoverable ones, which are the true repetitive relative motions occurring under dynamic loading.

The loads in laboratory bench tests are usually simplified. Muscle forces are often absent (e.g., 209,246) or restricted to the representation of the abductor muscles only (e.g., 18,158). In the latter case, a strap is usually attached to the greater trochanter and connected to the loading rig. A problem may arise when different prosthetic designs are tested. Ideally, the positions where the loads are applied should be the same in all cases. However, because of the different prosthetic shapes and implantation procedures, the position of load application may vary considerably (e.g., as a consequence of different offsets). This can affect the local loading conditions considerably (a smaller offset results in reduction of the bending moment) and obscures the interpretation of the results obtained with the various designs.

Laboratory studies with series of cadaver femurs are hampered by the variety in geometric and mechanical properties of human femurs. To overcome this problem, synthetic composite femurs can be used. It has been shown that the mechanical properties of these femurs, such as their bending stiffness, are similar to those of bones (163). This indicates that the cortical bone is adequately represented. However, the inner side of the synthetic bone consists of a foamy substance, and there is no intramedullary canal. Hence, the interior of the bone is not adequately represented, and one should be aware of these weaknesses when selecting this type of bone for experiments.

The second type of laboratory bench tests are the ones that focus on stress analysis in the bone–implant composite (42,48,60,62,90,106, 129,150,173,197). These studies are usually applied on laboratory models, using bone specimens or bone substitutes. In all cases, deformations are actually measured and then either visually interpreted or used to calculate the stresses utilizing elasticity theory. The common methods used to measure deformations in biomechanics are strain-gauge analysis, holography, photoelastic analysis (with photoelastic models, coatings, or films), and thermography.

The most popular method is strain-gauge analysis whereby an electrical gauge is glued to a free surface of an object (38). The gauge contains one or more electrical filaments, which deform with the surface to which they are attached. A strain gauge works on the principle that a deformation of the filament is proportional to a change in its electrical resistance; thus, the strain of the material at the point where the gauge is applied can be measured by simply measuring the difference in electrical resistance. Because the filament is a lineal element, a strain gauge can measure strain in only one direction. To determine the complete strain state (two lineal strains and one shear strain) at a free surface, a strain-gauge rosette can be used. A rosette contains three filaments (usually oriented at 30° or 45° from each other) that measure three lineal strains at the point of application. These three lineal strains may be used to calculate the complete strain state as well as the principal strain values and principal directions. When the elastic properties of the object are known, the stresses can be calculated using the generalized Hooke's law.

In biomechanics, strain gauges have been applied mostly to assess deformation patterns at periosteal bone surfaces (48,60,62,106, 150,173). In an example of this procedure (Fig. 29B), 100 rosette strain gauges have been glued to the surface of the femur, and these gauges are used to assess strain patterns in the bone before and after prosthetic fixation. Strain gauges applied for this purpose have some limitations, however. First, the deformation patterns, and therefore stress patterns, at the outside bone surface are not very sensitive to the details of stress transfer far away within the structure at implant–bone interfaces. Further, from the surface measurements, no information exists about the stress state within the structure. Hence, this method lacks the required sensitivity for artificial-joint design. Second, strains are obtained in a particular region of finite dimensions. The number of spots to be sampled is limited by

space, instrumentation, and cost restrictions. Hence, to obtain a good representation of the stress patterns, one must either know *a priori* where the values of interest might occur or have a method of interpolating the data. For example, diaphyses of long bones, such as the femur, behave in accordance with beam theory (94,106); hence, this theory can be used to interpolate strain values measured from a limited number of locations. Strain gauges have also been applied on the surface of prosthetic components (124) and have even been enclosed in acrylic cement (33). In the latter case, strain within the material is measured. It is uncertain as yet, however, whether this method possesses sufficient accuracy (61).

Continuous strain patterns on the outside surface of bone specimens can be visualized by using photoelastic coatings (263). The deformations in the coating, which is thin and flexible, follow precisely those of the bone surface and can be visualized as optical fringe patterns when viewed under polarized light. Photoelastic coatings have the same limitations as strain gauges because information is obtained only about the outside surface of the bone. They have an additional disadvantage of being difficult to quantify accurately. However, they do give continuous strain patterns that provide easy qualitative interpretation. Methods with similar results, advantages, and limitations are holography and thermography. These methods also display continuous deformation patterns on the outside surface of structures. Holography has been used to provide very accurate measurements of deformation, whereas thermography usually provides rough qualitative pictures of the deformation field. These methods have been occasionally used in this area of biomechanics (140).

A method suitable for the assessment of strain patterns inside materials is three-dimensional photoelasticity (51). In this case, a laboratory model of the structure to be analyzed must be constructed from a birefringent plastic. When this model is loaded and viewed under polarized light, optical fringes develop representing the deformation patterns in the plastic material. In the three-dimensional model, the deformation patterns in the plastic material are "frozen in" by heating the model in the deformed state and physically slicing it when it has cooled off. An important limitation of three-dimensional photoelastic analysis is the requirement for building a physical model of the structure with correct properties of the components of the composite structure. This is often impossible because the birefringent plastics are available only in a relatively narrow range of elastic moduli. Thus, at present, this method is rarely used. In addition, the required information can be obtained more easily using FE analysis.

Computer-Simulation Analysis

Computer-simulation methods are useful for the purpose of research in THR, preclinical testing, and design. Particularly in the last decade, their applicabilities were improved tremendously through research and developments in computer hardware (117). As tools of research of failure processes, computer-simulation models are conceptually similar to others, such as laboratory models, *in vitro* culture models, animal models, and clinical models. In any investigation, one must consider closeness to reality of the model used versus experimental control. A patient is very real, but when one is used for investigative purposes as a clinical model, there is very little control over the experimental parameters. Conversely, a computer simulation provides virtually absolute experimental control but is remote from reality. Other models can be positioned between these two extremes. In using computer-simulation models one can investigate pure cause–effect relationships for well-defined sets of parameters. A single parameter can be varied to estimate its role in a particular process. Another advantage is that computer simulation is relatively cheap. For example, THR designs can be tested directly from the drawing board; no prototypes are required. These advantages can be exploited and weighted against the limitations of remoteness from reality.

Creep in Acrylic Cement

Creep of a material is defined as the time-dependent deformation of a material under constant loading conditions. Significant creep may occur in plastic materials such as acrylic cement and polyethylene. In this paragraph we show how cement creep can be simulated using FE techniques.

The constitutive theory used in a creep simulation is based on the same concepts as used in the flow theory of plasticity. It is assumed that the total strain is composed of an elastic and a creep strain. The next paragraph describes how the creep properties of bone cement can be implemented in an FE model.

The stress state in the cement mantle around femoral hip implants is typically three-dimensional. Hence, three principal stress components and the principal stress orientations determine the local stress state. Experimental creep data are based on uniaxial tests, which consider the presence of only one stress component (27,236,237). For this reason, the uniaxial creep laws can not be applied directly to structures with three-dimensional stress states. The solution for this problem is to define an equivalent stress, which relates the three-dimensional stress state to the uniaxial one and can be used in the creep laws. We selected the Von Mises stress as the equivalent stress, in accordance with what is usually used in creep simulations (80).

Another problem that obstructs the direct use of the creep laws is the fact that these were determined assuming stress conditions that were either purely static (27) or cyclic dynamic (236,237). Assuming bonded or frictionless unbonded stem–cement interface conditions, the stress state is purely dynamic, and the creep laws determined under cyclic dynamic stress conditions can be applied. However, when the stem–cement interface is assumed to be unbonded, and friction occurs, the stress state is neither purely static nor cyclic dynamic (Fig. 30). Because of frictional forces at the interface, the stresses are not completely released after unloading (240). Therefore, the local Von Mises stress level is divided into a static residual stress (σ_{res}) and a dynamic (cyclic) one (σ_{dyn}). Obviously, the Von Mises stress level at full loading (σ_{vm}) will be affected by the creep process and is a function of the number of loading cycles (N), according to

$$\sigma_{vm}(N) = \sigma_{dyn}(N) + \sigma_{res}(N) \qquad (22)$$

The ratio (R) of the Von Mises stress levels in the cement in the unloaded and loaded conditions can be determined before the actual creep simulation by loading and subsequently unloading the structure. Hence, the ratio (R) is assumed to remain constant during the whole creep process and is described by

$$R = \frac{\sigma_{vm}^{unloaded}}{\sigma_{vm}^{loaded}}, \qquad (23)$$

which produces

$$\sigma_{res}(N) = R\sigma_{vm}(N) \qquad (24)$$

and

$$\sigma_{dyn}(N) = (1 - R)\,\sigma_{vm}(N) \qquad (25)$$

For the case of the bonded stem–cement interface conditions, σ_{res} and R are zero.

Similar to the application of the Boltzmann principle, which can be used for linear viscoelastic materials (262), the total creep strain

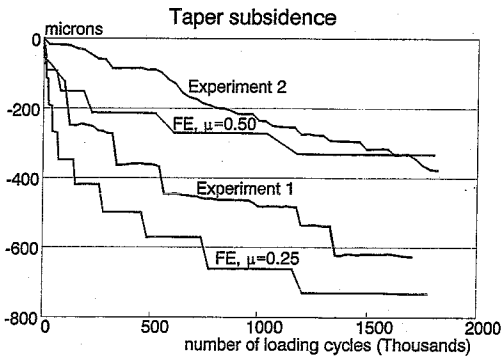

FIG. 30. Subsidence patterns of an unbonded taper within the cement mantle caused by cement creep, assuming friction coefficients (μ) of 0.25 and 0.5, shown together with experimental results. (From Verdonschot and Huiskes, ref. 239, with permission.)

can be expressed by superimposing the creep strains caused by the residual load and those by the dynamic loads, as

$$\epsilon^c(N,\sigma_{vm},R) = \epsilon^c_{dyn}(N,\sigma_{dyn}) + \epsilon^c_{res}(N,\sigma_{res}) \quad (26)$$

To determine the creep strain attributable to the residual stress component, the creep law determined by Chwirut (27),

$$\epsilon^c_{stat} = 1.798\ 10^{-6}\ N^{0.283}\sigma^{1.858}_{res} \quad (27)$$

was used, where N is the number of loading cycles, and σ_{res} the residual stress level (in megapascals). In this formula, the original time variable (27) must be transformed to the number of loading cycles for the frequency of 1 Hz we applied. To determine the creep strain caused by the dynamic stress amplitude, two creep laws are available. The first one describes the creep strain under dynamic tensile loading (236), whereas the second one was established for dynamic compressive loading conditions (237). The creep strains related to the dynamic stress amplitude can be calculated using one of these laws, depending on whether the local maximal principal stress (σ_{prmax}) was tensile or compressive. Hence,

$$\epsilon^c_{dyn} = 7.985\ 10^{-7}\ N^{0.4113}\ \sigma^{1.9063}_{dyn}\ N^{-0.116\log\sigma_{dyn}}, \quad if\ \sigma_{prmax} > 0, \quad (28a)$$

$$\epsilon^c_{dyn} = 1.225\ 10^{-5}\ N^{0.314}\ 10^{0.033\sigma_{dyn}}, \quad if\ \sigma_{prmax} < 0, \quad (28b)$$

where N is the number of loading cycles, and σ_{dyn} is the dynamic stress amplitude (in megapascals).

As the creep process develops, the stress levels in the structure change. Hence, an incremental procedure is required, for which incremental creep strains can be calculated, using an appropriate time step. The value of the time step is defined by the ratio of the creep strain increment permitted to the elastic strain. This ratio has a maximal value of 0.05 and ensures that the creep strain increments are small relative to the elastic strains; hence,

$$\Delta\varepsilon^c/\varepsilon^{el} < 0.05 \quad (29)$$

The creep-strain increment can then be used in the FE code to calculate the various three-dimensional creep-strain components ($\Delta\epsilon^c_{ij}$), using a flow rule that identifies how the Von Mises stress is affected by the various stress components:

$$\Delta\epsilon^c_{ij} = \Delta\epsilon^c \frac{\partial\sigma_{vm}}{\partial\sigma_{ij}} \quad (30)$$

From the creep-strain components and the stiffness matrix, a nodal force vector is calculated, which is subtracted from the force vector already present. Then a new FE iteration is performed with the modified force vector.

The first example to which the theory was applied is an axisymmetric structure consisting of a metal taper in a cement mantle (239). Figure 30 shows the subsidence of the taper within the cement mantle produced by the creep simulation and obtained with laboratory experiments. The subsidence pattern of the tapers was not continuous but had a stepwise appearance as a result of stick–slip mechanisms at the interface. Changing the coefficient of friction from 0.25 to 0.5 led to a significant reduction in subsidence.

When the method is applied to a three-dimensional FE model of a cemented femoral THR (242), it can be shown that creep of acrylic cement indeed has a stress-relaxing effect in the cement mantle, particularly at the exterior side (Fig. 31). At the interior side, however, cement stresses are not reduced significantly, resulting in maximal cement stresses that are virtually constant in time.

Accumulated Damage Analysis

The accumulated-damage failure scenario is one of the most prominent ones in cemented THR, particularly where the femoral component is concerned. As described above, this scenario involves the accumulation of mechanical damage in materials and interfaces caused by repetitive dynamic loading, eventually resulting in gross loosening. When the theory of continuum damage mechanics (CDM) is combined with FE techniques, the process of damage accumulation can be simulated (238,239). In this section, a method is described for ways the

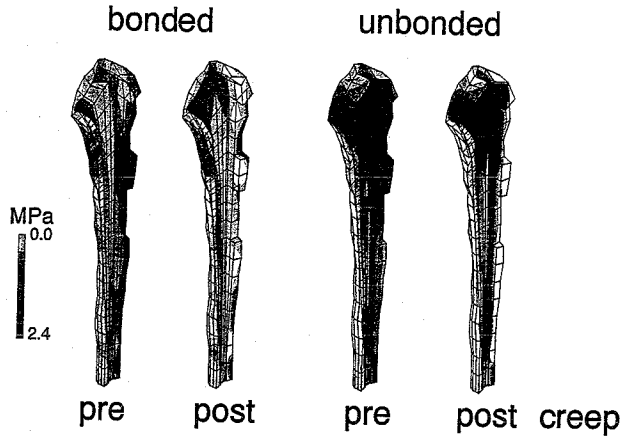

FIG. 31. Tensile stress distributions in the cement mantle (only the anterior part of the cement mantle is shown) before and after the simulation of cement creep, assuming either bonded or frictional unbonded stem–cement interface conditions. (From Verdonschot and Huiskes, ref. 242, with permission.)

theory of CDM can be implemented in FE simulations.

When a material is dynamically loaded, microcracks may be initiated. When this occurs, the material is damaged. The amount of damage accumulated in a material can be measured by a reduction in stiffness, strength, or residual lifetime (23,24). Assuming constant environmental conditions, the amount of damage depends on the applied load and the number of loading cycles. Consider, for the sake of simplicity, the one-dimensional case, where damage can be described with a scalar variable. When only the load level is varied during the damage process, the amount of damage (D) becomes a function of the number of cycles (n) and the load level (S):

$$D = F(n,S) = f(n/N) \qquad (31)$$

with the restrictions: $D = 0.0$ when $n = 0$, and $D = 1.0$ when $n = N$, where N is the number of cycles to failure for constant-amplitude loading in a fatigue bench test of the same material. In these tests, specimens are exposed to a dynamic load with a constant load level, and the number of cycles to failure is recorded. Repeating these tests with different load levels allows the relationship between load level (S) and the number of cycles to failure (N) to be determined. Results of fatigue tests are often presented as S–N curves.

The function $f(n/N)$ in equation 31, which is called the damage rule, defines the relationship between the amount of damage and the ratio of number of cycles of loading to number of cycles to failure. In the analyses, a linear cumulative damage rule is chosen, which is called the "Palmgren–Miner" rule (164). This damage rule, which itself is stress-independent, states that the damage is a linear function of the number of cycles of operations (n):

$$D = f(n/N) = n/N \qquad (32)$$

The rate of microcrack development in acrylic bone cement can be determined with fatigue experiments (44,143). These experiments provide a relationship between the stress amplitude σ and the number of cycles to failure N at that stress level, according to (44)

$$\log N = 4.68 - \log \sigma + 8.77 \qquad (33)$$

In reality, structures are often exposed to dynamic loads in which the load level varies in time. The damage sum accumulated during fatigue loading for a number of cycles of n_i at load levels S_i can be written as (122):

$$D = \sum_{i=1}^{m} \Delta D_i \qquad (34)$$

where ΔD_i represents the amount of damage accumulation during fatigue at load level S_i, and m is the number of load levels.

Because of the elastic relationship between stresses and strains, the amount of damage in an element can be coupled to the elastic prop-

erties (151). However, when the material is brittle, it can be assumed that the damage and the stiffness of the cement material are uncoupled. This means that the elastic properties of the cement are assumed constant until the damage is complete ($D = 1.0$). In the two- and three-dimensional cases, the damage (D) becomes a tensor. Because of cyclic loading in a particular direction, the material can be completely damaged in one direction, whereas it may be unaffected in another one. Perpendicular to the damage directions (the crack direction), the material loses its stiffness, resulting in anisotropic postdamage material behavior. In most FE codes, material anisotropy can be fed into the FE program. However, one may also use cracking options, which are available in some FE packages to simulate the postcracking material behavior. The stress patterns in the cement mantle change when the cement cracks locally. Hence, after creation of a cement crack, a new FE iteration is required to calculate the new stress distribution, resulting in an iterative FE simulation of the accumulation of damage in the cement mantle (Fig. 32).

Application of this method to an FE model of a cemented femoral THR reconstruction facilitates the analysis of parametric effects and the mechanisms involved during the damage accumulation process in THR reconstructions. An important mechanism is shown in Fig. 33. This figure shows that the accumulation of cement cracks does not result in an increase of cement stresses, as one might expect. On the contrary, tensile stresses are released after the material has cracked and lost its stiffness in the tensile hoop direction.

It should be realized that the method of accumulated damage as described in this paragraph has not been extensively validated as yet. Hence, this method can be used only to provide insight in the mechanisms involved in cement failure. It can determine the time-dependent effects of parametric variations only on a qualitative and relative basis.

Debonding and Micromotion

Loosening of THR components is often accompanied by disruption or noningrowth of interfaces. Finite-element studies have considered the interface debonding and micromotion processes (73,136,147,153,199,241,245,248).

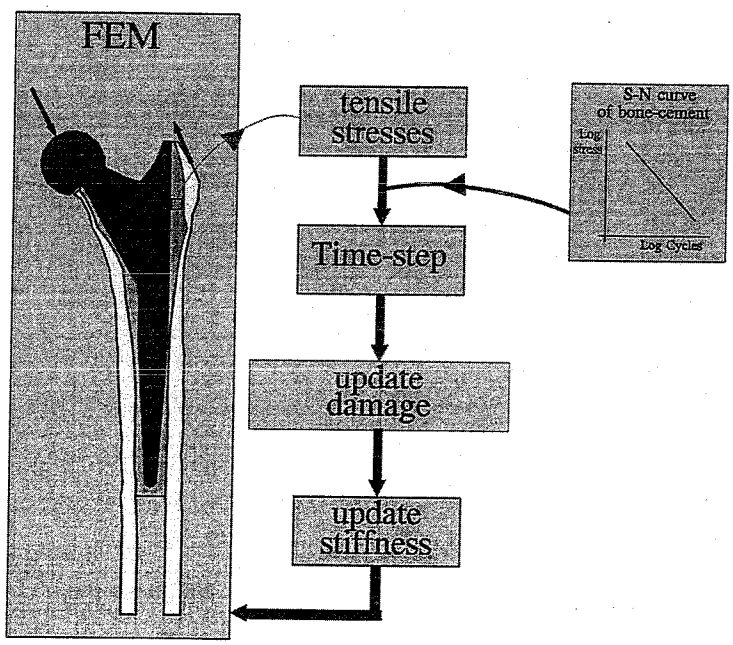

FIG. 32. Iteration scheme of the accumulative damage simulation in the cement mantle.

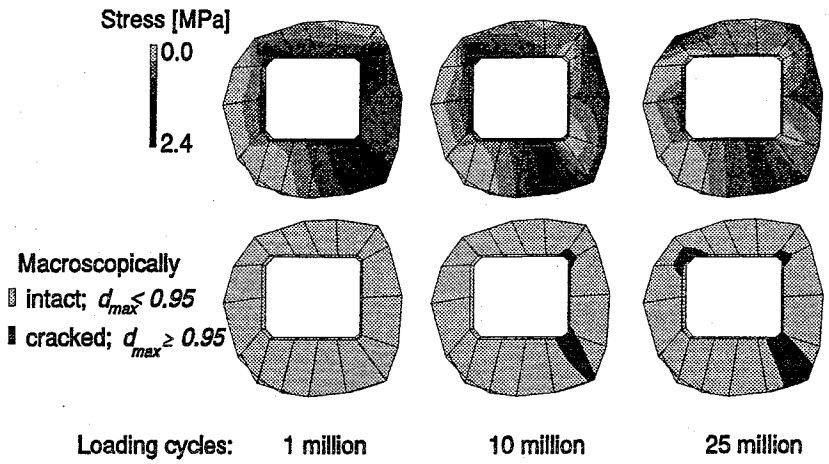

FIG. 33. The stress distribution **(top)** and crack distribution **(bottom)** in a transverse cross section of the cement mantle in the finite-element model at various times (from left to right) in the damage process. Stem–cement interface conditions were assumed as unbonded, with a friction coefficient of $\mu = 0.25$. (From Verdonschot and Huiskes, ref. 243, with permission.)

Clinically, debonding of the stem–cement interface does occur, if not immediately postoperatively, then most certainly after long-term dynamic loading (74,103,127). Debonding of the stem–cement interface is governed by the stresses relative to the fatigue strength of the stem–cement interfacial bond. There are, however, little data about the fatigue strength of the interface reported in the literature. This makes it impossible to simulate the debonding process in a realistic time frame. However, if we assume that debonding does occur, we can determine where debonding is most likely to be initiated and how it progresses. To determine where local debonding will occur, a multiaxial Hoffman's failure index (82) can be used. Hoffman used this index to determine material failure exposed to a multiaxial stress situation. The same procedure was successfully applied by Stone et al. (221) to establish failure of cancellous bone. Weinans et al. (251) incorporated this index in a finite-element model simulating the process of prosthesis–bone disruption. The failure index (*FI*) can be defined as

$$FI = \frac{1}{S_t S_c}\sigma^2 + \left(\frac{1}{S_t} - \frac{1}{S_c}\right)\sigma + \frac{1}{S_s^2}\tau^2 \quad \text{where bonded,} \qquad (35a)$$

and

$$FI = 0 \quad \text{where debonded} \qquad (35b)$$

where $S_t = 8$ MPa is the tensile strength of the metal–cement interface (137), $S_c = 70$ MPa is the compressive strength of the interface (the compressive strength of acrylic cement according to Saha and Pal [202]), $S_s = 6$ MPa is the shear strength of the interface (6,8,190, 222), and σ the normal and τ the shear stress at the interface. When *FI* has a value equal to 1.0, the stress situation at the interface equals that of the static interfacial strength. Hence, a value of *FI* beyond 1.0 indicates immediate failure. A lower value would indicate that no immediate static interface failure can be expected. For a particular value of the shear stress, *FI* is higher for tensile stresses than for compressive ones. Hence, a combination of shear and tension is assumed to be more harmful to the interfacial bond than shear in combination with compression. The debonding process requires an iterative FE simulation, starting with a completely bonded stem–cement interface. In every increment, the maximal *FI* is calculated, and the interface is debonded at that location. This change in local interface condition will affect the inter-

face stresses elsewhere in the structure and requires a new FE iteration to calculate these changes. This procedure is repeated until the whole interface is debonded.

When this method is applied to a three-dimensional FE model of a cemented femoral THR, the debonding process can be simulated (Fig. 34). In this model, debonding started in the distal and proximal regions. These regions expanded until the whole interface was debonded.

Stem–cement debonding not only elevates the cement stresses, thereby intensifying the accumulated-damage failure scenario as demonstrated previously, but it also allows the stem to move relative to the cement mantle. Depending on the roughness and the relative motions, this can lead to the production of metal and acrylic cement wear products, which promote the particulate-reaction failure scenario. Finite-element models can be used to determine the micromotions at the debonded interface (240). A result of this type of analysis is depicted in Fig. 35. The cyclic slip at the stem–cement interface is shown under dynamic loaded (stance-phase loading) and unloaded (swing-phase) conditions. It is clear that friction (and surface roughness) does affect these motions considerably. Assuming no friction at the interface, a cyclic slip at the interface is generated in the range of 200 μm (Fig. 35). After load release, the stem returns to its original position. In any consecutive load cycle, this behavior is repeated. When friction is assumed, the stem sticks to the cement mantle after the first loading cycle, which leads to a considerable reduction of the micromotions at the stem–cement interface (Fig. 35).

According to the failed-bonding scenario, large gaps and relative motions between the implant and the bone play a dominant role in the failure process of noncemented components (102). High cyclic micromotions can be generated because of the lack of mechanical stability and may prevent the bone from growing into the surface of the implant. Finite-element computer simulations have been utilized to analyze this problem (136,147,199,245,248). An example of such an analysis is shown in Fig. 36. The analysis is performed with a two-dimensional side-plated FE model using three different loading modes (147). The analysis shows that implant–bone motions are clearly affected by interface friction and material stiffness properties. If the stem is made of a material that has a similar stiffness to cortical bone (an "isoelastic" material), higher micromotions are produced as compared to the cases with a stiffer titanium implant. A limitation of these

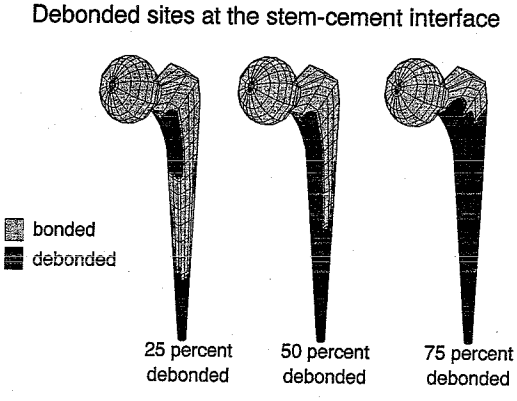

FIG. 34. Sites of stem–cement debonding at various stages in a debonding process during dynamic loading. (Adapted from Verdonschot and Huiskes, ref. 241.)

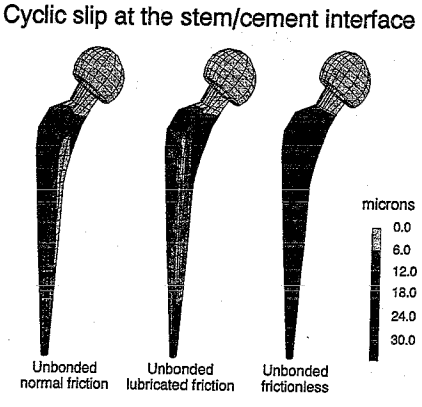

FIG. 35. Cyclic micromotion patterns between the stem and the cement, assuming friction coefficients of 0.25, 0.05, and 0.0 (from left to right). (From Verdonschot and Huiskes, ref. 240, with permission.)

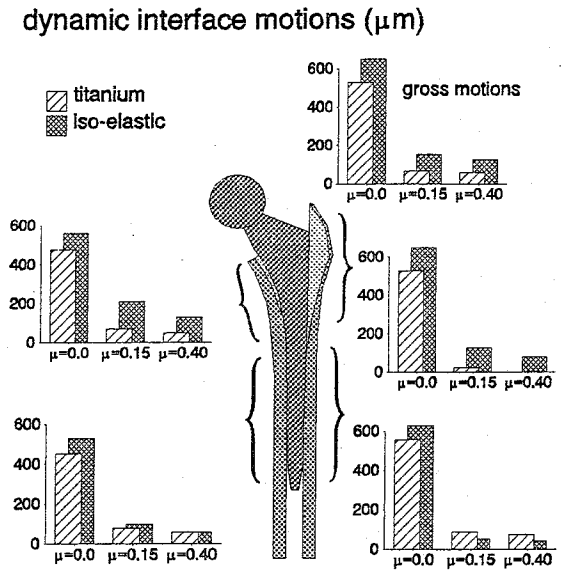

FIG. 36. Amplitudes of the cyclic movements along the implant–bone interface for two values of the prosthetic Young's modulus and three values of the coefficient of friction between bone and implant. (Adapted from Kuiper and Huiskes, ref. 147.)

FE micromotion studies is that they do not usually consider the mismatch of the shape of the implant and the bone cavity created by the surgeon. Hence, these studies only consider the stability of the implant assuming a perfect fit. Although this is a serious limitation, they can provide important information about the inherent stability of the implant, depending on shape, material properties, and interface characteristics, and thus provide the possibility of testing this at a preclinical stage, before patients are put at risk.

Motion-Induced Interface Resorption

Bone resorption and fibrous tissue formation between implants and bone are important determinants for clinical loosening. They can be the result of reactions to wear particles but can also be induced by relative motions between implant and bone (16,180,182,188,216). A conceptual scheme for such a process is shown in Fig. 37. Relative motions in a local interface region are the effects of external joint and muscle loads in combination with the structural and bonding characteristics of the THR reconstruction as a whole. It is assumed that if these local motions exceed 150 μm, bone ingrowth or osseus integration does not occur, and fibrous tissue starts to develop (186,216). The motion-induced interface resorption paradigm now implies that the repetitive deformations in that fibrous membrane are the driving forces for its growth (Fig. 37). Which mechanical signal derived from the tissue deformation would in fact stimulate the cells in the tissues, we do not know.

For a first conceptual analysis of this process, we assumed that the growth rate of the tissue membrane is proportional to the strain in the tissue; hence,

$$db/dt = c_{ij}\varepsilon_{ij} \qquad (36)$$

where $b(t)$ is the actual tissue thickness, and ε_{ij} is the strain tensor (Fig. 38). For the purpose of the computer simulation in conjunc-

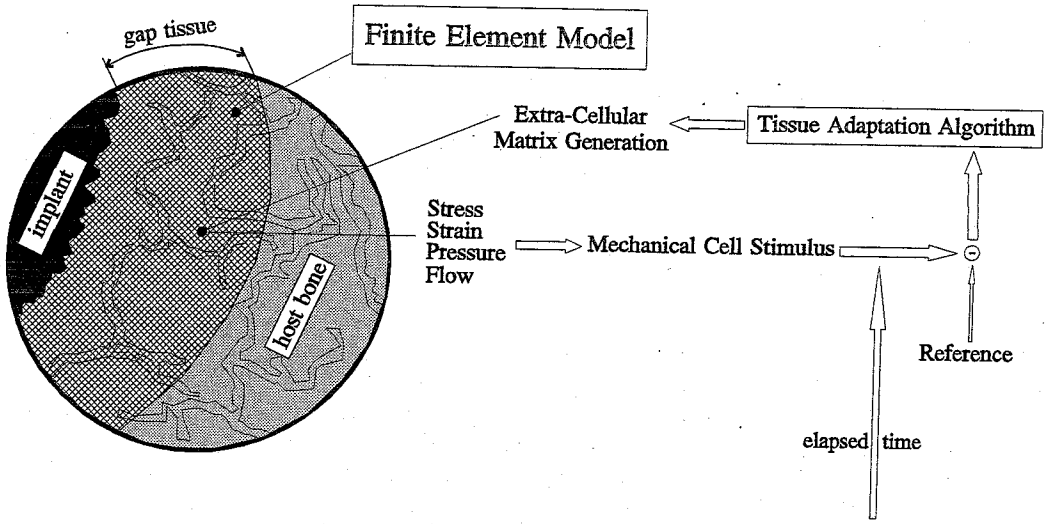

FIG. 37. A conceptual scheme for bone resorption and fibrous-tissue formation around implants.

tion with an FE model, we reduced this feedback relationship to the iterative formula

$$\Delta b = (c'\Delta u_n/b + c''\Delta u_p/b)\Delta t \qquad (37)$$

where c' and c'' are constants, and Δu_n and Δu_p are the overall elastic displacements of the implant relative to bone in normal and tangential directions (Fig. 38A). This relationship is for a plane-strain state and assumes that the fibrous layer is relatively thin (248). For the purpose of FE analysis, we modeled the fibrous tissue as a nonlinear elastic material with negligible resistance against shear and tension (251).

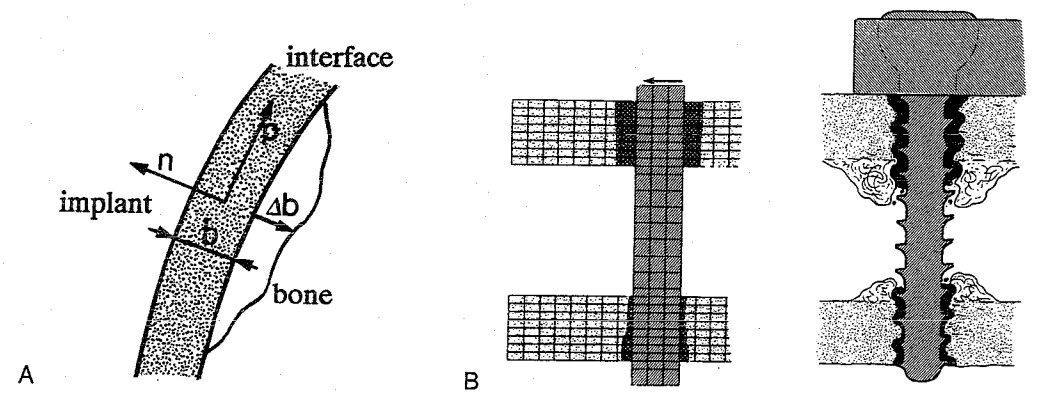

FIG. 38. (A) Interface layer with implant at the left and bone at the right. The coordinates n and p are taken parallel and normal to the interface. The thickness and growth of the interface are expressed by b and Δb, respectively. (From Weinans et al., ref. 251, with permission.) **(B)** *Left:* Simulation of the resorption process around a bone screw. The resorbed bone is indicated in black. (Reproduced from [251].) *Right:* The general resorption pattern around the bone screw fixations with fibrous tissue indicated in black. (Adapted from [180].)

This model was used to simulate loosening processes of a number of implant configurations (251). It concerns a screw used in fracture fixation with bone plates, which gradually loosens as an effect of repetitive transverse forces (182). The simulation model is able to predict the typical resorption patterns around the screw in both bone-cortex regions it penetrated (Fig. 38B). Similarly, the typical resorption patterns of femoral-head surface replacements (65) could be predicted in this way (249).

This model is very simple indeed. It neglects the three-dimensional viscoelastic properties of the fibrous tissue, important in relation to the dynamic character of the load, and the mechanical signal for the bone-resorbing cells in the membrane is not specified (Fig. 37). The first results, however, are promising. To develop this model further, biphasic theory (168) was used in FE analyses of mechanical variables during fibrous-tissue differentiation in periimplant tissues (188). In a well-controlled animal experimental model (216), the differentiation of tissue from fibrous to cartilaginous and eventually to bone could be explained as the effects of mechanical stimuli, such as strain, hydrostatic pressure, and fluid flow. It is expected that these results can be used to develop a valid computer-simulation model to predict implant loosening processes as effects of dynamic loads.

Strain-Adaptive Bone Remodeling Analysis

The ability of bone to form optimal structures to support loads and to adapt structurally to changing loads has been qualitatively described by Wolff's law (198,258). The ability implies that bone must have some internal sensors to detect stresses and strains. It also implies that bone must possess a mechanochemical transduction mechanism to translate these mechanical signals to biochemical ones at the cellular level. Figure 39 shows the chain of events generally assumed for Wolff's law. A local change in mechanical signal is sensed by the bone and is translated by an as yet unknown transducer to a chemical remodeling potential. When this potential is integrated with genetic, hormonal, and metabolic factors, a remodeling signal is generated for modulating osteoblast and osteoclast activities, causing a net increase or decrease of bone mass. This entire process is known as the strain-adaptive remodeling paradigm.

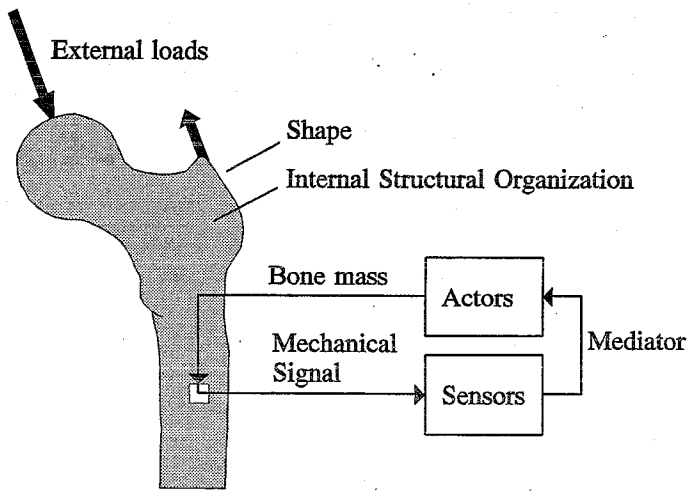

FIG. 39. A hypothesis for the mechanisms of Wolff's law.

In recent years, a number of strain-adaptive bone-remodeling theories have been formulated (22,30,75,110). These theories are mathematical descriptions of the process depicted in Fig. 39, thus providing a quantitative formulation of Wolff's law. The theories assume a relationship between local, strain-related variables and the net change of bone mass. Such variables are called remodeling signals, and the relationships are called remodeling rules. These rules are written as mathematical statements and are combined with an FE model of the bone or the bone–prosthesis structure. Thus, computer simulations of these strain-adaptive bone remodeling processes may be achieved numerically. These models have been used to explain the density patterns and trabecular architectures of bones as effects of their external loads (11,22,169,250). Similar models have also been applied to predict long-term bone remodeling around prostheses, to evaluate the consequences of stress shielding, and to preclinically test THR stem designs (113,116,119,249,253). The theory used for these computer-simulation analyses is briefly summarized in this section.

We assume that the bone cells react to a mechanical signal S, which is the local expression of the bone deformation patterns caused by the external load. The distribution of S is calculated in an FE model of the bone with prosthesis. The signal value is compared to a target value S_{ref}, taking into account a threshold level s. Hence, the target signal value range is

$$(1 - s)S_{ref} \leq S \leq (1 + s)S_{ref} \qquad (38)$$

where s is expressed as a fraction. S_{ref} is the local signal value for the normal bone under remodeling equilibrium. The distribution of S_{ref} is also determined in an FE model representing these conditions. If the signal exceeds the target range, then net bone mass M is added ($dM/dt > 0$); if it is below the target range, bone is removed ($dM/dt < 0$), as illustrated in Fig. 40. The adaptive process in the operated femur can then be expressed in the rate of net bone turnover

$$dM/dt = \tau A(\rho)[S - (1 - s)S_{ref}] \quad \text{if } S \leq (1 - s)S_{ref}$$

$$dM/dt = 0 \quad \text{if } (1 - s)S_{ref} < S < (1 + s)S_{ref}$$

$$dM/dt = \tau A(\rho)[S - (1 + s)S_{ref}] \quad \text{if } S \geq (1 + s)S_{ref}$$

$$0.01 \geq \rho \geq 1.73 \text{ gr/cm}^3 \qquad (39)$$

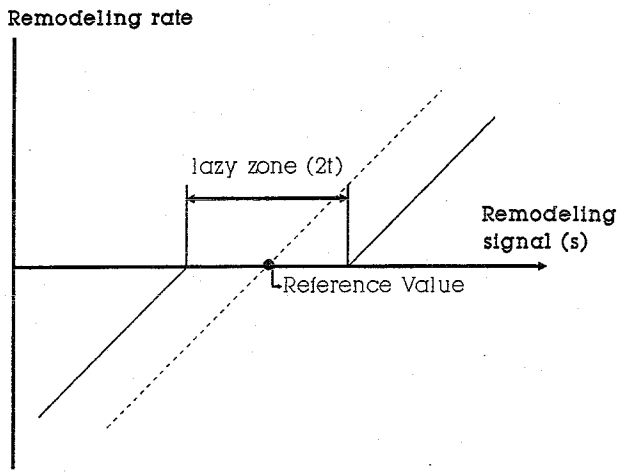

FIG. 40. Relationship between remodeling rate and remodeling signal, with *(solid lines)* and without *(dotted lines)* a lazy zone (110).

where τ is a time constant expressed in grams per millimeters^2[joules/gram]/month, ρ is the apparent density of the bone (in g/cm^3), with a maximal value of 1.73, $A(\rho)$ is the free surface available for remodeling at the periosteum or in the internal bone structure, and s represents the threshold level. The time t is given in units of months.

In the simulation, remodeling takes place within the bone (internal remodeling, a change in apparent density ρ) and at its periosteal surface (external or surface remodeling, a change in shape). The rate of net bone turnover dM/dt can now be expressed as a rate of change of the external (periosteal) geometry, dx/dt, by

$$dM/dt = \rho A(dx/dt) \tag{40}$$

with A the external surface area at which the rate of mass change dM/dt takes place (the external face of the element concerned) and x a characteristic surface coordinate, perpendicular to the periosteal surface. For the adaptation of the internal bone mass as a result of porosity changes we use

$$dM/dt = V(d\rho/dt) \tag{41}$$

with V the volume in which the bone mass change takes place (the volume of the element concerned) and $d\rho/dt$ the rate of change in apparent density. Equation 39 can now be written in terms of dx/dt for surface remodeling and in terms of $d\rho/dt$ for internal remodeling. If we substitute this in equation 39, the proportionality parameters τ/ρ and $\tau A/V$ appear, which regulate the rates of the remodeling processes at the surface and internally, respectively. In the latter location, $A(\rho)$ is the pore surface in the bone, which can be expressed in the apparent density ρ by using a theory of Martin (161).

For the mechanical signal S we take the average elastic energy per unit of mass (joules/gram) from a series of m external loading configurations, each consisting of joint and muscle forces; hence,

$$S = \frac{1}{m}\sum_{i=1}^{m}\frac{U_i}{\rho} \tag{42}$$

where U_i is the strain-energy density (see equation 4) for loading case i. The distribution of S_{ref} is determined accordingly in an FE model of the intact (preoperative) bone. The distribution of the actual signal S in the THR is updated iteratively. The external loading configurations are always assumed identical before and after the operation. Through forward Euler integration, the equations can be

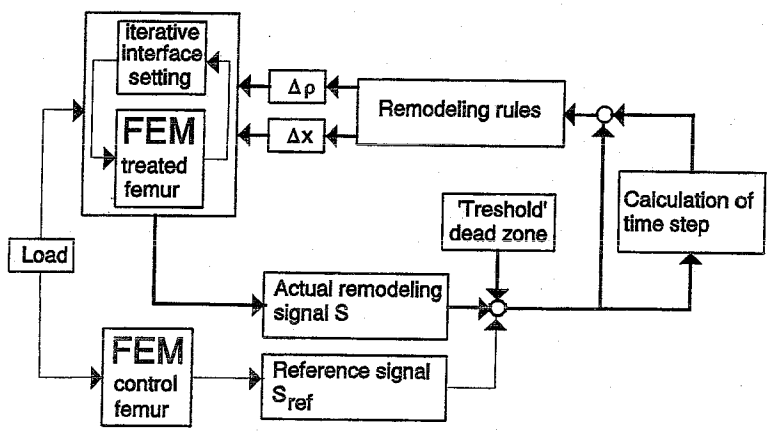

FIG. 41. Schematic representation of the iterative computer simulation model of bone remodeling around implants. (Adapted from Weinans et al., ref. 252.)

solved iteratively to find the new coordinates of the surface nodes and new apparent density values in the integration points after every iterative step. In the computer program, the integration is carried out in steps of $\tau\Delta t$, which represents the proceeding of the processes at an arbitrary computer time scale. The time step in the integration process is variable and determined in each iterative step such that the maximal density change in the integration point where the maximal rate of density change occurs will not exceed $^1/_2\rho_{max}$ (= 0.865 g/cm^3) (229). The iterative simulation process is depicted in Fig. 41.

The value of the threshold s was determined experimentally for dogs as $s = 0.35$. The time constant τ was empirically determined in the same study as $\tau = 130$ g/[mm^2(J/g)month] to have the time t given in units of 1 month (252). For humans the threshold level is taken as $s = 0.75$ (116). A realistic time constant is not known for this case.

The simulation model presented above was validated with respect to six series of animal experiments with THR in dogs (118,229,252). In each series different stem materials and coating conditions were applied. The cortical bone areas and medullary bone densities were measured postmortem 6 months and 2 years postoperatively and compared to the predictions of the simulation model. As shown in Fig. 42, the predictions by the model and the actual morphology found in the dogs were very similar, even in detail. When the predictions of overall bone remodeling were compared per series to the experimental averages and standard deviations, significant correspondence was obtained, as shown for one series in Fig. 43.

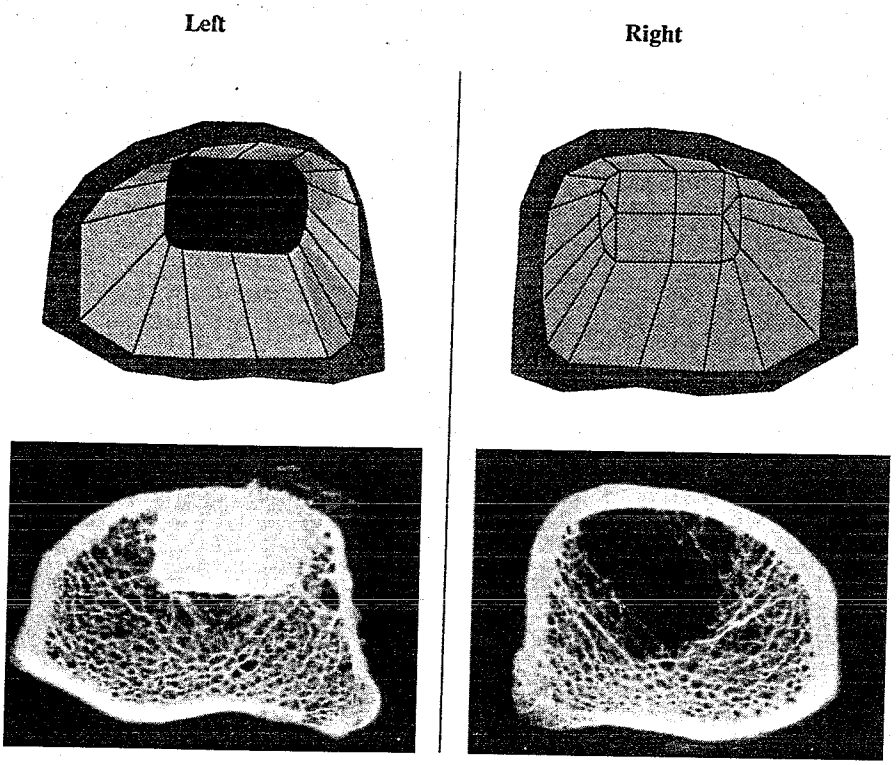

FIG. 42. Animal experimental results (2 years' follow-up) of bone remodeling in canine femurs with fully bonded prostheses compared with the prediction using the remodeling simulation. The **left** femur is the treated case, and the **right** is the control. (Adapted from Van Rietbergen et al. [229].)

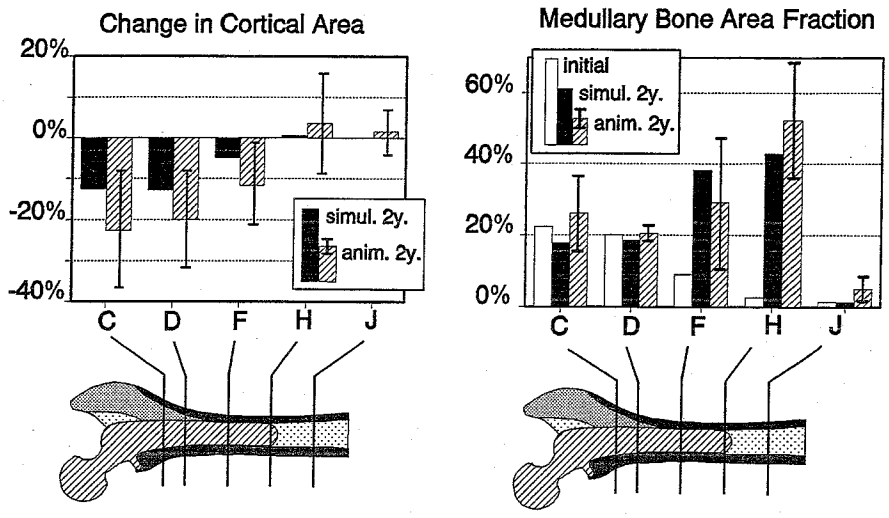

FIG. 43. A comparison between 2-year experimental results in animals and those of the simulation for the uncoated-stem series. The predicted CBA and MBAF are within the 95% confidence interval of the experimental values. (Adapted from Van Rietbergen et al., ref. 229.)

In regard to human configurations, we have hitherto only used internal remodeling because in humans cortical porosis is the main mechanism of bone loss. Figure 44 shows an example of predicted long-term bone loss around a titanium stem in THR. These results were verified relative to mean bone resorption values measured in a series of retrieved THR bone specimens (55,101,104). One-to-one validation relative to the individual patients in this series is in progress.

The computer simulation method discussed here is now used routinely to test prosthetic designs preclinically relative to the stress-shielding failure scenario, on a relative basis, always comparing one configuration with another (116,119,228,249,253).

Numerical Design Optimization

It is evident from the discussion of failure scenarios that many design goals in THR are incompatible. In order to improve fit of noncemented prostheses, modular components to be assembled at the operating table are useful. However, modularity implies more connections subject to wear. Hence, to prevent the failed-bonding failure scenario, components should be modular, but to prevent the particulate-reaction scenario, they should be monoblocs. They can not be both at the same time, so sensible compromises will have to be found. There are many examples of incompatible design goals in THR (102). In an earlier section, we discussed the effects of femoral stem stiffness on bone and interface stresses. Basically, when the stiffness of the stem increases, the interface stresses reduce, but stress shielding increases. So a rigid stem promotes the stress-shielding scenario, and a flexible one promotes both the failed-bonding and the accumulated-damage scenarios. This is another notorious incompatibility in THR design goals, and again sensible compromises are indicated. To assist the designer in finding the best compromise available, numerical design optimization, using FE models, can be a useful tool (39,45,111,112,144–146,261).

The usual approach to FE analysis is to take a particular design (shape and material properties) and determine the stress patterns within the structure under specified loads. In optimization analysis, this procedure is conceptually reversed in that a desired stress pattern in a THR structure is specified and the

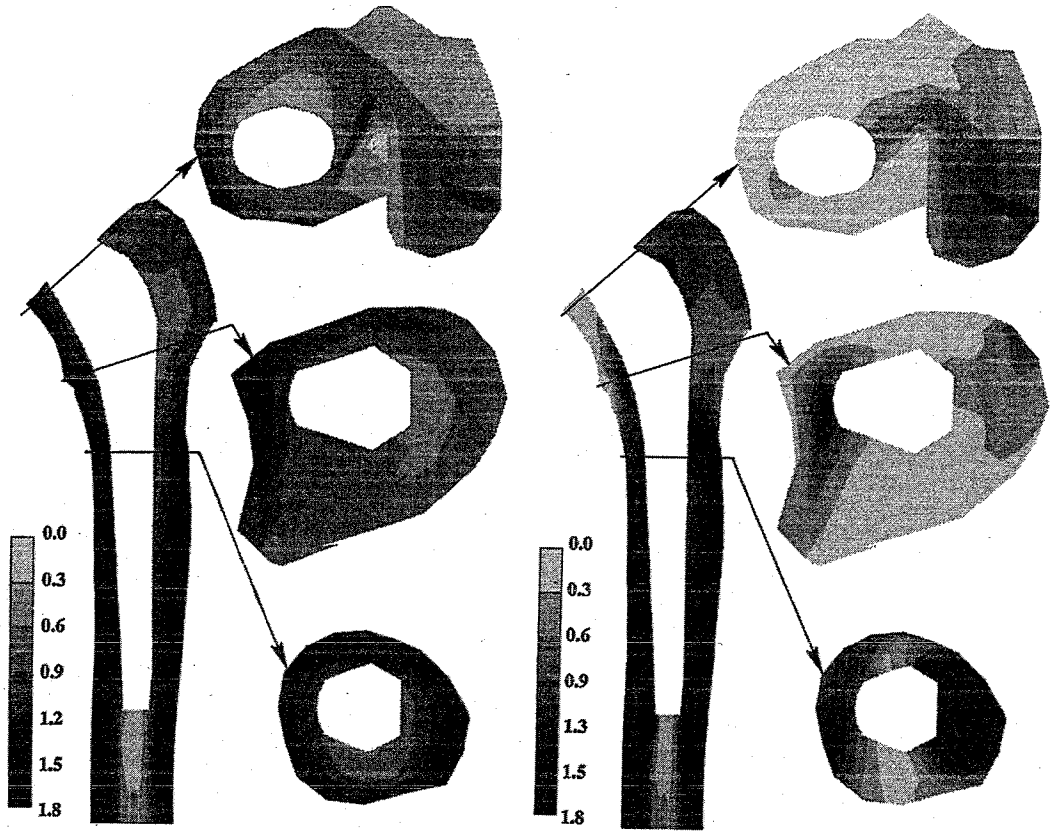

FIG. 44. Immediate postoperative density distribution, as based on CT scan **(left),** and density distribution after long-term remodeling simulation **(right).** (From Huiskes, ref. 101, with permission.)

design characteristics by which it is realized are determined. As in the computer simulations discussed above, this is accomplished in an iterative procedure (Fig. 45). The process is started with an initial design for which the stresses, strains, or other mechanical variables (e.g., strain-energy density, SED) are determined from the initial FE model. If the stress distributions deviate from the desired ones, the shape or material

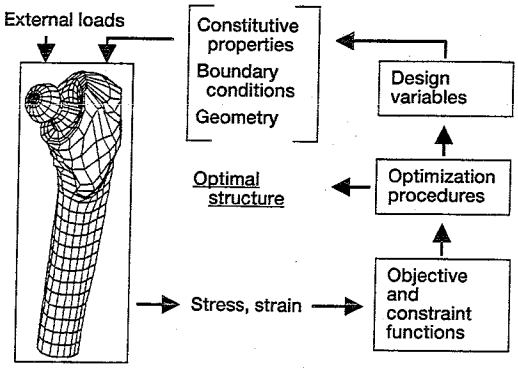

FIG. 45. A general scheme for iterative optimization in combination with a FE-model. (Reproduced from [102]).

characteristics of the design are adapted in such a way that the stresses and strains are changed toward the specified values. This iterative process is repeated until the desired stress patterns are approximated as closely as possible or within a specified range of error. The way in which the shape of the prosthesis is adapted in each iteration is determined by a search procedure that determines the search direction. Experience shows that it is an exception, rather than a rule, that the desired stress and strain distributions are realized precisely by the final design. One must be satisfied with a reasonable approximation of the desired stress and strain distributions.

An optimization process is conducted relative to particular criteria, for instance, minimal stress shielding, minimal interface tension, or minimal cement stress. These criteria are written in mathematical forms as *objective functions* to be minimized. In the optimization procedure, the values of these objective functions are minimized by the particular design characteristics evolved from the iterative process. Hence, these characteristics are "optimal" only relative to the particular objective function selected. This means the criteria must be defined very carefully by the prosthesis designer. This optimization procedure must also include a check against unrealistic properties. For example, the stem of a femoral prosthesis cannot be bigger than the bone into which it is to be fixed. Or the elastic modulus of a material must fit into the range of what can be actually produced. For this reason, certain *boundary constraints* are required for use in the optimization procedure. Finally, the design variations considered in a particular prosthesis are limited to a particular, limited number of dimensional or material parameters, called *design variables*, for instance, parameters that define length or cross-sectional shape of a femoral stem or the parameters of a function that describe the allowable elastic modulus distribution field in a structure. The values of the selected design variables are varied in the process, but all other parameters remain fixed.

As an illustration (Fig. 46), an optimization procedure is applied to optimize the design of a "metal-backed" acetabular cup (100,115). Previous FEM analysis has shown that a metal-backed polyethylene acetabular cup reduces some cement and cement–bone interface stresses (179). However, it was also found that this metal backing tends to in-

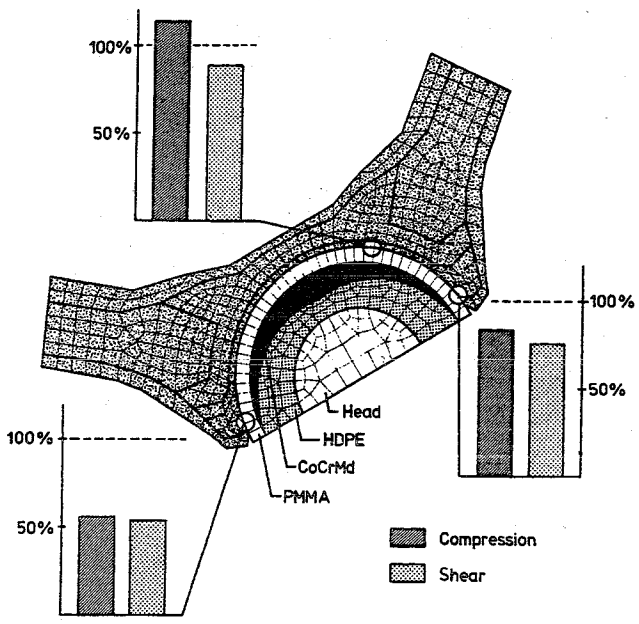

FIG. 46. Compressive and shear-stress values at the cement–bone interface in an acetabular reconstruction for an "optimized" metal-backed shell normalized against the uniform-thickness case (100%) (100,115).

crease interface shear stresses near the edges of the cup (43,109), as discussed in an earlier section. Hence, the question posed was whether a metal-backing shape could be found that would minimize the cement and interface stresses over the whole cup.

The solution procedure was based on a two-dimensional FE model with nonuniform bone properties (179). Other conditions simulated by the FE model included the complete removal of the subchondral bone layer, a uniform cement-layer thickness of 3 mm, a femoral head diameter of 28 mm, and a unit hip-joint force in a direction corresponding to the maximal force during the stance phase of gait. The metal backing shell was assumed to be made out of CoCrMd. A maximal shell thickness of 5 mm and a minimal thickness of zero were taken as boundary constraints in the optimization procedure. Three design variables were used: the thickness of the shell at the dome of the cup, the thickness at the lateral edge, and the thickness at the medial edge. The objective function was the sum of the strain-energy density function for all nodal points at the cement elements. In this sense, the minimization procedure seeks a solution in which minimal load-transfer stresses would occur at the cement–bone interface. The mathematical formulation of the problem may be described as follows:

Design variables:

$$\mathbf{v} = (t_l, t_d, t_m) \tag{43}$$

where t_l = lateral shell thickness, t_d = shell thickness at the dome, t_m = medial shell thickness (linear interpolation between).

Boundary constraints:

$$0 < t_l \leq 5,\ 0 < t_d \leq 5,\ 0 < t_m \leq 5 \tag{44}$$

Objective function:

$$F(\mathrm{v}) = \sum_{k=1}^{n} [U_k(\mathrm{v})]^p \tag{45}$$

where U_k is the strain-energy density at nodal point k of the cement, n is the total number of nodal points, and p is an exponent.

Figure 46 shows the resulting optimal shape of the metal shell and the maximal cement/bone interface stress values (compression and shear) relative to those found for a shell of 2-mm uniform thickness. The optimal inner contour of the shell tends to make it as thick as possible at the cup dome (the maximal value of 5 mm) and as thin as possible at the cup edges. The reductions of stress compared to the case of the uniform shell thickness are on the order of about 15% at the medial and about 45% at the lateral side. At the cranial side, above the hip-joint load, the compressive stress is slightly higher, and shear is slightly lower, than in the case of a uniformly thick metal backing.

A similar optimization procedure applied to a cemented stem produced a typical shape, with a taper at the proximal/medial side, a belly-shaped middle region, and a strongly tapered distal end. Relative to a conventional femoral stem design, cement and interface stress reductions of 30% to 70% could be obtained with this optimized shape (111,112).

For FE analysis of structures, parametric studies require selected design parameters that depend on the intuition and experience of the designer. For optimization analysis, the selection is automated, and the search for the optimal parameters is defined with respect to assumed physical and geometric constraints and criteria. Thus, FE integrated optimization can be a powerful tool in the prosthesis design process. These concepts are obviously not limited to shape optimization but can also be applied to optimization of material properties and boundary conditions, taking adaptive bone remodeling into account.

For this purpose, optimization studies were conducted in which the probability of mechanical interface failure of a cemented stem was formulated mathematically as an objective criterion for an optimization analysis. The integrated elastic energy in the bone was used for a constraint function, in the sense that the maximal amount of bone loss would be limited to a particular maximum value. To accomplish that, the elastic modulus distribution of the stem material was varied between zero and a maximum of 100 GPa. The parameters describing the potential modulus distribution were used as

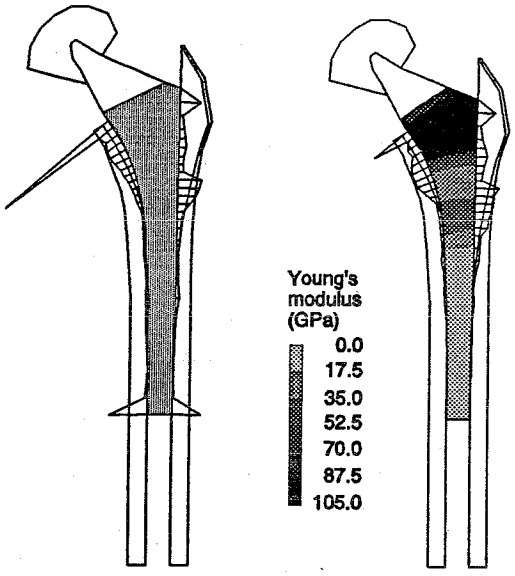

FIG. 47. The stem stiffness distribution before **(left)** and after **(right)** an optimization procedure. (Adapted from Kuiper and Huiskes, ref. 145.)

the design variables. Analyses were conducted in two- and three-dimensional models (144–146). Figure 47 shows an example of a configuration obtained in which the stem elastic modulus varies from high proximally to low distally. Compared to a full titanium stem (modulus 115 GPa), the amount of bone resorption predicted would reduce from 26% to 7.5%. This would also be realized by an "isoelastic" stem with a uniform modulus of 36 GPa, but for such a stem the peak interface stress would be a factor of three higher than for the optimized design. Evidently, it is questionable whether a material distribution as in Fig. 47 could actually be produced, so the matter is presently rather academic. However, these results illustrate that in principle, solutions for incompatible design goals are to be found with numerical optimization methods.

REFERENCES

1. Ahmed, A. M., Raab, S., and Miller, J. E. (1984): Metal–cement interface strength in cemented stem fixation. *J. Orthop. Res.*, 2:105–118.
2. Ahnfelt, L., Herberts, P., Malchau, H., and Andersson, G. B. J. (1990): Prognosis of total hip replacement. *Acta Orthop. Scand. [Suppl.]*, 238.
3. American Academy of Orthopaedic Surgeons (1981): *Musculoskeletal System Research, Current and Future Research Needs.* AAOS Publication TFR-81, Chicago.
4. Amstutz, H. C., Nasser, S., More, R. C., and Kabo, J. M. (1989): The anthropometric total hip femoral prosthesis. Preliminary clinical and roentgenographic findings of exact-fit cementless application. *Clin. Orthop.*, 242:104–119.
5. Amstutz, H. C., Campbell, P., Kossovsky, N., and Clarke, I. C. (1992): Mechanism and clinical significance of wear debris-induced osteolysis. *Clin. Orthop.*, 276:7–18.
6. Arroyo, N. A., and Stark, C. F. (1987): The effect of textures, surface finish and precoating on the strength of bone cement/stem interfaces. *Proc. Soc. Biomat.*, 13:218.
7. Bakhvalov, and Panasenko (1989): *Homogenisation: Averaging Process in Periodic Media.* Kluwer Academic Publisher, Dordrecht.
8. Barb, W., Park, J. B., Kenner, G. H., and Recum, A. F. (1982): Intramedullary fixation of artificial hip joints with bone cement-precoated implants. Interfacial strengths. *J. Biomed. Mater. Res.*, 16:447–458.
9. Bargar, W. L. (1989): Shape the implant to the patient. A rationale for the use of custom-fit cementless total hip implants. *Clin. Orthop.*, 249:73–78.
10. Bartel, D. L., Bickness, V. L., and Wright, T. J. (1986): The effect of conformity, thickness, and material on stresses in ultra-high molecular weight components for total joint replacement. *J. Bone Joint Surg.*, 68-Am:1041–1051.
11. Beaupré, G. S., Orr, T. E., and Carter, D. R. (1990): An approach for time-dependent bone modeling and remodeling—application: a preliminary remodeling simulation. *J. Orthop. Res.*, 8:662–670.
12. Bergmann, G., Graichen, F., and Rohlmann, A. (1993): Hip joint loading during walking and running, measured in two patients. *J. Biomech.*, 26:969–990.
13. Bobyn, J. D., Mortimer, E. S., Glassman, A. H., Engh, C. A., Miller, J. E., and Brooks, C. E. (1992): Producing and avoiding stress shielding. Laboratory and clinical observations of noncemented total hip arthroplasty. *Clin. Orthop.*, 274:79–96.
14. Brand, R. A., and Pedersen, D. R. (1984): Computer modeling of surgery and a consideration of the mechanical effects of proximal femoral osteotomies. In: *The Hip,* edited by R. B. Welch, pp. 193–210. C. V. Mosby, St. Louis.
15. Brand, R. A., Pedersen, D. R., Davy, D. T., Kotzar, G. M., Heiple, K. G., and Goldberg, V. M. (1994): Comparison of hip force calculations and measurements in the same patient. *J. Arthropol.*, 9:45–51.
16. Brunski, J. B., Aquilante, F. M., Pollack, S. R., Korostoff, E., and Trachtenberg, E. I. (1979): The influence of functonal use of endosseous dental implants on tissue–implant interface. I. Histological aspects. *J. Dent. Res.*, 10:1953–1969.
17. Burke, D. W., O'Connor, D. O., Zalenski, E. B., Jasty, M., and Harris, W. H. (1991): Micromotion of cement and uncemented femoral components. *J. Bone Joint Surg.*, 73-B:22–37.
18. Carlsson, L., Albrektsson, B., and Freeman, M. A. R.

(1988): Femoral neck retention in hip arthroplasty. *Acta Orthop. Scand.,* 59:6–8.
19. Carter, D. R. (1978): Anisotropic analysis of strain rosette information from cortical bone. *J. Biomech.,* 11:199–202.
20. Carter, D. R., and Hayes, W. C. (1977): The behavior of bone as a two-phase porous structure. *J. Bone Joint Surg.,* 59-A:954–962.
21. Carter, D. R., Vasu, R., and Harris, W. H. (1982): Stress distributions in the acetabular region—II: effects of cement thickness and metal backing of the total hip acetabular component. *J. Biomech.,* 15:165–170.
22. Carter, D. R., Fyhrie, D. P., and Whalen, R. T. (1987): Trabecular bone density and loading history: regulation of connective tissue biology by mechanical energy. *J. Biomech.,* 20:785–794.
23. Chaboche, J. L. (1988): Continuum damage mechanics: Part I—General concepts. *J. Appl. Mech.,* 55:59–64.
24. Chaboche, J. L. (1988): Continuum damage mechanics: Part II—Damage growth, crack initiation, and crack growth. *J. Appl. Mech.,* 55:65–72.
25. Charnley, J. (1970): *Acrylic Cement in Orthopaedic Surgery.* E. and S. Livingstone; Edinburgh.
26. Charnley, J. (1978): *Low Friction Arthroplasty of the Hip.* Springer Verlag, New York.
27. Chwirut, D. J. (1984): Long-term compressive creep deformation and damage in acrylic bone cements. *J. Biomed. Mater. Res.,* 18:25–37.
28. Cohen, B., and Rushton, N. (1995): Accuracy of DEXA measurement of bone mineral density after total hip arthroplasty. *J. Bone Joint Surg.,* 77-Br:479–483.
29. Concensus Development Panel (1982): *Total Hip Replacement in the United States.* Report of Concensus Conference, NIH, 1-3 March 1982, Bethesda, MD. *JAMA,* 248:1817–1821.
30. Cowin, S. C., and Hegedus, D. H. (1976): Bone remodeling I: theory of adaptive elasticty. *J. Elasticity,* 6:313–326.
31. Crolet, J. M., Aoubiza, B., and Meunier, A. (1993): Compact bone: numerical simulation of mechanical characteristics. *J. Biomech.,* 26:677–689.
32. Crowninshield, R. D., and Brand, R. A. (1981): A physiologically based criterion of muscle force prediction in locomotion. *J. Biomech.,* 14:793–801.
33. Crowninshield, R. D., and Tolbert, J. R. (1983): Cement strain measurement surrounding loose and well-fixed femoral component stems. *J. Biomed. Mater. Res.,* 17:819–828.
34. Crowninshield, R. D., Johnston, R. C., and Andrews, J. G. (1978): A biomechanical investigation of the human hip. *J. Biomech.,* 11:75–86
35. Crowninshield, R. D., Brand, R. A., and Pedersen, D. R. (1983): A stress analysis of acetabular reconstruction in protrusio acetabuli. *J. Bone Joint Surg.,* 65-Am: 495–499.
36. Culleton, T. P., Prendergast, P. J., and Taylor, D. (1993): Fatigue failure in the cement mantle of an artificial joint. *Clin. Mater.,* 12:95–102.
37. Currey, J. (1984): *The Mechanical Adaptations of Bone.* Princeton University Press, Guildford, UK.
38. Dally, J. W., and Riley, W. F. (1965): *Experimental Stress Analysis.* McGraw-Hill, New York.
39. Dalstra M. (1993): *Biomechanical aspects of the pelvic bone and design criteria for acetabular prostheses.* Ph.D. thesis, Nijmegen University, The Netherlands.
40. Dalstra, M., and Huiskes, R. (1994): Prestresses around the acetabulum generated by screwed cups. *Clin. Mater.,* 16:145–154.
41. Dalstra, M., and Huiskes, R. (1995): Load transfer across the pelvic bone. *J. Biomech.,* 28:715–724.
42. Dalstra, M., Huiskes, R., and Van Erning, L. (1995): Development and validation of a three-dimensional finite element model of the pelvic bone. *J. Biomech. Eng.,* 117:272–278.
43. Dalstra, M., and Huiskes, R. (1997): The effects of total hip replacement on pelvic load transfer. *J. Orthop. Res.* (in press).
44. Davies, J. P., Burke, D. W., O'Connor, D. O., and Harris, W. H. (1987): Comparison of the fatigue characteristics of centrifuged and uncentrifuged Simplex P bone cement. *J. Orthop. Res.,* 5:366–371.
45. Davy, D. T., and Katoozian, H. (1994): Three-dimensional shape optimization of femoral components of hip prostheses with frictional interfaces. *Trans. ORS,* 40:223.
46. Davy, D. T., Kotzar, G. M., Brown, R. H., Heiple, K. G., Goldberg, V. M., Heiple, K. G., Jr., Berilla, J., and Burstein, A. H. (1988): Telemetric force measurements across the hip after total arthroplasty. *J. Bone Joint Surg.,* 70-Am:45–50.
47. DiCarlo, E. F., and Bullough, P. G. (1992): The biological responses to orthopaedic implants and their wear debris. *Clin. Mater.,* 9:235–260.
48. Diegel, P. D., Daniels, A. U., and Dunn, H. K. (1989): Initial effect of collarless stem stiffness on femoral bone strain. *J. Arthroplasty,* 4:173–179.
49. Dostal, W. F., and Andrews, J. F. (1981): A three dimensional biomechanical model of hip musculature. *J. Biomech.,* 14:802–881.
50. Duparc, J., and Massin, P. (1992): Results of 203 total hip replacements using a smooth, cementless femoral component. *J. Bone Joint Surg.,* 74-Br:251–256.
51. Durelli, A. J. (1977): The difficult choice: evaluation of methods used to determine experimentally displacements, strains and stresses. *Appl. Mech. Rev.,* 30(9): 1167–1174.
52. Eftekar, M. S., Doty, S. B., Johnston, A. D., and Parisien, M. V. (1985): Prosthetic synovitis. In: *The Hip,* edited by R. H. Fitzgerald, pp. 169–183. C. V. Mosby, St. Louis.
53. Engh, C. A., and Bobyn, J. D. (1988): The influence of stem size and extent of porous coating on femoral bone resorption after primary cementless hip arthroplasty. *Clin. Orthop.,* 231:7–28.
54. Engh, C. A., and Massin, P. (1989): Cementless total hip replacement using the AML stem. 0–10 year results using a survivorship analysis. *Nippon Seikeigeka Gakkai Zasshi,* 63:653–666.
55. Engh, C. A., McGovern, T. F., Bobyn, J. D., and Harris, W. H. (1992): A quantitative evaluation of periprosthetic bone-remodeling after cementless total hip arthroplasty. *J. Bone Joint Surg.,* 74-Am:1009–1020.
56. Engh, C. A., Hooten, J. P., Jr., Zettl-Schaffer, K. F., Ghaffarpour, M., McGovern, T. F., Macalino, G. E., and Zicat, B. A. (1994): Porous-coated total hip replacement. *Clin. Orthop.,* 298:89–96.
57. Faro, L. M., and Huiskes, R. (1992): Quality assurance of joint replacement. Legal regulation and medical judgement. *Acta Orthop. Scand. [Suppl.],* 250:1–33.
58. Feith, R. (1975): Side-effects of acrylic cement, implanted into bone. *Acta Orthop. Scand. [Suppl.],* 161.

59. Felts, W., and Yelin, E. (1989): The economic impact of the rheumatic diseases in the United States. *J Rheumatol.,* 16:867–884.
60. Finlay, J. B., Bourne, R. B., Landsberg, R. P. D., and Andreae, P. (1986): Pelvic stresses *in vitro*—I. Malsizing of endoprostheses. *J. Biomech.,* 19:703–714.
61. Finlay, J. B., and Bourne, R. B. (1989): Potential reinforcement-errors from the use of foil strain-gauges. *Trans. Orthop. Res. Soc.,* 14:491.
62. Finlay, J. B., Rorabeck, C. H., Bourne, R. B., and Tew, W. M. (1989): *In vitro* analysis of proximal femoral strains using PCA femoral implants and a hip-abductor muscle simulator. *J. Arthroplasty,* 4:335–345.
63. Freeman, M. A. R., and Plante-Bordeneuve, P. (1994): Early migration and late aseptic failure of proximal femoral prostheses. *J. Bone Joint Surg.,* 76-Br:432–438.
64. Furlong, R. (1993): Six years use of the unmodified Furlong hydroxyapatite ceramic coated total hip replacement. *Acta Orthop. Belg.,* 59(Suppl. 1):323–325.
65. Geesink, R. G. T., Groot, K. de, and Klein, C. P. A. T. (1987): Chemical implant fixation using hydroxyl-apatite coatings. *Clin. Orthop.,* 225:147–170.
66. Geesink, R. G., and Hoefnagels, N. H. (1995): Six-year results of hydroxyapatite-coated total hip replacement. *J. Bone Joint Surg.,* 77-Br:534–547.
67. Gilbert, J. L., Blommfield, R. S., Lautenschlager, E. P., and Wixson, R. L. (1992): A computer-based biomechanical analysis of the three-dimensional motion of cementless hip prostheses. *J. Biomech.,* 25:329–340.
68. Goldring, S. R., Schiller, A. L., Roelke, M., Rourke, C. M., O'Neill, D. A., and Harris, W. H. (1983): The synovial-like membrane at the bone–cement interface in loose total hip replacements and its proposed role in bone lysis. *J. Bone Joint Surg.,* 65A:575–583.
69. Goodman, S. B., Aspenberg, P., Song, Y., Regual, D., Doshi, A., and Lidgren. L. (1994): Effects of intermittent micromotion versus polymer particles on tissue ingrowth: experiment using a micromotion chamber implanted in rabbits. *J. Appl. Biomater.,* 5:117–123.
70. Goulet, R. W., Goldstein, S. A., Ciarelli, M. J., Kuhn, J. L., Brown, M. B., and Feldkamp, L. A. (1994): The relationship between the structural and orthogonal compressive properties of trabecular bone. *J. Biomech.,* 27:375–389.
71. Grazier, K. L., Holbrook, T. L., Kelsey, J. L., and Stauffer, R. N. (1984): *The Frequency of Occurence, Impact and Cost of Musculoskeletal Conditions in the United States.* American Academy of Orthopaedic Surgeons, Chicago.
72. Gruen, T. A., McNeic, G. M., and Amstutz, H. C. (1979): "Modes of failure" of cemented stem-type femoral components: A radiographic analysis of loosening. *Clin. Orthop.,* 141:17–23.
73. Harrigan, T., and Harris, W. H. (1991): A three-dimensional non-linear finite element study of the effect of cement-prosthesis debonding in cemented femoral total hip components. *J. Biomech.,* 24:1047–1058.
74. Harris, W. H. (1992): Is it advantageous to strengthen the cement–metal interface and use a collar for cemented femoral components of total hip replacement? *Clin. Orthop.,* 285:67–72.
75. Hart, R. T., Davy, D. T., and Heiple, K. G. (1984): A computational method of stress analysis of adaptive elastic materials with a view toward application in strain induced remodeling. *J. Biomech. Eng.,* 106:342–350.
76. Havelin, L. I., Espehaug, B., Vollset, S. E., and Engesaeter, L. B. (1995): The effect of the type of cement on early revision of Charnley total hip prostheses. A review of eight thousand five hundred and seventy-nine primary arthroplasties from the Norwegian Arthroplasty Register. *J. Bone Joint Surg.,* 77-Am:1543–1550.
77. Havelin, L. I., Espehaug, B., Vollset, S. E., and Engesaeter, L. B. (1995): Early aseptic loosening of uncemented femoral components in primary total hip replacement. A review based on the Norwegian Arthroplasty Register. *J. Bone Joint Surg.,* 77-Br:11–17.
78. Hayes, W. C., and Snyder, B. (1981): Toward a quantitative formulation of Wolff's law in trabecular bone. In: *Mechanical Properties of Bone,* edited by S. C. Cowin, pp. 43–69. American Society of Mechanical Engineers, New York.
79. Herberts, P., Ahnfelt, L., Malchau, H., Strömberg, C., and Andersson, G. B. J. (1989): Multicenter clinical trials and their value in assessing total joint arthroplasty. *Clin. Orthop.,* 249:48–55.
80. Hinton, E. (1992): *NAFEMS Introduction to Nonlinear Finite Element Analysis.* Bell and Bain, Glasgow.
81. Hodge, W. A., Andriacchi, T. P., and Galante, J. O. (1991): A relationship between stem orientation and function following total hip arthroplasty. *J. Arthopl.,* 6:229–235.
82. Hoffman, O. (1967): The brittle strength of orthotropic materials. *J. Comp. Mater.,* 1:200–206.
83. Hollister, S. J., Fyhrie, D. P., Jepsen, K. J., and Goldstein, S. A. (1991): Application of homogenization theory to the study of trabecular bone mechanics. *J. Biomech.,* 24:825–839.
84. Hollister, S. J., and Kikuchi, N. (1992): Direct analysis of trabecular bone stiffness and tissue level mechanics using an element-by-element homogenization method. *Trans. ORS,* 38:559.
85. Hollister, S. J., Brennan, J. M., and Kikuchi, N. (1992): Homogenization sampling analysis of trabecular bone microstructural mechanics. In: *Recent Advances in Computer Methods in Biomechanics and Biomedical Engineering,* edited by J. Middleton, G. N. Pande, and K. R. Williams, pp. 308–317. Books & Journals Int. LTD, Swansea.
86. Hollister, S. J., Brennan, J. M., and Kikuchi, N. (1994): A homogenization sampling prodedure for calculating trabecular bone effective stiffness and tissue level stress. *J. Biomech.,* 27:433–444.
87. Holman, J. P. (1978): *Experimental Methods for Engineers,* 3rd ed. McGraw-Hill Kogakusha, Tokyo.
88. Horikoshi, M., Macaulay, W., Booth, R. E., Crossett, L. S., and Rubash, H. E. (1994): Comparison of interface membranes obtained from failed cemented and cementless hip and knee prostheses. *Clin. Orthop.,* 309:69–87.
89. Horowitz, S. M., Doty, S. B., Lane, J. M., and Burstein, A. H. (1993): Studies of the mechanism by which the mechanical failure of polymethylmethacrylate leads to bone resorption. *J. Bone Joint Surg.,* 75-Am:802–813.
90. Hua, J., and Walker, P. S. (1995): Closeness of fit of uncemented stems improves the strain distribution in the femur. *J. Orthop. Res.,* 13:339–346.
91. Hughes, T. J. R. (1987): *The Finite Element Method; Linear Static and Dynamic Finite Element Analysis.* Prentice-Hall, Englewood Cliffs, NJ.
92. Hughes, J. R., Ferencz, R. M., and Hallquist, J. O. (1987): Large-scale vectorized implicit calculations in

solid mechancs on a cray S-MP/48 utilizing EBE preconditioned conjugate gradients. *Comp. Meth. Appl. Mech. Eng.,* 61:215–248.

93. Huiskes, R. (1980): Some fundamental aspects of human-joint replacement. *Acta Orthop. Scand. [Suppl.],* 185.
94. Huiskes, R. (1982): On the modelling of long bones in structural analyses. *J. Biomech.,* 15:65–69.
95. Huiskes, R. (1984): Principles and methods of solid biomechanics. In: *Functional Behavior of Orthopaedic Materials. Vol. I: Fundamentals,* edited by P. Ducheyne and G. Hastings, pp. 51–98. CRC-Press, Boca Raton, FL.
96. Huiskes, R. (1984): Design, fixation, and stress analysis of permanent orthopedic implants: the hip joint. In: *Functional Behavior of Biomaterials. Vol. II: Applications,* edited by P. Ducheyne and G. Hastings, pp. 121–162. CRC-Press, Boca Raton, FL.
97. Huskes, R., (1985): Properties of the stem–cement interface and artificial hip-joint failure. In: *The Bone–Implant Interface,* edited by J. L. Lewis and J. O. Galante, pp. 86–101. American Academy of Orthopaedic Surgeons, Chicago.

97a. Huiskes, R., Strens, P.H.G.E., Heck, J. van, and Slooff, T.J. (1985) Interface stresses in the resurfaced hip. *Acta Orthop. Scand.*, 56, pp. 474–478.

98. Huiskes, R. (1987): Finite element analysis of acetabular reconstruction. *Acta Orthop. Scand.,* 58:620–625.
99. Huiskes, R. (1990): The various stress patterns of press-fit, ingrown and cemented femoral stems. *Clin. Orthop.* 261:27–38.
100. Huiskes, R. (1991): New approaches to cemented hip-prosthetic design. In: *Safety of Implants,* edited by G. Buchorn and H. G. Willert, pp. 227–236. Hans Huber Verlag, Bern.
101. Huiskes, R. (1993): Stress shielding and bone resorption in THA: clinical versus computer-simulation studies. *Acta Orthop. Belg.,* 59(Suppl. 1):118–129.
102. Huiskes, R. (1993): Failed innovation in total hip replacement. *Acta Orthop. Scand.,* 64:699–716.
103. Huiskes, R. (1993): Mechanical failure in total hip arthroplasty with cement. *Curr. Orthop.,* 7:239–247.
104. Huiskes, R. (1995): Bone remodeling around implants can be explained as an effect of mechanical adaptiation. In: *Total Hip Revision Surgery,* edited by J. O. Galante, A. G. Rosenberg, and J. J. Gallaghan, pp. 159–171. Raven Press, Ltd., New York.
105. Huiskes, R. (1996): Biomechanics of noncemented total hip arthroplasty. *Curr. Orthop.* 7:32–37.
106. Huiskes, R., Janssen, J. D., and Slooff, T. J. (1981): A detailed comparison of experimental and theoretical stress-analyses of a human femur. In: *Mechanical Properties of Bone,* edited by S. C. Cowin, pp. 211–234. The American Society of Mechanical Engineers, New York.
107. Huiskes, R., and Chao, E. Y. S. (1983): A survey of finite element methods in orthopaedic biomechanics. *J. Biomech.,* 16:385–409.
108. Huiskes, R., and Nunamaker, D. (1984): Local stresses and bone adaptation around orthopaedic implants. *Calcif. Tissue Int.,* 36:S110–S117.
109. Huiskes, R., and Slooff, T. J. (1987): Stress transfer across the hip joint in reconstructed acetabuli. In: *Biomechanics: Basic and Applied Research,* edited by G. Bergmann, R. Koelbel, and A. Rohlmann, pp. 333–340. Martinus Nijhoff, Dordrecht.
110. Huiskes, R., Weinans, H., Grootenboer, H. J., Dalstra, M., Fudala, B., and Slooff, T. J. (1987): Adaptive bone-remodeling theory applied to prosthetic-design analysis. *J. Biomech.,* 20(11/12):1135–1150.
111. Huiskes, R., and Boeklagen, R. (1988): The application of numerical shape optimization to artificial joint design. In: *Computational Methods in Bioengineering,* edited by R. L. Spilker and B. R. Simon, pp. 185–198. The American Society of Mechanical Engineers, New York.
112. Huiskes, R., and Boeklagen, R. (1989): Mathematical shape optimization of hip-prosthesis design. *J. Biomechanics,* 22:793–804.
113. Huiskes, R., Weinans, H., and Dalstra, M. (1989): Adaptive bone remodeling and biomechanical design considerations for noncemented total hip arthroplasty. *Orthopedics,* 12:1255–1267.
114. Huiskes, R., Strens, P. Vroemen, W., and Slooff, T. J. (1990): Post-loosening mechanical behavior of femoral resurfacing prostheses. *Clin. Mater.,* 6:37–55.
115. Huiskes, R., Venne, R. van der, and Spierings, P. T. J. (1990): Numeral shape optimization applied to cemented acetabular-cup design in THA. *Proc. Ann. Meet. ORS,* 255.
116. Huiskes, R., Weinans, H., and Van Rietbergen, B. (1992): The relationship betweeen stress shielding and bone resoption around total hip stems and the effects of flexible materials. *Clin. Orthop.,* 272:124–134.
117. Huiskes, R., and Hollister, S. J. (1993): From structure to process, from organ to cell: recent developments of FE-analysis in orthopaedic biomechancics. *J. Biomech. Eng.,* 115:520–527.
118. Huiskes, R., Van Rietbergen, B., Weinans, H., Sumner, D. R., Turner, T., and Galante, J. O. (1994): Validation of strain-adaptive bone-remodeling simulation models. *World Cong. Biomech.,* 2:57.
119. Huiskes, R., and Van Rietbergen, B. (1995): Preclinical testing of total hip stems; The effects of coating placement. *Clin. Orthop.,* 319:64–76.
120. Hungerford, D. S., Hedley, A., Habermann, E. T., Borden, L. S., and Kenna, R. V. (1984): *Total Hip Arthroplasty: A New Approach.* University Park Press, Baltimore.
121. Huracek, J., and Spirig, P. (1994): The effect of hydroxyapatite coating on the fixation of hip prostheses. A comparison of clinical and radiographic results of hip replacement in a matched-pair study. *Arch. Orthop. Trauma Surg.,* 113:72–77.
122. Hwang, W., and Han, K. S. (1986): Cumulative damage models and multi-stress fatigue life prediction. *J. Comp. Mater.,* 20:125–153.
123. Ilchmann, T., Franzén, H., Mjöberg, G., and Wingstrand, H. (1992): Measurement accuracy in acetabular cup migration. A comparison of four radiologic methods versus roentgen stereo-grammetric analysis. *J. Arthroplasty,* 7:121–127.
124. Jacob, H. A. C., and Huggler, A. H. (1980): An investigation into biomechanical causes of prosthesis stem loosening within the proximal end of the human femur. *J. Biomech.,* 13:159–171.
125. Jacobs, C. R., Mandell, J. A., and Beaupré, G. S. (1993): A comparative study of automatic finite ele-

ment mesh generation techniques in orthopaedic biomechanics. *ASME,* 24:512–514.
126. Jacobs, J. J., Galante, J. O. and Sumner, D. R. (1992): Local response to biomaterials: bone loss in cementless femoral stems. *Instr. Course Lect.,* 41:119–125.
127. Jasty, M., Maloney, W. J., Bragdon, C. R., O'Connor, D. O., Haire, T., and Harris, W. H. (1991): The initiation of failure in cemented femoral components of hip arthroplasties. *J. Bone Joint Surg.,* 73-Br:551–558.
128. Jasty, M., Jiranek, W., and Harris, W. H. (1992): Acrylic fragmentation in total hip replacements and its biological consequences. *Clin. Orthop.,* 285:116–128.
129. Jasty, M., O'Connor, D. O., Henshaw, R. M., Harrigan, T. P., and Harris, W. H. (1994): Fit of the uncemented femoral components and the use of cement influence the strain transfer to the femoral cortex. *J. Orthop. Res.,* 12:648–656.
130. Johnston, R. C. (1987): The case for cemented hips. *Iowa Orthop. J.,* 6:60–64.
131. Kang, Y. K., Park, H. C., Youm, Y., Lee, I. K., Ahn, M. H., and Ihn, J. C. (1993): Three dimensional shape reconstruction and finite element analysis of femur before and after the cementless type of total hip replacement. *J. Biomed. Eng.,* 15:497–504.
132. Kaplan, E. L., and Meier, P. (1958): Nonparametric estimation from incomplete observations *Am. Stat. Assoc. J.,* 54:457–557.
133. Kärrholm, J. (1989): Roentgen stereophotogrammetry. Review of orthopaedic applications. *Acta Orthop. Scand.,* 60:491–503.
134. Kärrholm, J., and Snorrason, F. (1992): Migration of porous coated acetabular prostheses fixed with screws. *J. Orthop. Res.,* 10:826–835.
135. Kärrholm, J., Borssén, B., Löwenhielm, G., and Snorrason, F. (1994): Does early micromotion of femoral stem prostheses matter? *J. Bone Joint Surg.,* 76-Br:912–917.
136. Keaveny, T. M., and Bartel, D. L. (1993): Effects of porous coating and collar support on early load transfer for a cementless hip prosthesis. *J. Biomech.,* 26: 1205–1216.
137. Keller, J. C., Lautenschlager, E. P., Marshall, G. W., Meyer, P. R. (1980): Factors affecting surgical alloy/bone cement interface adhesion. *J. Biomed. Mater. Res.,* 14:1639–1651.
138. Keyak, J. H., Meagher, J. M., Skinner, H. B., and Mote, C. D., Jr. (1990): Automated three-dimensional finite element modelling of bone: a new method. *J. Biomed. Eng.,* 12:389–397.
139. Keyak, J. H., and Skinner, H. B. (1992): Three-dimensional finite element modelling of bone: effects of element size. *J. Biomed. Eng.,* 14:483–489.
140. Kohles, S. S., Vanderby, R., Manley, P. M., Belloli, D. M., Sandar, B. I., and McBeath, A. A. (1989): A comparison of strain gage analysis to differential infraved thermography in the proximal canine femur. *Trans. Orthop. Res. Soc.,* 14:490.
141. Kotzar, G. M., Davy, D. T., Goldberg, V. M., Heiple, K. G., Berilla, J., Heiple, K. G., Jr., Brown, R. H., and Burstein, A. H. (1991): Telemetrized *in vivo* hip joint force data: a report on two patients after total hip surgery. *J. Orthop. Res.,* 9:621–633.
142. Krause, W. R., Krug, W., and Miller, J. (1982): Strength of the cement-bone interface. *Clin. Orthop.,* 163: 290–299
143. Krause, W. R., Mathis, R. S., and Grimes, L. W. (1988): Fatigue properties of acrylic bone cement: S-N, P-N, and P-S-N data. *J. Biomed. Mater. Res.,* 22:221–244.
144. Kuiper, J. H., and Huiskes, R. (1992): Numerical optimization of hip-prosthetic material. *Recent Advances in Computer Methods in Biomechanics and Biomedical Engineering,* edited by J. Middleton, G. N. Pande, and K. R. Williams, pp. 76–84. Books & Journals Int., Swansea, UK.
145. Kuiper, J. H., and Huiskes, R. (1997): Mathematical optimization of elastic properties—Application to cementless hip stem design. *J Biomech. Eng.,* 14:36–43.
146. Kuiper, J. H., and Huiskes, R. (1997): The predictive value of stress shielding for quantification of adaptive resorption around hip replacements. *J. Biomech. Eng.* (in press).
147. Kuiper, J. H., and Huiskes, R. (1996): Friction and stem stiffness affect dynamic interface motion in total hip replacement. *J. Orthop. Res.* 14:36–43.
148. Kwong, L. M., O'Connor, D. O., Sedlacek, R. C., Krushell, R. J., Maloney, W. J., and Harris, W. H. (1994): A quantitative *in vitro* assessment of fit and screw fixation on the stability of a cementless hemispherical acetabular component. *J. Arthroplasty,* 9:163–170.
149. Landjerit, B., Jacquard-Simon, N., Thourot, M., Massin, P. H. (1992): Physiological loadings on human pelvis: a comparison between numerical and experimental simulations. *Proc. Eur. Soc. Biomech.,* 8:195.
150. Lanyon, L. E., Paul, I. L., and Rubin, C. T. (1981): *In vivo* strain measurements from bone and prosthesis following total hip replacements. *J. Bone Joint Surg.,* 63A:989–994.
151. Lemaitre, J. (1984): How to use damage mechanics. *Nucl. Eng. Design,* 80:233–245.
152. Lionberger, D., Walker, P. S., and Granholm, J. (1985): Effects of prosthetic acetabular replacement on strains in the pelvis. *J. Orthop. Res.,* 3:372–379.
153. Lu, Z., Ebramzadeh, E., and Sarmiento, A. (1993): The effect of failure of the cement interfaces on gross loosening of cemented total hip femoral components. *Trans. ORS,* 39:519.
154. Mackerle, J. (1992): Finite and boundary element methods in biomechanics: A bibliography. *Eng. Comput.,* 9:403–435.
155. Malchau, H., Herberts, P., and Ahnfelt, L. (1993): Prognosis of total hip replacement in Sweden. Follow-up of 92,675 operations performed 1978–1990. *Acta Orthop Scand.,* 64:497–506.
156. Malchau, H. (1995): *On the importance of stepwise introduction of new hip implant technolgy.* Ph.D. thesis, Göteborg University, Sweden.
157. Malchau, H., Kärrholm, J., Wang, Y. X., and Herberts, P. (1995): Accuracy of migration analysis in hip arthroplasty. *Acta Orthop. Scand.,* 66:418–424.
158. Maloney, W. J., Jasty, M., Burke, D. W., O'Connor, D. O., Zalenski, E. B., Bragdon, C., and Harris, W. H. (1989): Biomechanical and histologic investigation of cemented total hip arthroplasties. A study of autopsy-retrieved femurs after *in vivo* cycling. *Clin. Orthop.,* 249:129–140.
159. Maloney, W. J., Smith, R. L., Schmalzried, T. P., Chiba, J., Huene, D., and Rubash, H. (1995): Isolation and characterization of wear particles generated in patients

who have had failure of a hip arthroplasty without cement. *J. Bone Joint Surg.,* 77-Am:1201–1210.
160. Mann, K. A., Bartel, D. L., Wright, T. M., and Burstein, A. H. (1995): Coulomb frictional interfaces in modeling cemented total hip replacements: a more realistic model. *J. Biomech.,* 28:1067–1078.
161. Martin, R. B. (1972): The effects of geometric feedback in the development of osteoporosis. *J. Biomech.,* 5:447–455.
162. McKellop, H., Campbeel P., Park S.H., Schmalzried T.P., Grigoris P., Amstutz H.C., Sarmiento A. (1995) The origin of submicron polyethylene wear debris in total hip arthroplasty. *Clin. Orthop.*, 311: 3–20.
163. McNamara BP, Cristofolini L, Toni A, and Tayor D (1995): Evaluation of experimental and finite element models of synthetic and cadaveric femora for pre-clinical design-analysis. *Clin. Mater.,* 17:131–140.
164. Miner, M. A. (1945): Cumulative damage in fatigue. *J. Appl. Mech.,* 159–164.
165. Mjöberg, B. (1986): Loosening of the cemented hip prosthesis. The importance of heat injury. *Acta Orthop. Scand. [Suppl.],* 221.
166. Mjöberg, B. (1991): Fixation and loosening of hip prostheses. A review. *Acta Orthop. Scand.,* 62:500–508.
167. Mjöberg, B., Hanson, L. I., and Selvik, G. (1984): Instability, migration and laxity of total hip prostheses. A röntgen stereophotogrammetric study. *Acta Orthop. Scand.,* 55:504–506.
168. Mow, V. C., Ateshian, G. A., and Spilker, R. L. (1993): Biomechanics of diathrodial joints: a review of twenty years of progress. *J. Biomech. Eng.,* 115:460–467.
169. Mullender, M. G., and Huiskes, R. (1995): Proposal for the regulatory mechanism of Wolff's Law. *J. Orthop. Res.,* 13:503–512.
170. NIH (1995): Total hip replacement. NIH Consensus Development Panel on Total Hip Replacement. *NIH Concen. Conf.,* 273:1950–1956.
171. Noble, P. C., Alexander, J. W., Granberry, M. L., et al. (1988): *The myth of "press-fit" in the proximal femur.* Scientific Exhibit, 55th AAOS, Atlanta GA, February 4–9.
172. Noble, P. C., Alexander, J. W., Lindahl, L. J., Yew, D. T., Granberry, W. M., and Tullos, H. S. (1988): The anatomic basis of femoral component design. *Clin. Orthop.,* 235:148–165.
173. Oh, I., and Harris, W. H. (1978): Proximal strain distribution in the loaded femur. *J. Bone Joint Surg.,* 60A:75–85.
174. Olsson, E. (1986): Gait analysis in hip and knee surgery. *Scand. J. Rehabil. Med. Suppl.,* 15:1–55.
175. Osborn, J. F. (1987): The biological behavior of the hydroxyapatite ceramic coating on a titanium stem of a hip prosthesis. *Biomed. Technol.,* 32:177–183.
176. Otani, T., Whiteside, L. A., White, S. E., and McCarthy, D. S. (1995): Reaming technique of the femoral diaphysis in cementless total hip arthroplasty. *Clin. Orthop.,* 311:210–221.
177. Pal, S., and Saha, S. (1982): Stress relaxation and creep behaviour of normal and carbon fibre reinforced acrylic bone cement. *Biomaterials,* 3:93–95.
178. Pazzaglia, U. E. (1990): Pathology of the bone–cement interface in loosening of total hip replacement. *Arch. Orthop. Trauma Surg.,* 109:83–88.
179. Pedersen, D. R., Crowninshield, R. D., Brand, R. A., and Johnston, R.C. (1982): An axial symmetric model of acetabular components in total hip arthroplasty. *J. Biomech.,* 15:305–315.
180. Perren, S. M. (1983): Induction der Knochenresorptio bei Prothesenlockering. In: *Die Zementlose Fixation von Hüftendoprothesen,* edited by E. Morcher, pp. 38–40. Springer Verlag, Berlin.
181. Perren, S. M., Ganz, R., and Rüter, A. (1975): Oberflächliche Knochenresorption um Implantate. *Med. Orthop. Techn.,* 95:6–10.
182. Perren, S. M., Rahn B.A. (1980): Biomechanics of fracture healing. *Can. J. Surg.,* 20:228–231.
183. Perrin, T., Dorr, L. D., Perry, J., Gronley, J., and Hull, D. B. (1985): Functional evaluation of total hip arthroplasty with five- to ten-year follow-up evaluation. *Clin. Orthop.,* 195:252–260.
184. Petty, W., Miller, G. J., and Piotrowski, G. (1980): *In vitro* evaluation of the effect of acetabular prosthesis implantation on human cadaver pelvis. *Bull. Pros. Res.,* 17:80–89.
185. Pierson, J. L., and Harris, W. H. (1993): Extensive osteolysis behind an acetabular component that was well fixed with cement—a case report. *J. Bone Joint Surg.,* 75-Am:305–315.
186. Pilliar, R. M., Lee, J. M., and Maniatopoulos, C. (1986): Observation on the effect of movement on bone ingrowth into porous-surfaced implants. *Clin. Orthop. Rel. Res.,* 208:108–113.
187. Poss, R., Walker, P., Spector, M., Reilly, D. T., and Robertson, D. D. (1988): Strategies for improving fixation of femoral components in total hip arthroplasty. *Clin. Orthop.,* 235:181–194.
188. Prendergast, P. J., Huiskes, R., and Søballe, K. (1997): Biophysical stimuli during tissue differentiation at implant interfaces. *J. Biomech.* (in press).
189. Pritchett, J. W. (1995): Femoral bone loss following hip replacement. *Clin. Orthop. Rel. Res.,* 314:156–161.
190. Raab, S., Ahmed, A., and Provan, J. W. (1981): The quasistatic and fatigue performance of the implant/bone interface. *J. Biomed. Mater. Res.,* 15:159–182.
191. Radin, E. L., Rubin, C. T., Thrasher, E. L., Lanyon, L. E., Crugnola, A. M., Schiller, A. S., Paul, I. L., and Rose, R. M. (1982): Changes in the bone-cement interface after total hip replacement. *J. Bone Joint Surg.,* 64A:1188–1194.
192. Rapperport, D. J., Carter, D. R., and Schurman, D. J. (1985): Contact finite elment stress analysis of the hip joint. *J. Orthop. Res.,* 3:435–446.
193. Reilly, D. T., and Burstein, A. H. (1975): The elastic and ultimate properties of compact bone tissue. *J. Biomed.,* 8:393–405.
194. Renaudin, F., Lavst, F., Skalli, W., Pecheux, C., and Schmitt, V. (1992): A 3D finite element model of pelvis in side impact. *Proc. Eur. Soc. Biomech.,* 8:194.
195. Rice, J. C., Cowin, S. C., and Bowman, J. A. (1988): On the dependence of the elasticity and strength of cancellous bone on apparent density. *J. Biomech.,* 21:155–168.
196. Ries, M., Pugh, J., Au, J. C., Gurtowski, J., and Dee, R. (1989): Cortical pelvic strains with varying size hemiarthroplasty in vitro. *J. Biomech.,* 22:775–780.
197. Ries, M. D., Gomez, M. A., Eckhoff, D. G., Lewis, D. A., Brodie, M. R., and Wiedel, J. D. (1994): An *in vitro* study of proximal femoral allograft strains in revision hip arthroplasty. *Med. Eng. Phys.,* 16:292–296.
198. Roesler, H. (1987): The history of some fundamental

concepts in bone biomechanics. *J. Biomech.,* 20(11/12): 1025–1034.
199. Rohlmann, A., Cheal, J., Hayes, W. C., and Bergmann, G. (1988): A nonlinear finite element analysis of interface condition in porous coated hip endoprostheses. *J. Biomech.,* 21:605–611
200. Rosenthal, D., (1974): *Resistance and Deformation of Solid Media.* Pergamon Press, New York.
201. Ryd, L. (1986): Micromotion in knee arthroplasty. *Acta Orthop. Scand. [Suppl.],* 220.
202. Saha, S., and Pal, S. (1984): Mechanical properties of bone cement: A review. *J. Biomed. Mater. Res.,* 18:435–462.
203. Saikko, V. O., Pavolainen, P. O., and Slätis, P. (1993): Wear of the polyethylene acetabular cup. Metallic and ceramic heads compared in a hip simulator. *Acta Orthop. Scand.,* 64:391–402.
204. Sanchez-Palencia, E. (1980): *Non-homogeneous Media and Vibration Theory.* Springer, Berlin.
205. Sandborn, P. M., Cook. S. D., Spires, W. P., and Kester, M. A. (1988): Tissue response to porous-coated implants lacking initial bone apposition. *J. Arthroplasty,* 3:337–346.
206. Schimmel, J. W., and Huiskes, R. (1988): Primary fit of the Lord cementless total hip. *Acta Orthop. Scand.,* 59:638–642.
207. Schmalzried, T. P., Kwong, L. M., Jasty, M., Sedlacek, R. C., Haire, T. C., O'Connor, D. O., Bragdon, C. R., Kabo, J. M., Malcolm, A. J., and Harris, W. H. (1992): The mechanism of loosening of cemented acetabular components in total hip arthroplasty. Analysis of specimens retrieved at autopsy. *Clin. Orthop.,* 274:60–78.
208. Schmitt, J., Lengsfeld, M., Alter, P., and Leppek, R. (1995): Use of voxel-oriented femur models for stress analysis. Generation, calculation and validation of CT-based FEM models. *Biomed. Tech. Berl.,* 40:175–181.
209. Schneider, E., Kinast, C., Eulenberger, J., Wyder, D., Eskilsson, G., and Perren, S. M. (1989): A comparative study of the initial stability of cementless hip prostheses. *Clin. Orthop.,* 248:200–209.
210. Schneider, E., Eulenberger, J., Steiner, W., Wyder, D., Friedman, R. J., and Perren, S. M. (1989): Experimental method for the *in vitro* testing of the initial stability of cementless hip prostheses. *J. Biomech.,* 22:735–744.
211. Schreurs, B. W., Buma, P., Huiskes, R., Slagter, J. L., and Slooff, T. J. (1994): Morsellized allografts for fixation of the hip prosthesis femoral component. A mechanical and histological study in the goat. *Acta Orthop. Scand.,* 65:267–275.
212. Selvik, G. (1989): *A roentgen stereophotogrammetric method for the study of the kinematics of the skeletal system.* Thesis, Lund, 1974. Reprinted as *Acta Orthop. Scand. [Suppl.],* 232.
213. Shanbhag, A. S., Jacobs, J. J., Glant, T. T., Gilbert, J. L., Black, J., and Galante, J. O. (1994): Composition and morphology of wear debris in failed uncemented total hip replacement. *J. Bone Joint Surg.,* 76-Br:60–67.
213a. Skinner H.B., Kilgus D.J., Keyak J., Shimaoka E.E., Kim A.S., Tipton J.S. (1994) Correlation of computed finite element stresses to bone density after remodeling around cementless femoral implants. *Clin. Orthop.,* 305:178–189.
214. Snorrason, F., and Kärrholm, J. (1990): Primary stability of revision total hip arthroplasty: A roentgen stereophotogrammetric analysis. *J. Arthroplasty,* 5:217–229.
215. Snorrason, F., and Kärrholm, J. (1990): *Roentgen stereophotogrammetric analysis of acetabular prostheses.* Scientific Exhibit, 57th Annual Meeting AAOS, Feb. 8–12, New Orleans.
216. Søballe, K., Hansen, E. S. B., Rasmussen, H., Jørgensen, P. H., and Bunger, C. (1992): Tissue ingrowth into titanium and hydroxyapatite-coated implants during stable and unstable mechanical conditions. *J. Orthop. Res.,* 10:285–299.
217. Södeqvist, I., and Wedin, P. A. (1993): Determining the movements of the skeleton using well-configured markers. Technical Note. *J. Biomech.,* 26:1473–1477.
218. Spector, M., Shortkroff, S., Hsu, H. P., Lande, N., Sledge, C. B., and Thornhill, T. S. (1990): Tissue changes around loose prostheses. A canine model to investigate the effects of an antiinflammatory agent. *Clin. Orthop.,* 261:140–152.
219. Spilker, R. L., Donzelli, P. S., and Mow, V. C. (1992): A transversely isotropic biphasic finite element model of the mensicus. *J. Biomech.,* 25:1027–1046.
220. Stauffer, R. N. (1982): Ten-year follow-up study of total hip replacement. *J. Bone Joint Surg.,* 64A:983–990
221. Stone, J. L., Beaupré, G. S., and Hayes, W. C. (1983): Multiaxial strength characteristics of trabecular bone. *J. Biomech.,* 16:743–752.
222. Stone, M. H., Wilkinson, R., and Stother, I. G. (1989): Some factors affecting the strength of the cement–metal interface. *J. Bone Joint Surg.,* 71-Br:217–221.
223. Sugiyama, H., Whiteside, L. A., and Kaiser, A. D. (1989): Examination of rotational fixation of the femoral component in total hip arthroplasty. *Clin. Orthop.,* 249:122–128.
224. Tanner, K. E., Bonfield, W., Nunn, D., and Freeman, M. A. R. (1988): Rotational movement of femoral components of total hip replacements in response to an anteriorly applied load. *Eng. Med.,* 17:127–129.
225. Thanner, J., Freij-Larsson, C., Karrholm, J., and Malchau, H. (1995): Evaluation of Boneloc. Chemical and mechanical properties, and a randomized clinical study of 30 total hip arthroplasties. *Acta Orthop. Scand.,* 66:207–214.
226. Timoshenko, S. P. and Gere, J. M. (1977): *Mechanics of Materials.* Van Nostrand Reinhold, New York.
227. Turner, C. H., Cowin, S. C., Rho, J. Y., Ashman, R. B., and Rice, J. C. (1990): The fabric dependence of the orthotropic elastic constants of cancellous bone. *J. Biomech.,* 23:549–561.
228. Van Lenthe, H., de Waal Malefijt, M., and Huiskes, R. (1996): Distal femoral resorption after total knee arthroplasty. *Trans. ORS,* 21:152.
229. Van Rietbergen, B., Huiskes, R., Weinans, H., and Sumner, D. R. (1993): ESB Research Award 1992. The mechanism of bone remodeling and resorption around press-fitted THA stems. *J. Biomech.* 26:369–382.
230. Van Rietbergen, B., Weinans, H., Huiskes, R., Odgaard A., and Kabel, J. (1995): A new method to determine trabecular bone elastic properties and loading using micromechanial finite element models. *J. Biomech.,* 28:69–81.
231. Van Rietbergen, B., Weinans, H., Polman, B. J. W., and Huiskes, R. (1996): Computational strategies for iterative solutions of large FEM applications employing voxel data. *Int. J. Num. Meth. Eng.* 39:2743–2767.

232. Van Rietbergen, B., Odgaard, A., Kabel, J., and Huiskes, R. (1996): The inherent mechanical quality of trabecular bone architecture can be accurately predicted from fabric and apparent density. *Trans. ORS,* 42:82.
233. Vasu, R., Carter, D. R., and Harris, W. H. (1982): Stress distributions in the acetabular region—I. before and after total joint replacement. *J. Biomech.,* 15:155–164.
234. Verdonschot, N. (1995): *Biomechanical faiure scenarios for cement total hip replacement.* Ph.D. thesis, Nijmegen University, The Netherlands.
235. Verdonschot, N. and Huiskes, R. (1990): FEM analyses of hip prostheses: validity of the 2-D side-plate model and the effects of torsion. In: *Proceedings 7th Meeting of the European Society of Biomechanics,* July 8–11, Arhus, Denmark, p. A20.
236. Verdonschot, N., and Huiskes, R. (1994): The creep behavior of hand-mixed Simplex P bone cement under cyclic tensile loading. *J. Appl. Biomater.,* 5:235–243.
237. Verdonschot, N., and Huiskes, R. (1995): Dynamic creep behavior of acrylic bone cement. *J. Biomed. Mater. Res.,* 29:575–581.
238. Verdonschot, N., and Huiskes, R. (1995): The application of continuum damage mechanics to pre-clinical testing of cemented hip prostheses; the effects of cement-stem debonding. In: *Second International Symposium on Computer Methods in Biomechanical & Biomedical Engineering,* edited by J. Middleton, pp. 25–33. Gordon and Breach, The Netherlands.
239. Verdonschot, N., and Huiskes, R. (1996): Subsidence of THA stems due to acrylic cement creep is exteremely sensitive to interface friction. *J. Biomech.* 29:1569–1575.
240. Verdonschot, N., and Huiskes, R. (1996): Mechanical effects of stem–cement interface characteristics in total hip replacement. *Clin. Orthop.* 329:326–336.
241. Verdonschot, N., and Huiskes, R. (1997): The cement debonding process of THA stems and its effects on cement stresses. *Clin. Orthop.* (in press).
242. Verdonschot, N., and Huiskes, R. (1997): The effects of bone cement creep on the mechanical endurance of femoral total hip reconstructions. *J. Bone Joint Surg.* (in press).
243. Verdonschot, N., and Huiskes, R. (1997): The effects of cement–stem debonding in THA on the long-term failure probability of cement. *J. Biomech.* (in press).
244. Verdonschot, N., Dalstra, M., and Huiskes, R. (1991): The relevance of implant telemetry for mechanical analyses of total hip arthroplasties. In: *Proceedings Book Workshop "Implantable Telemetry in Orthopaedics," Berlin.* Edited by Bergmann G, Graichen F, Rohlmann A. pp. 249–258. Freie Universitat Berlin, Berlin.
245. Verdonschot, N., Huiskes, R., and Freeman, M. A. R. (1993): Pre-clinical testing of hip prosthetic designs: a comparison of finite element calculations and laboratory tests. *J. Eng. Med.,* 207:149–154.
246. Walker, P. S., Schneeweis, D., Murphy, S., and Nelson, P. (1987): Strains and micromotions of press-fit femoral stem prostheses. *J. Biomech.,* 20:693–702.
247. Walker, P., Mai, S. F., Cobb, A. G., Bentley, G., and Hua, J. (1995): Prediction of clinical outcome of THR from migration measurements on standard radiographs. *J. Bone Joint Surg.,* 77-Br:705–714.
248. Weinans, H., Huiskes, R., and Grootenboer, H. J. (1990): Trends of mechanical consequences and modeling of a fibrous membrane around femoral hip prostheses. *J. Biomech.,* 23:991–1000.
249. Weinans, H., Huiskes, R., and Grootenboer, H. J. (1992): Effects of material properties of femoral hip components on bone remodeling. *J. Orthop. Res.,* 10:845–853.
250. Weinans, H., Huiskes, R., and Grootenboer, H. J. (1992): The behavior of adaptive bone-remodeling simulation models. *J. Biomech.,* 25:1425–1441.
251. Weinans, H., Huiskes, R., and Grootenboer, H. J. (1993): Quantitative analysis of bone reactions at implant–bone interfaces. *J. Biomech.,* 26:1271–1281.
252. Weinans, H., Huiskes, R., Van Rietbergen, B., Sumner, D. R., Turner, T. M., and Galante, J. O. (1993): Adaptive bone remodeling around bonded noncemented total hip arthroplasty: a comparison between animal experiments and computer simulation. *J. Orthop. Res.,* 11:500–513.
253. Weinans, H., Huiskes, R., and Grootenboer, H. J. (1994): Effects of fit and bonding characteristics of femoral stems on adaptive bone remodeling. *J. Biomech. Eng.,* 116:393–400.
254. Weinans, H., Igloria, R., Turner, T. M., Sumner, D. R., Natarajan, R. N., and Galante, J. O. (1995): Animal specific adaptive bone remodeling response to femoral hip components in dogs. *Trans. ORS,* 41:718.
255. Whiteside, L. A. (1989): The effect of stem fit on bone hypertrophy and pain relief in cementless total hip arthoplasty. *Clin. Orthop.,* 247:138–147.
256. Wiklund, I., Romanus, B., and Hunt, S. M. (1988): Self-assessed disability in patients with arthrosis of the hip joint. Reliability of the Swedish version of the Nottingham Health Profile. *Int. Disabil. Stud.,* 10:159–163.
257. Willert, H. G., Ludwig, J., and Semlitsch, M. (1974): Reaction of bone to methacrylate after hip arthroplasty. *J. Bone Joint Surg.,* 56-A:1368–1382.
258. Wolff, J. (1892): *Das Gesetz der Transformation der Knochen [The Law of Bone Remodeling].* Springer-Verlag, Berlin.
259. Wroblewski, B. M. (1988): Wear and loosening of the socket in the Charnley low-friction arthroplasty. *Orthop. Clin. North Am.,* 19:627–630.
260. Yelin, E. (1992): Arthritis. The cumulative impact of a common chronic condition. *Arthritis Rheum.,* 35: 489–497.
261. Yoon, Y. S., Jang, G. H., and Kim, Y. Y. (1989): Shape optimal design of the stem of a cement hip prosthesis to minimize stress concentration in the cement layer. *J. Biomechanics,* 22:1279–1284.
262. Young, R. J., and Lovell, P. A. (1991): *Introduction to Polymers.* The University Press, Cambridge.
263. Zhou, X. M., Walker, P. S., and Robertson, D. D. (1990): Effect of pres-fit femoral stems on strains in the femur. *J. Arthroplasty,* 5:71–82.
264. Zienkiewicz, O. C. (1977): *The Finite Element Method,* 3rd ed., McGraw-Hill, London.